Salen-type Metal Complexes with a Hydroxylamine Function and their Application in Aerobic Alcohol Oxidation

Hardeep Singh

A Thesis

In the Department

Of

Chemistry and Biochemistry

Presented in Partial Fulfillment of the Requirements

For the Degree of

Master of Science (Chemistry) at

Concordia University

Montreal, Quebec, Canada

November 2020

CONCORDIA UNIVERSITY
School of Graduate Studies

This is to certify that the thesis prepared

By: Hardeep Singh

Entitled: Salen-type Metal Complexes with a Hydroxylamine Function and their Application in Aerobic Alcohol Oxidation

and submitted in partial fulfillment of the requirements for the degree of

Master of Science in Chemistry

complies with the regulations of the University and meets the accepted standards with respect to originality and quality.

Signed by the final examining committee:

Dr. Judith Kornblatt Chair

Dr. Louis Cuccia Examiner

Dr. Marek Majewski Examiner

Dr. Xavier Ottenwaelder Supervisor

Approved by:

Dr. Yves Gélinas, Graduate Program Director

Dr. Pascale Sicotte, Dean, Faculty of Arts and Science

Date: November 4th, 2020

Abstract

Salen-type Metal Complexes with a Hydroxylamine Function and their Application in Aerobic Alcohol Oxidation

Hardeep Singh, M.Sc.

Aromatic compounds containing a redox-active hydroxylamine functionality are of great importance in biology and in synthetic organic chemistry. For example, arylhydroxylamines can act as a nitric oxide donor in mammals under certain conditions. They also participate as substrates in organic reactions for C–N bond formation, *e.g.* the metal-catalyzed nitroso-ene reaction. The redox conversions of arylhydroxylamines are, however, not well studied because of the high reactivity of these compounds and the ensuing formation of undesired side products. To address this challenge and gain insight into the redox behaviour of arylhydroxylamines in a systematic manner, we designed a family of ligands that possess an arylhydroxylamine function and can accommodate a variety of metal ions. This thesis reports the synthesis of these ligands, their complexation with three metal ions and the capacity of the complexes to catalyze a test organic reaction, the aerobic oxidation of alcohols into aldehydes.

Ligand design is based on the well-known family of salen ligands. We installed a pendant nitro group ($ArNO_2$) on one side of the ligand *via* a sulphonamide linkage, while substitutions on the salicylimine side afford structural and electronic variety. Partial reduction of the nitro group provides access to the corresponding arylhydroxylamine (ArNHOH) ligand, but the reduction conditions have to be fine-tuned to avoid over-reduction to the amine ($ArNH_2$) function. This was achieved either by catalytic hydrogenation over a poisoned palladium/charcoal catalyst or by stoichiometric transfer hydrogenation with zinc and ammonium formate. After optimization, these methods yielded four NHOH-containing ligands.

Subsequent complexation of the ligands with copper(II), nickel(II) and zinc(II) did not trigger a reaction with the redox-active NHOH function, contrary to the common belief that hydroxylamines disproportionate in the presence of metal ions. These unique complexes have been characterized by single-crystal X-ray diffraction, ^{1}H-NMR, and mass spectrometry. These studies reveal that the hydroxylamine function is engaged in an intramolecular hydrogen bond, which we hypothesized is responsible for the metastability of the NHOH function.

The complexes were screened as pre-catalysts for the aerobic oxidation of primary and benzylic alcohols to produce aldehydes. Only with benzylic alcohols was significant turnover observed, and only with the copper complexes (copper is known to enable oxygen-activation turnover). More importantly, control experiments reveal that the NHOH function is crucial for catalysis, which portends a similar mechanism as in the Markó alcohol oxidation system.

Further studies will focus on characterizing the fate of the NO bond during turnover, with the prospect of designing a novel family of catalysts for two-electron oxidation reactions.

Acknowledgments

This thesis is dedicated to the eternal guru “Shri Guru Granth Sahib Ji” for bestowing me with colossal strength, patience, and determination to complete my degree.

First and foremost, I gratefully acknowledge my profound sense of gratitude and regards to my research supervisor, Dr. Xavier Ottenwaelder, for his scientific guidance, meticulous attention to my work, fruitful discussions, and constant encouragement at every stage of my research work at Concordia. I would also like to thank Xavier for his patience and kind-heartedness throughout my entire studies.

I also extend many thanks and deepest appreciation to my supervisory committee members; Dr. Louis Cuccia and Dr. Marek Majewski for their inspiring guidance and invaluable suggestions in carrying out the research during the committee meetings.

I also wish to express my most heartful and tremendous thanks to all the administrative and exceptional technical staff members especially Marika, Maria, Alain (mass spectrometry experiments) and Costa (NMR experiments) who made my life and research easier and more enjoyable.

The words are not enough to express my love and thankfulness to XoRG members, especially Farshid Effaty, Paul Hoschtettler, Louis Paton and dearest friends at Concordia; Zujhar Singh, Kamal Kaur, Shubam Bhagat, Cynthia Messina, Arman, Gourav Shrivastava, Keegan Mckibbon who always supported me in all aspects of graduate life and finding me the ways to make life happier and cheerful. You people will always be remembered in my heart and I will always venerate your friendship. I would also like to convey my most warm and sincere thanks to Amanteshwar Singh and Zujhar Singh who really supported and encouraged me during the difficult times of my life during past two years. I am really thankful to Gurpreet Singh and Gurpreet kour for their pre-admission guidance to choose such a prestigious institution for higher studies to foster career and academic growth in this field.

Finally, and the most important of all, I would like to express my sincere gratitude and appreciation to my parents, Gurmeet Singh and Harmeet Kour, my brother Jaspreet Singh, for their constant support, unconditional care, and immense love. I would not have achieved as much throughout my life without their unstinting encouragement and blessings. I would also like to express my love and special honours to my fiancée, Parvinder Kour for her immense support, patience, and encouragement during the last year of my degree. I could not ask for a more supportive partner.

Table of Contents

List of Figures

List of Schemes

List of Tables

List of Abbreviations

ACN	Acetonitrile
ap	*ortho*-Amidophenolate
bq	*ortho*-Benzoquinone
cat	Catecholate
DBAD	Di-*tert*-butyl azodicarboxylate
DCM	Dichloromethane
DEAD	Diethyl azodicarboxylate
diq	*ortho*-Diiminoquinone
disq	*ortho*-Diiminosemiquinone
DMAP	4-*N,N*-Dimethylaminopyridine
DMSO	Dimethyl sulfoxide
EDTA	Ethylenediaminetetraacetic acid
en	ethylenediamine
EPR	Electron Paramagnetic resonance
equiv.	Equivalents
ESI-MS	Electrospray ionisation mass spectrometry
GOase	Galactose oxidase
HbO_2	Oxyhemoglobin
^{1}H-NMR	Proton nuclear magnetic resonance
HOMO	Highest occupied molecular orbital
ibq	*ortho*-iminobenzoquinone
isq	*ortho*-iminosemiquinone
IR	Infrared spectroscopy
L	Ligand
LUMO	Lowest unoccupied molecular orbital
MbO_2	Oxymyoglobin
MHz	Megahertz
m/z	Mass-to-charge ratio
NMI	*N*-methylimidazole
ORTEP	Oak Ridge thermal ellipsoid plot
pda	*ortho*-Phenylenediamine
sq	*ortho*-Semiquinone
TBP	Trigonal Bipyramidal
THF	Tetrahydrofuran
TLC	Thin-layer chromatography
TMPD	*N,N,N',N'*-tetramethyl-1,3-propanediamine
UV-Vis	Ultraviolet-visible
XRD	X-ray diffraction

Chapter 1: Introduction

1.1 Noninnocent Ligands

1.1.1 Redox properties of ligands

In 1966, Jørgensen[1] coined the term "noninnocent" to describe that "ligands are innocent when they allow oxidation states of the central atom to be defined". It implies that oxidation states of metal centers coordinated to a noninnocent ligands are ambiguous. While metal centers are normally the site of redox processes, ligand-centered redox processes can occur due to the unusual electronic structure of the noninnocent ligand scaffold. The combination of metal and ligand redox activity therefore broadens the scope of redox events that a complex can undergo.[2–12] Four different ways can be adopted to broaden metal reactivity (Figure 1-1).[13] Noninnocent ligands can: (A) act as electron reservoirs to provide a required number of electrons in electron-transfer reactions, (B) enhance the ability of the metal to accept or lose electrons in redox-processes, (C) afford ligand radical precursors, which can facilitate bond making/breaking reactions, (D) promote single-electron transfer processes.[13]

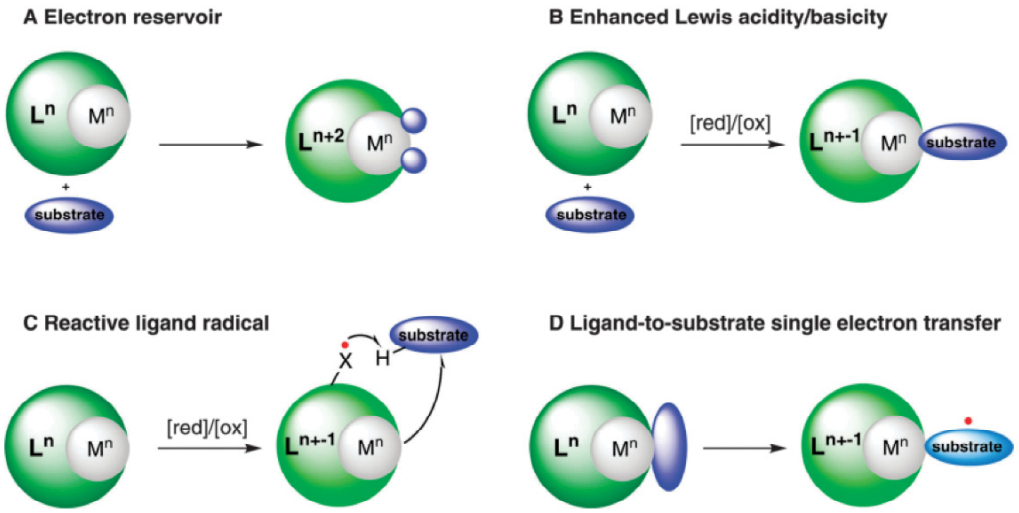

Figure 1-1: Different modes of enhancing metal reactivity by redox-active ligands (adapted from reference 13).

The higher energy of the HOMO (highest occupied molecular orbital) or lower energy of the LUMO (lowest unoccupied molecular orbital) of these ligands, as compared with charged-defined traditional ligands[14] such as H_2O, NH_3 or Cl^-, are responsible for their participation in electron-transfer processes through an inverted bonding process.[15] In general, noninnocent ligands possess energetically accessible levels through which they can change their oxidation states by loss of gain of an electron.[16,17] In further

descriptions, Ward and McCleverty introduced the term "ambivalent", which emphasized that noninnocence is not a function of ligand alone but also depends upon the central metal ion.[18]

The different oxidation states of a noninnocent ligand result in significantly modified metrical parameters of their metal complexes.[19,20] Various characterization techniques can be employed for the proper assignment of ligand and metal physical oxidation states, *viz*: X-ray crystallography, electrochemistry, density functional theory (DFT) to calculate spin densities, nuclear magnetic resonance (NMR) and electron paramagnetic resonance (EPR).[13]

1.1.2 Dioxygen

Several biologically important systems are involving redox-active ligands that generate radical species upon electron transfer.[21–23] For example, dioxygen (O_2) can be considered as a redox-active ligand. The sequential $1e^-$ reduction of O_2 in two steps can afford $O_2^{\bullet-}$ (superoxide) and O_2^{2-} (peroxide) anions (Scheme 1-1).[24]

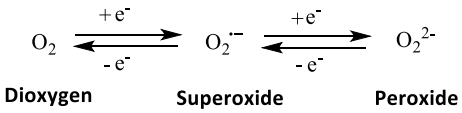

Scheme 1-1: Molecular oxygen as a redox-active ligand.

Dioxygen-storing and -transporting proteins,[25] oxymyoglobin (MbO_2) and oxyhemoglobin (HbO_2) also show redox processes between coordinated oxygen and iron.[26,27] In 1964, Pauling[26] showed that there is a simultaneous change in the spin state from high spin ferrous state (S = 2) to low spin ferrous state (S = 0) during the binding of dioxygen to the heme unit. This formulation was further revamped by Weiss[27] who best described this transformation as a one-electron transfer process from Fe(II) to O_2 to form an antiferromagnetically coupled Fe(III)-superoxide ($O_2^{\bullet-}$) pair (Scheme 1-2).

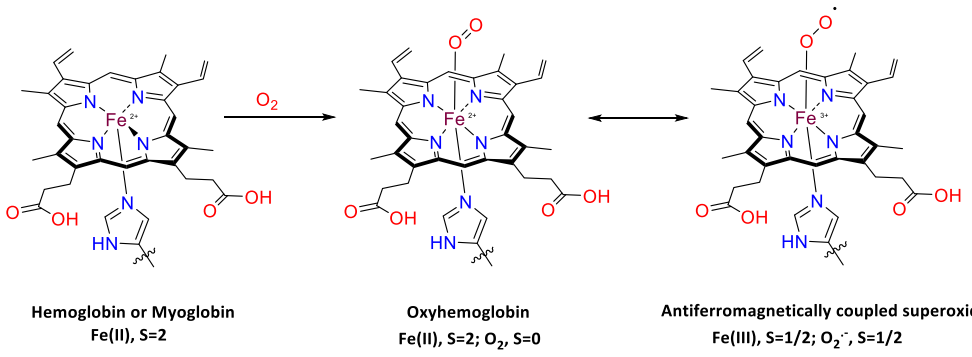

Scheme 1-2: Redox-active behaviour of dioxygen upon coordination to heme unit in hemoglobin.

1.1.3 *Ortho*-benzoquinones

Benzoquinones are some of the most studied compounds in the family of redox-active ligands as they are involved in numerous biological processes.[13,28] These ligands can exist in three oxidation states ranging from neutral benzoquinone (bq) to one electron reduced semiquinone (sq) and finally to fully reduced dianionic catecholate, as illustrated in Scheme 1-3a for the *ortho* topology, which is the most relevant in the context of noninnocent ligands.[29–31] Derivatives of these species, *ortho*-aminophenols and *ortho*-phenylenediamines find numerous applications in oxidation reactions due to the versatility of substitution at their nitrogen groups.[32,33] They exhibit similar kind of oxidation-reduction pattern as *ortho*-benzoquinones to give neutral *ortho*-iminobenzoquinone (ibq) and *ortho*-diiminoquinone (diq), monoanionic radical *ortho*-iminosemiquinone (isq) and *ortho*-diiminosemiquinone (disq) radical anions, and fully reduced *ortho*-amidophenolate (ap) and *ortho*-phenylenediamine (pda) dianions, respectively (Scheme 1-3b, c).

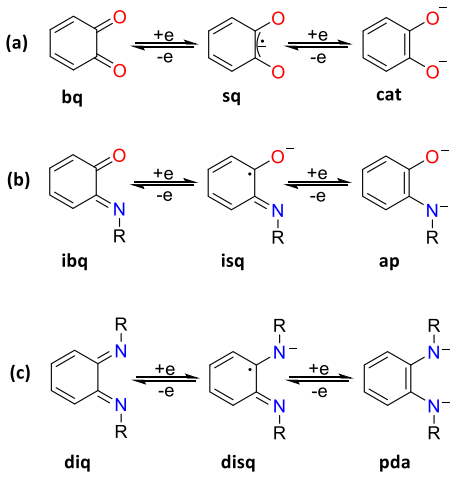

Scheme 1-3: Redox-active behaviour of: (a) *ortho*-benzoquinones, (b) *ortho*-aminophenol and (c) *ortho*-phenylene-diamine ligands.

1.1.4 Nitric oxide

Nitric oxide (NO) is a small molecule with many biological functions and effects.[34–36] This simple molecule had drawn much attention in recent decades due to its potential role in cellular signaling.[34] Due to its biological relevance, it was also announced as "molecule of the year" in 1962.[37] This reactive molecule was documented as a redox-active ligand in early 1960s by Jørgensen, who stated NO may be "the simplest case of suspect ligand".[1] The molecular orbital diagram of NO (Scheme 1-4a) provides a justification for the high reactivity of this molecule which is particularly attributed to the presence of one unpaired electron in an anti-bonding π* molecular orbital. Other factors that can contribute to the high

reactivity of nitric oxide are high electron affinity (0.024 eV, 2.31 kJ mol^{-1}) and low ionization potential (9.26 eV, 893 kJ mol^{-1}). This electronic configuration explains the redox versatility of this molecule that can exist in three different forms (Scheme 1-4b): one-electron oxidized nitrosonium ion (NO^+), one-electron reduced nitroxide ion (NO^-) and the nitric oxide radical ($NO^\bullet$).[38,39] These different oxidation states can be inferred by the stretching frequencies of the N–O bond (ν_{NO}), which increases with decreasing charge from 1470 (NO^-) through 1875 (NO) to 2377 (NO^+).[40]

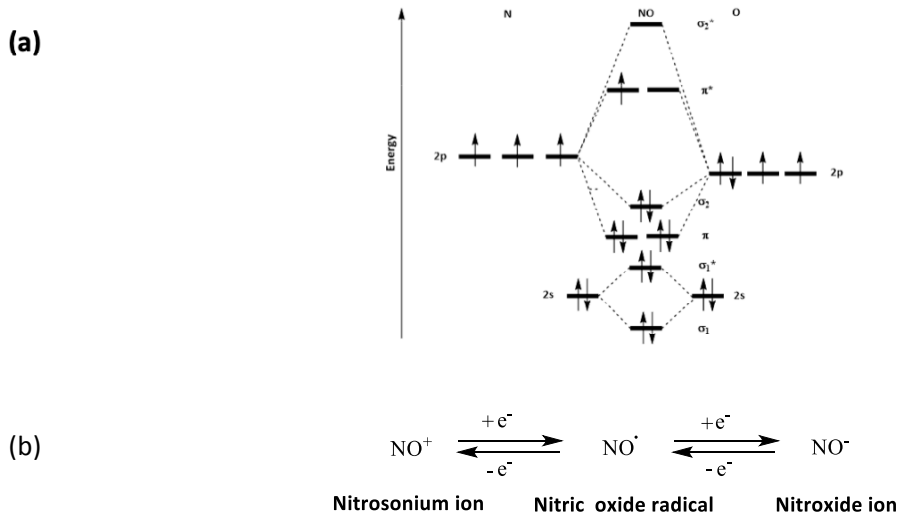

Scheme 1-4: (a) Molecular orbital diagram of nitric oxide. (b) Redox-active behaviour of NO.

1.1.5 Galactose Oxidase

Multielectron transfer processes can be facilitated in metalloenzymes with a noninnocent cofactor coordinated to the metal center.[41] One classic example of this synergistic reactivity is the two-electron aerobic alcohol oxidation by Galactose Oxidase (GOase). It is an extracellular, fungal copper metalloenzyme produced in Dactylium dendroides.[42] GOase converts galactose to galactohexodialdose, generating H_2O_2 as a by-product (Scheme 1-5a).[41] As this transformation is a two-electron process, it raises the question how it is performed at a mononuclear copper site because, in general, copper shuttles between +1 and +2 oxidation states.[43] In 1990, Whittaker was able to identify that the active site in GOase contains a tyrosyl radical coordinated to a Cu(II) ion.[44] The catalytic cycle of alcohol oxidation involves three steps (Scheme 1-5b): (i) substrate deprotonation and coordination to the metal center, (ii) intramolecular proton-coupled electron transfer, (iii) formation of aldehyde, which is then released from the active site, (iv) regeneration of active species by reaction with dioxygen.[45,46]

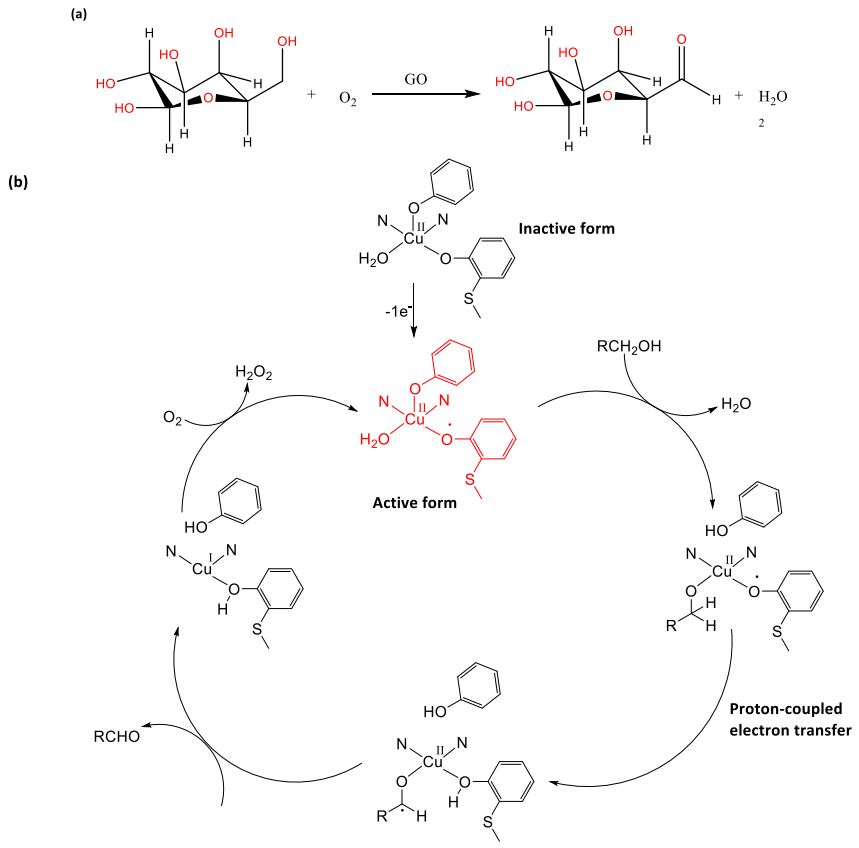

Scheme 1-5: (a) Galactose oxidase: general reaction equation. (b) Proposed catalytic cycle for alcohol oxidation catalyzed by galactose oxidase.[46]

1.1.6 Cytochrome P450

Another classic example of cooperativity between a metal ion and an organic radical during catalytic turnover is cyctochrome P450.[47,48] In this hemoprotein the active species contains a high-valent iron(IV)-oxo moiety coordinated by a ligand radical that is stabilized by the delocalisation over the electron-rich porphyrin system and axially bound sulfur atom.[47] The catalytic cycle (Scheme 1-6) starts with one-electron reduction of cytochrome P450 to generate a Fe(II)-heme unit. It will subsequently coordinate to O_2 and react with two equivalents of H^+, with further one electron reduction to afford a high-valent iron(IV)=O core named as compound I, where the heme is oxidized to a radical cation.[48,49] This metalloradical can hydroxylate very unreactive C–H bond of a typical hydrocarbon having a dissociation energy of 100 kcal mol^{-1}.[50]

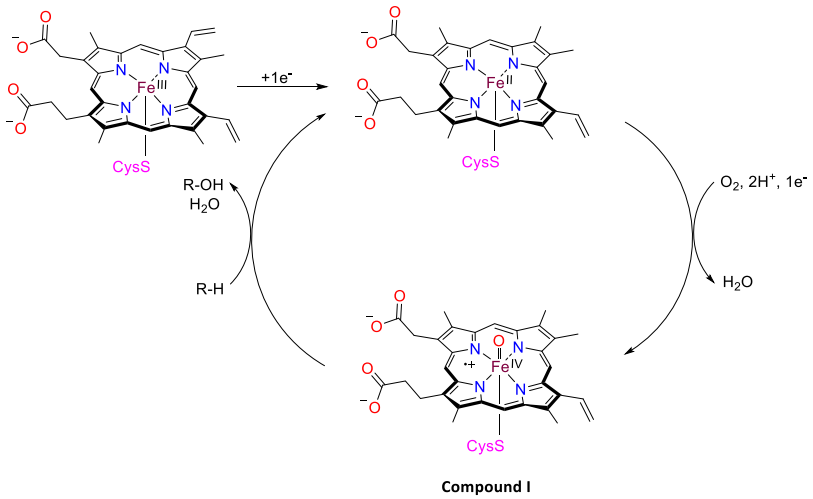

Scheme 1-6: Cytochrome P450 catalytic cycle.[48]

1.2 Redox-Noninnocent Ligands in Catalysis

Transition metal catalysts based on 4d and 5d series elements are generally expensive, rare, and toxic. Therefore, considerable attention have been given in recent years to employ inexpensive and earth-abundant base metal catalysts to perform desirable chemical transformations.[8] But these metals are limited by their tendency to undergo one-electron redox changes (i.e Cu^{1+} to Cu^{2+}, Fe^{2+} to Fe^{3+}) whereas noble metals typically show controlled two-electron redox changes and enable two-electron catalysis without deleterious radicals. Chirik and Wieghardt have proposed that the cooperative action of redox-active ligand and base metal ion can facilitate the multi-electron redox-reaction.[17] Traditional ligands coordinated to the metal center act as spectators (redox-inactive or innocent), which implies that the metal ion is the site of reactivity in catalytic cycles.[8] But, recently new approaches were highlighted in these papers,[51,52] where bond making and bond breaking steps in a catalytic cycle are generally catalyzed by the active participation of redox-active or noninnocent ligands coordinated to the metal center. In general, the cooperativity between the metal center and the redox-active ligand can facilitate the chemical reaction by breaking down the multi-electron reaction steps into smaller steps, thereby forcing the reactions to occur near thermodynamic potential.[53] In the previous section, we discussed about the synergistic behaviour in few metalloenzymes like galactose oxidase and cytochrome P450 where both metal center and ligand actively participate in catalytic reactions.[41,47,48] Inspired by such metalloenzymes, several catalytic systems have been developed by chemists in recent decades which find numerous applications in synthetic inorganic chemistry and homogenous catalysis.[51,54]

A prominent system illustrating the picture of redox cooperativity between metal center and coordinated ligand was reported by Markó and coworkers in 1996. They used CuCl/phen/DEAD system (phen: phenanthroline, DEAD: diethyl azodicarboxylate) to catalyze the aerobic oxidation of a broad range of alcohols. According to their mechanism, the added base facilitates deprotonation of the alcohol substrate to produce an alkoxide, which then coordinates to Cu(I) to produce A. In the next step, intramolecular hydrogen-atom transfer occurs from the alkoxide to produce $DEADH^-$ (B), which then releases the aldehyde to produce C. Binding of oxygen to C affords Cu(II)-hydrazide derivative D. The thermal conditions of the reaction reorganize D to produce Cu(I)-hydroxo intermediate E. The key diazo functionality (DEAD) in the catalytic system is regenerated by ligand-exchange producing water as a by-product (Scheme 1-7).[55] This system was further modified (supporting ligands and additives) for better yields and broader substrate scope.[56]

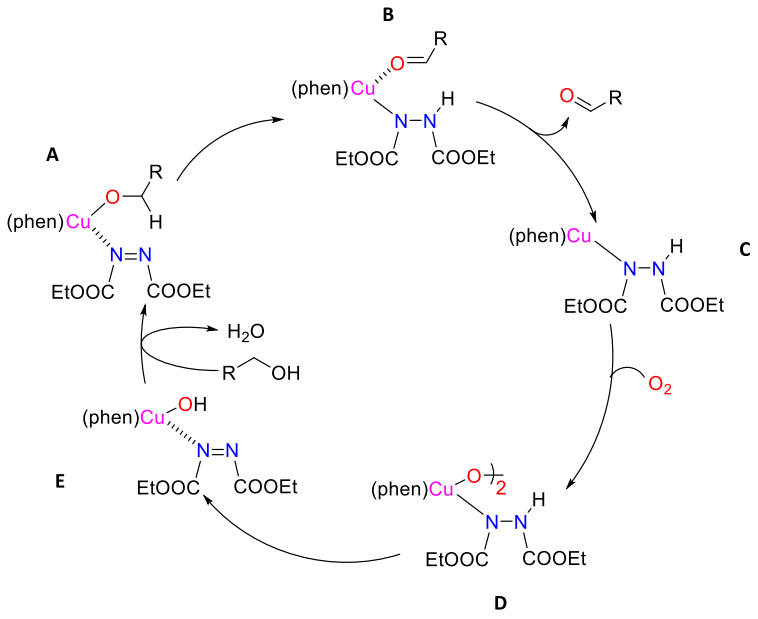

Scheme 1-7: Proposed catalytic cycle for alcohol oxidation by Markó and coworkers.[55]

In 2016,[57] Stahl investigated this mechanism in more detail with kinetic and *in-situ* spectroscopic studies. The revised mechanism involves two interdependent catalytic cycles (Scheme 1-8). In the first, slow cycle, Cu(II) mediates the alcohol oxidation without the involvement of DBAD (top, red cycle). In the second, fast cycle, the alcohol substrate is oxidized by two-electron oxidant di-*tert*-butyl azodicarboxylate (DBAD) (bottom, blue cycle). The fast Cu(II)/DBAD pathway can only turnover after the formation of Cu(I) by the slow process because only Cu(I) can activate O_2 to oxidize $DBADH_2$ back into

DBAD. Thus, the steady-state rate-law is determined by the slow Cu(II)-mediated oxidation of alcohol. Notwithstanding, this catalytic bicycle still involves redox cooperativity between Cu and DBAD.

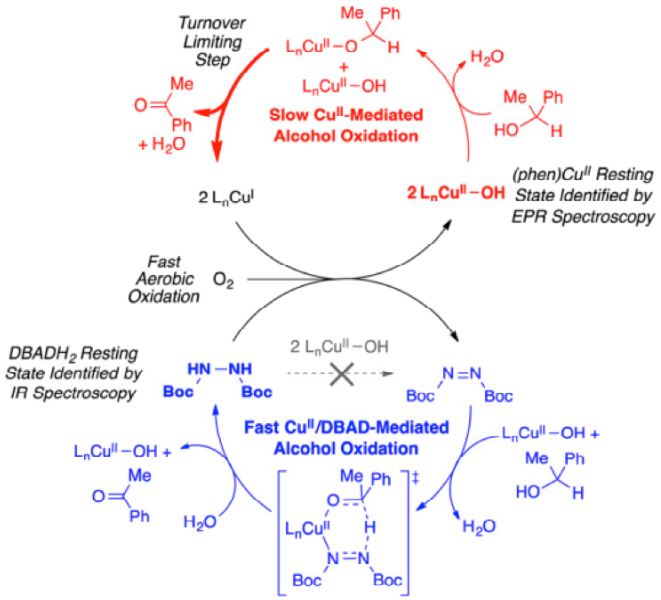

Scheme 1-8: Reinvestigated mechanism of Cu(II)/DBAD catalyzed aerobic alcohol oxidation.[57]

Another catalytic system exhibiting similar kind of ligand-metal interaction for their participation in catalysis was proposed by Paul and coworkers (Scheme 1-9) for the aerobic oxidation of primary and secondary benzylic alcohols using phenanthroline based redox-noninnocent azoaromatic pincer ligand coordinated to Fe^{2+} metal center.[5]

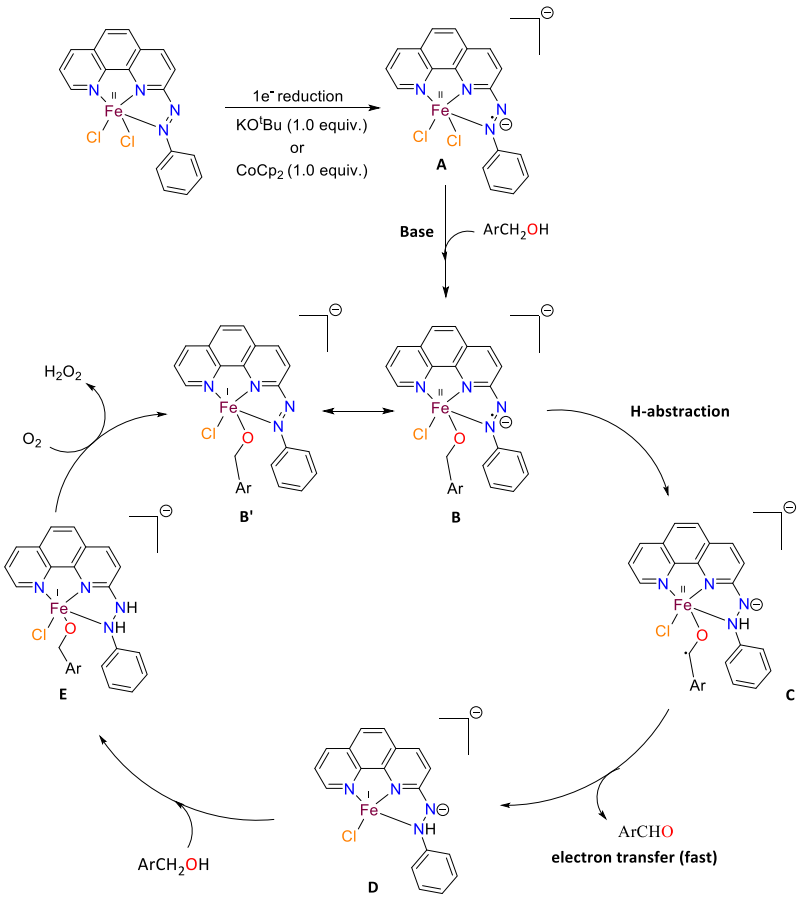

Scheme 1-9: Proposed catalytic cycle for alcohol oxidation.[5]

Upon one electron reduction, the coordinated azo ligand is reduced to afford active catalyst containing azo anion radical A. The catalytic cycle starts with the binding of deprotonated alcohol substrate to give intermediate B. Hydrogen-atom abstraction from alcohol gives intermediate C which can lose one electron to produce corresponding aldehyde along with intermediate D in which iron is proposed to be in +1 oxidation state. This intermediate then undergo another H abstraction to generate intermediate E which subsequently regenerates azo key functionality and H_2O_2 as a by-product.[5]

1.3 Redox Behaviour of Nitrogen Containing Functional Groups and their Reactivity

Nitrogen containing functional groups are versatile in terms of their redox behaviour and can possess different oxidation states in chemical compounds. For example, in direct route,[58,59] sequential two-electron reductions of a nitro compound (R–NO_2) affords the nitroso (R–N=O), hydroxylamine (R–NHOH) and finally amine (R–NH_2) derivatives (Scheme 1-10). Nitro hydrogenation can also proceed *via* a condensation route with the formation of azoxy, azo and hydrazine compounds. In addition, the hydroxylamine intermediate can disproportionate into nitroso and amine moieties.[58] Nitroso species

being reactive in nature can also form two dimers solid or liquid state viz: Z-azodioxy or E- azodioxy. These dimers are in equilibrium with their monomeric form.[60,61] This redox richness is what propels our research in studying how a metal ion can steer these reactions for catalytic use.

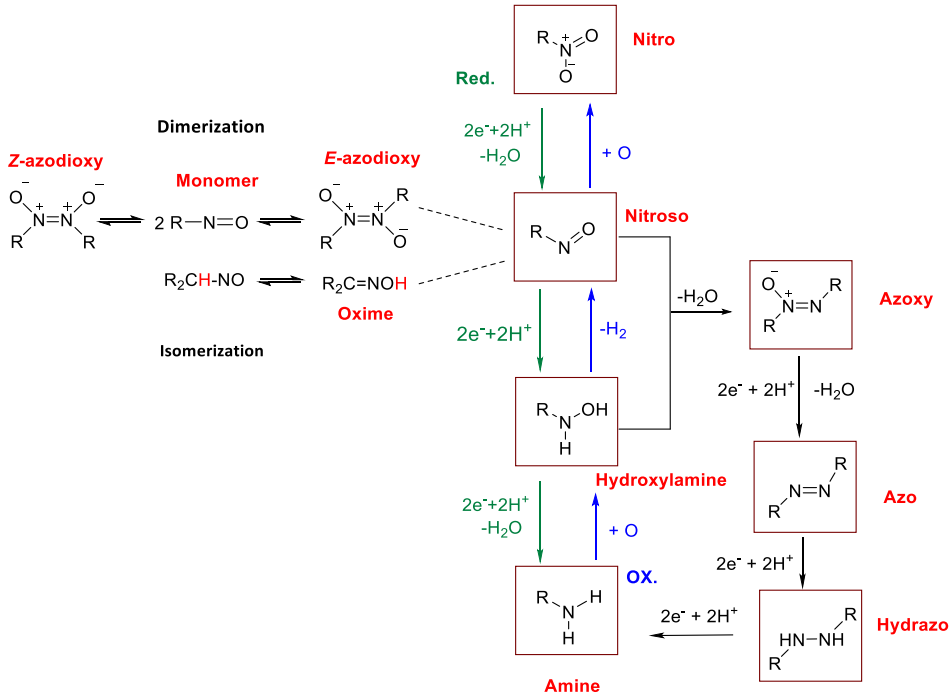

Scheme 1-10: Redox versatility of nitrogen-containing functional groups.

1.3.1 Nitrosoarenes and their Applications

C-nitroso compounds, due to their highly reactive nature, undergo numerous organic reactions,[62,63] some of which are highlighted in Scheme 1-11.

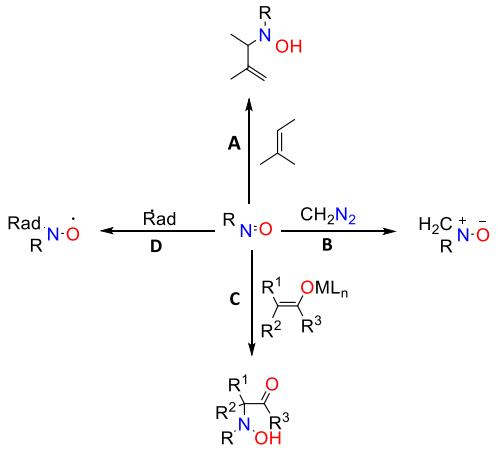

Scheme 1-11: Applications of nitroso compounds in organic synthesis.

One of the most typical reactions of nitroso compounds is the nitroso-ene reaction (path A). As the name suggests, it is a reaction between an alkene having an allylic hydrogen (ene) and a nitroso compound, which has an electron-deficient multiple bond (enophile). It is a pericyclic reaction involving the activation of allylic C–H bond to form *N*-allyl hydroxylamines. However, the hydroxylamine produced tends to disproportionate and form several side products, which is the major drawback of this reaction.[63] Nitrones are produced upon reaction with diazomethane (path B).[64] Being electrophilic in nature, C-nitroso compounds undergo nucleophilic addition with enolates to produce α-hydroxyamino carbonyl compounds (path C).[65–67] This method is named nitroso aldol reaction and specifically introduces a nitrogen atom to carbonyl compounds.[67] Nitrosos have also been used as radical scavengers in organic reactions to trap radical intermediates (path D). The transient radicals generated in the reaction will form nitroxide radicals with nitroso compounds which can be easily detected by Electron Paramagnetic Resonance (EPR) spectroscopy.[68–70] For example, Adam and coworkers had trapped 2-diphenylmethylene-1,3-cyclopentadiyl *via* nitroxide formation using nitrosobenzene as a spin-trapping agent (Scheme 1-12).[68]

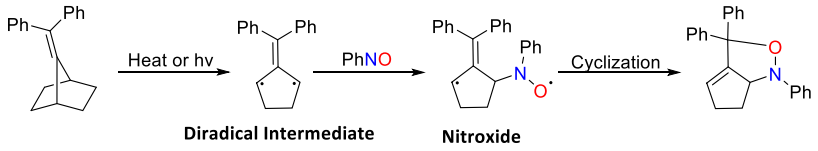

Scheme 1-12: Use of nitroso compound to trap radical intermediate.[68]

In addition to this, nitrosoarenes or nitrosoalkanes form complexes or simple adducts with metal centers by acting as ligands.[71,72] Due to the presence of lone pairs, π-bonding electrons and a π* system on both heteroatoms (N and O), C-nitroso compounds have wide range of binding modes in their metal complexes (Scheme 1-13).[61,73] The three different binding modes as characterized by X-ray crystallography are categorized as: sole N-bonding, sole O-bonding and N, O-bonding. Among these coordination modes, sole N-bonding (κN) is the most prevalent. X-ray crystallography and vibrational spectroscopy can be used to determine N–O bond lengths in different binding modes. However, N–O bond length may also vary due to differences in the nature and oxidation state of metal centers and the supporting ligands.

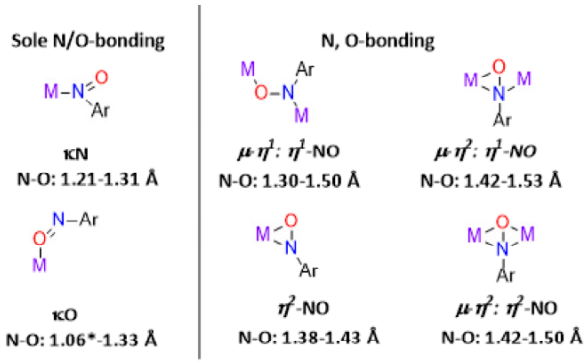

Scheme 1-13: Some common examples of metal- ArNO binding modes.* disorders in the structures.[61]

A recent report by XoRG member Mohammad S. Askari et al. demonstrated different binding modes of nitroso moiety in a series of copper/nitrosoarene complexes (Scheme 1-14).[74] They prepared a series of *para*-substituted derivatives of nitrosobenzene to form adducts with Cu(I) precursor complex of *N,N,N′,N′*-tetramethyl-1,3-propanediamine (TMPD). With an electron-donating group (NMe_2) on nitrosobenzene, the NO group binds to copper complex in a κN fashion. In this case, no electron-transfer is observed between the metal center and nitroso moiety which is further supported by N–O bond length of 1.293 Å, a typical value for N=O double bonds. In case of electron-neutral substituted (H, Cl, Br) derivatives, nitroso moiety undergoes one electron reduction to form monoanionic radical species (η^2-$PhNO^{\bullet-}$ or μ-η^2:η^1-$PhNO^{\bullet-}$). These adducts observed elongated N–O bond lengths of 1.327 Å consistent with this binding mode. Whereas two-electron reduction of NO group is observed in adducts of electron-poor (NO_2) nitrosobenzene derivatives to form dianionic NO^{2-} species (μ-η^2:η^2-$PhNO^{2-}$). The bond length in this case is 1.456 Å.[74]

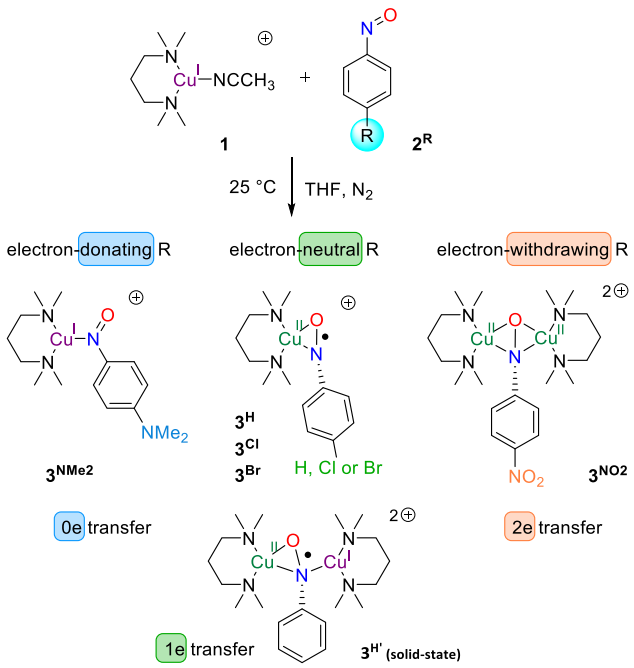

Scheme 1-14: Different binding modes of ArNO in Cu-TMPD adducts.[74]

1.3.2 Arylhydroxylamines and their Applications

Arylhydroxylamines (ArNHOH) can be formed by catalytic partial reduction of aromatic nitro compounds ($ArNO_2$) (Scheme 1-15).[58] Although very reactive in biological systems, ArNHOH and its two-electron oxidized counterpart ArNO can be formed as metabolic intermediates by the penetration of aniline ($ArNH_2$) or nitrobenzene inside red blood cells (Scheme 1-15).[75] *N*-phenylhydroxylamine is also formed as one of the intermediates by bioactivation sulfamethoxazole (a drug used in the treatment of Pneumocystis carinii pneumonia), which will initiate a cascade of events leading to idiosyncratic reactions.[76] In addition to this, hydroxylamines are produced endogenously in the production of nitric oxide.[77] Furthermore, its reaction with oxyhemoglobin can generate hydronitroxide radical ($H_2NO^{\bullet}$) and methemoglobin due to oxidative stress in erythrocyte.[78]

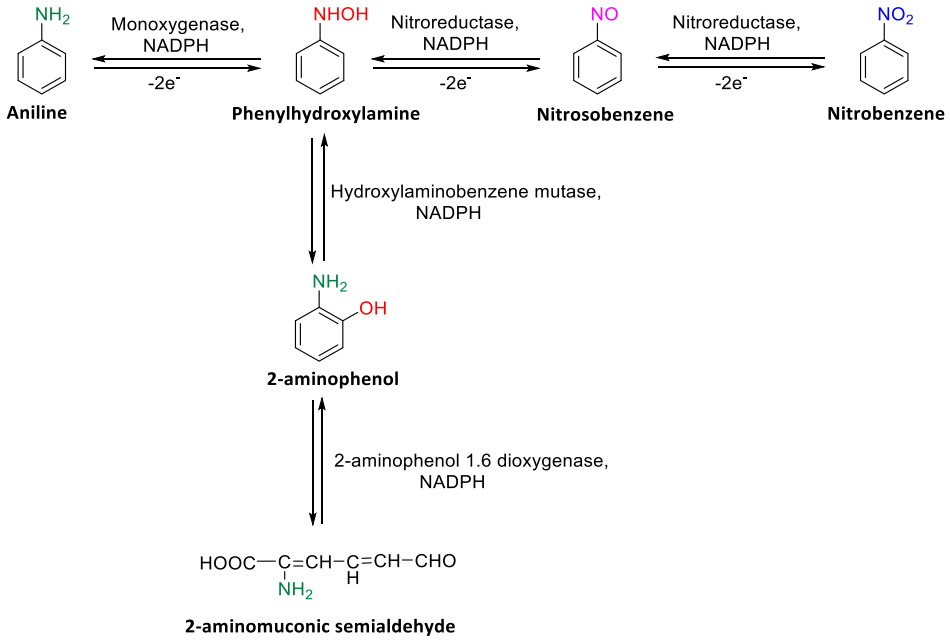

Scheme 1-15: Formation of metabolic intermediates inside red blood cells.[75]

Due to their high reactivity, *N*-arylhydroxylamines have been used as nitrogen-fragment donors in C–H amination of allylic substrates *via* a nitroso-ene reaction in the presence of metal catalysts.[63] The catalytic cycle starts with the oxidation of phenylhydroxylamine to corresponding nitrosobenzene, which then coordinates to the metal center (molybdenum, iron or copper) and catalyzes the reaction. In the molybdenum-catalyzed oxidative amination, the cycle starts with the oxidation of phenylhydroxylamine by Mo(VI) catalyst to form molybdenaoxaziridine complex (B).[79] This catalytic active species then reductively eliminates nitrosobenzene (PhNO) to undergo nitroso-ene reaction with allylic substrate (alkene) to form initial hydroxylamine ene product (C) and Mo(IV) intermediate. Reduction of C by Mo(IV) species affords the desired amine and regenerates the catalyst (A) to start new catalytic cycle (Scheme 1-16).

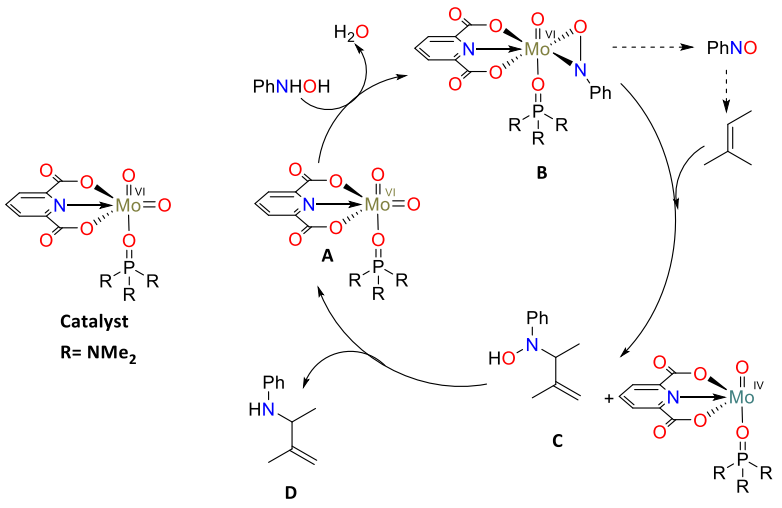

Scheme 1-16: Mo(VI) catalyzed nitroso-ene reaction.[79]

The catalytic cycle for the iron-catalyzed allylic amination is not yet confirmed.[63] However, an azo dioxide iron complex (Scheme 1-17) produced by the initial oxidation of PhNHOH was found to be the active aminating species. Its structure is confirmed by X-ray diffractometry.[80]

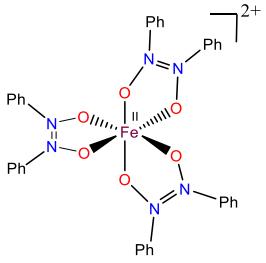

Scheme 1-17: Catalytic active aminating species in iron catalyzed nitroso-ene reaction.[80]

In 2000, Lau and coworkers reported allylic amination with phenylhydroxylamine using Cu(II) salts.[81]. In the first step of the catalytic cycle, PhNHOH is oxidized to free PhNO by Cu(II) which then undergoes nitroso-ene reaction with allylic substrate to form allylhydroxylamine. In the next step, Cu(I) produced in the first step reduces allylhydroxylamine to allylamine and regenerates Cu(II) to start a new cycle (Scheme 1-18).

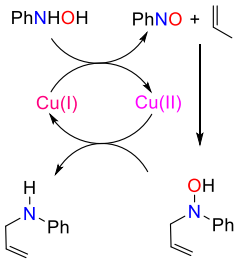

Scheme 1-18: Cu(II) catalyzed nitroso-ene reaction.[81]

Srivastava et al.[82] have proposed Cu(I) promoted allylic amination of alkenes. Reaction of pre-catalyst $[Cu^{I}(CH_3CN)_4]PF_6$ with phenylhydroxylamine generates $[Cu^{I}(\kappa N\text{-}PhNO)_3]^+$, a Cu(I)-bonded nitrosoarene complex which serves as active aminating species in the catalytic cycle.[83,84] This is contrary to Mo^{VI} catalyzed allylic amination as it involves the intervention of free PhNO.[63] The catalytic cycle (Scheme 1-19) begins with the reduction of PhNHOH by catalytic amount of Cu(I) to produce $PhNH_2$ and Cu(I). This Cu(II) will then oxidize phenylhydroxylamine to free nitrosobenzene, which affords catalytic active complex, $[Cu(\kappa N\text{-}PhNO)_3]^+$. This complex performs the nitroso-ene reaction and produce allylhydroxylamine which is further reduced by Cu(II) to give desired amine and Cu(I) to start a new cycle.[83,84] In both copper-catalyzed amination reactions, copper shuttles between +1 and +2 oxidation states during the transformation of PhNHOH to PhNO or $PhNH_2$. However, the conversion of these nitrogen-containing compounds required transfer of two electrons to shuttle between PhNHOH and PhNO or PhNHOH and $PhNH_2$. It still remains a question of interest how a single electron interconversion between Cu(I)/Cu(II) redox couple is promoting two electron transformations.

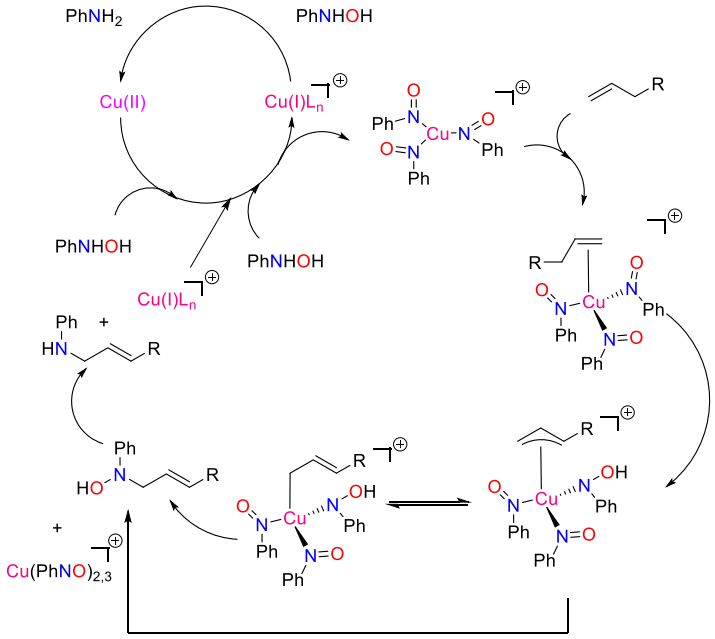

Scheme 1-19: Cu(I) catalyzed nitroso-ene reaction.[84]

1.4 Methods of Synthesis of Arylhydroxylamines

N-aryl compounds constitute an important class of compounds as they are important intermediates in the production of dyes, pharmaceuticals, and agrochemicals.[85] Some of the important pharmaceutical compounds containing arylamine substructures are paracetamol[86] (analgesic) and erlotinib[87] (anticancer lung/pancreatic) (Scheme 1-20).

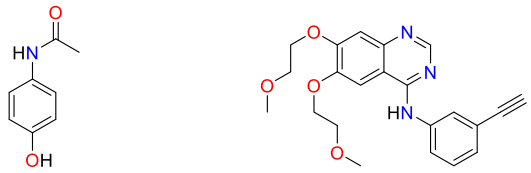

Paracetamol (Analgesic) **Erlotinib Anticancer (Pancreatic/Lung)**

Scheme 1-20: Medicinal compounds with amino functionalized substructures.

The large-scale manufacturing of these reactive compounds is accomplished by hydrogenation of aromatic nitro compounds under a wide range of conditions.[88,89] Catalytic reduction of aromatic nitro compound ($ArNO_2$) can proceed *via* the formation of reactive nitrosoarene (ArNO) and arylhydroxylamine (ArNHOH) intermediates (Scheme 1-10). Makaryan and Savchenko proposed another route for the formation of amine as a result of hydroxylamine disproportionation rather than hydrogenation(Scheme 1-21).[90] All of these interconversions involve sequential two-electron processes

at each step. On the other side, condensation route beginning with reaction of reactive hydroxylamine and nitroso intermediates suggests alternative route for production of aromatic amines through sequential formation of azoxy, azo and hydrazo derivatives.[58]

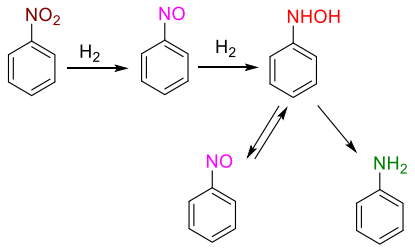

Scheme 1-21: Conversion of aryl nitro to aniline by disproportionation mechanism proposed by Makaryan and Savchenko.[91]

The reduction of nitro compounds to amines can be achieved by various methods. The most general and conventional methods are catalytic hydrogenation[88] using Raney Ni and PtO_2 or metal-based reducing systems such as Fe/HCl,[92] Zn/NH_3,[93] Zn/HCl,[94] and Sn/HCl.[95] However, carrying out reduction with these reagents have several limitations. For example, they are not selective in nature and can also reduce other groups in functionalized nitro compounds leading to unwanted side products.[96]

Partial reduction to get hydroxylamine and nitroso intermediates is considerably more difficult. This is due to instability of these derivatives and their ability to react with each other to form other compounds (Scheme 1-10). Still, a few reports are known to partially hydrogenate aryl nitro compounds to these reactive compounds under mild reduction conditions.[88] For example, nitroso compounds can be obtained by catalytic reductive deoxygenation of nitro compounds.[97] Hydroxylamines can be obtained by using a Pt catalyst with DMSO under H_2 pressure (Scheme 1-22).[88] Entwistle and coworkers achieved this conversion *via* transfer hydrogenation from phosphonic acid or sodium phosphinate in bi-phasic H_2O-THF system with palladium-charcoal catalyst.[98]

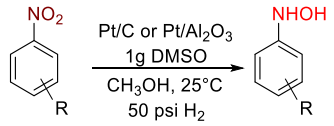

Scheme 1-22: Controlled reduction of nitroarenes to aryl hydroxyalmines.[88]

Catalytic hydrogenation methods are clean, but overreduction of nitroarenes to produce amines can be problematic. Therefore, new approaches were introduced to achieve maximum yield of hydroxylamine using stoichiometric reducing agents. Kamm reported a convenient and facile reduction

method using non-toxic Zn dust in aqueous NH_4Cl to selectively reduce nitrobenzene to *N*-phenyl hydroxylamine at a temperature range of 60-65 °C (Scheme 1-23).[99,100] This method is advantageous because of its mild reaction conditions and low cost. But large consumption of NH_4Cl and ample wastewater generation are some of the drawbacks that urge chemists to develop more environmentally benign methods.[101]

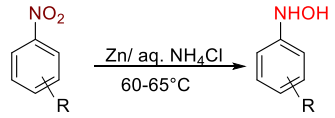

Scheme 1-23: Traditional method of synthesizing aryl hydroxylamines using Zn in aqueous NH_4Cl.[99,100]

Liu et al.[101] reported an environmentally friendly system, which removes the use of aq. NH_4Cl for partial reduction of nitro compounds to aryl hydroxylamines using cheap and commercially available Zn dust in a CO_2/H_2O system. Carrying out the reaction at room temperature for 1.5 h under 0.1 MPa CO_2 and 3 equivalents of Zn affords 88% yield of desired hydroxylamine. This method proves to be more efficient than the one reported by Kamm[99,100] in view of environmental concerns. Furthermore, this system was modified by using ultrasonic waves, which significantly increase the yield of hydroxylamine to 95% under the optimized conditions with a lesser quantity of zinc (2.2 equiv.) and shorter reaction time (1 h).[102]

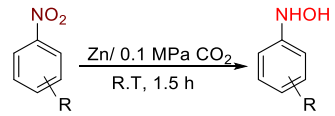

Scheme 1-24: Green method of partial reduction of nitroarenes reported by Liu et al.[101]

1.5 Objectives of the Thesis

The aims of this thesis are:

1) To optimize the reaction conditions for controlled/partial hydrogenation of asymmetric salen-type nitro ligands and perform this reaction with highest selectivity in NHOH function.

2) To synthesize metal complexes for studying the interaction of redox-active NHOH function in the vicinity of metal centers.

3) To screen these novel metal complexes for aerobic alcohol oxidation to produce aldehydes under different reaction conditions.

To study the redox-noninnocent behaviour of hydroxylamine function in the vicinity of metal centers, the first step is to partially hydrogenate NO_2 functionality on these asymmetric salen-type chelating ligands to get maximum amount of NHOH function. Two different types of ligands have been employed in this research project based on linker attached to ethylene backbone: imine-based ligands and amine-based ligands. Further modifications on these ligands can change the steric and electronic properties. I reoptimized the hydrogenation conditions to get maximum amount of NHOH-containing ligands. For imine-based ligands, catalytic reduction method is selected which employs Pd/C catalyst poisoned with diphenyl sulfide under H_2 pressure. On the other side, for amine-based ligands stoichiometric reducing agent is used consisting of zinc dust in presence of ammonium formate (NH_4HCO_2). The purity of the hydrogenated ligands can be determined using ^{1}H-NMR.

In the next stage of this project, these hydrogenated ligands were used for complexation with several metal ions, *viz.* copper(II), nickel(II) and zinc(II), to study the behaviour of redox-active NHOH function upon interaction with metal centers. To our surprise, all of these complexes bear an intact NHOH function, which is contrary to the belief that NHOH disproportionates upon interaction with transition metal centers. The NHOH function in these complexes is stabilized by intramolecular hydrogen bonding. All of these complexes are well characterized by single crystal X-ray diffraction and ^{1}H-NMR. Furthermore, disproportionated products of nickel(II) hydroxylamine complexes (L^{I}_{H}-NHOH-Ni and L^{I}_{tBu}-NHOH-Ni) are also presented and characterized by mass spectrometry.

In the third objective, these synthesized complexes were tested for catalytic activity. Based on the assumption that the NHOH/NO shuttle is a two-electron processes, it can catalyze two electrons oxidation reaction such as the oxidation of alcohols to aldehydes. Among the complexes we prepared, only copper-based complexes show promising results for the oxidation of benzyl alcohols and its derivatives with no traces of overoxidized carboxylic acids under different reaction conditions. Yields are determined by gas chromatography using hexamethylbenzene as internal standard. L^{I}_{tBu}-NHOH-Cu shows maximum conversion upto 97% for 3-methoxybenzyl alcohol.

1.6 Organization of the Thesis

Chapter 1 (introductory chapter) discusses the redox noninnocent behaviour of ligands and their complexes with transition metal centers, their applications in coordination chemistry. More precisely, the chemistry of nitrogen-containing functional groups possessing redox-active properties is explored. This chapter also throw a light on various reduction methods for converting nitro to hydroxylamine function and catalytic systems based on transition metals.

Chapter 2 focuses on the approach, design and syntheses of nitro containing asymmetric salen-type ligands, optimization procedures for partial hydrogenation of nitro to hydroxylamine moiety. Both catalytic (Pd/C poisoned with thioether under hydrogen pressure) and stoichiometric (Zn/NH_4HCO_2 mediated transfer hydrogenation) methods are used for reduction purposes.

Chapter 3 highlights the complexation of the ligands with copper(II), nickel(II) and zinc(II) metal ions. The metal complexes are well-characterized by single-crystal X-ray diffraction, ^{1}H-NMR and mass spectrometry.

Chapter 4 presents the screening and the results of using these novel metal complexes in catalysis of aerobic oxidations of alcohols to aldehydes. Copper-based catalysts show promising results specifically for benzylic and its substituted derivatives oxidation.

The final chapters comprise the experimental section, characterization data, conclusions, and future research directions.

Chapter 2: Ligand Design, Approach, Synthesis of Nitro Ligands, and their Optimization for Partial Hydrogenation

2.1 Ligand Design and Approach

Our research group has long had an interest in the chemistry of reactive nitrogen-containing functional groups, especially nitrosoarenes (ArNO)[74,103] and aromatic hydroxylamines (ArNHOH) to understand their redox behaviour in the vicinity of transition metal centers. To serve the purpose, our design is to synthesize asymmetric salen-type ligands having a pendant nitro group, which can be partially hydrogenated to give hydroxylamine-containing coordinating ligands. The synthesis of multidentate salen-type ligands is well-established, facile and quite straightforward.[104,105] Several structural manipulations can be carried out on salen ligand system to tune both steric and electronic properties around the metal center.[106] The N_2O_2 donor sites (N_2: two imine nitrogens, O_2: two deprotonated phenolic oxygens) offer a strong multidentate coordination environment known to form stable complexes with various transition metals.[105,107–112] The first salen-type metal complex was reported by Pfeiffer et al. in 1933.[113]

Herein, we functionalized the ethylenediamine ('en' in salen) backbone to generate asymmetric salen-type ligands bearing one salicylimine ('sal' in salen) moiety and one *ortho*-nitro-containing aromatic moiety (Scheme 2-1). This ligand design can suitably place the nitro group in close proximity to a metal center upon coordination. Also, various substitutions at diamine linkage and aromatic ring can be carried out to produce derivatives of salen ligand system with desirable properties. For instance, substituents at positions 3 and 5 on the salicylimine moiety can enhance the solubility of the ligand and its metal complexes. Furthermore, these substituents can prevent dimerization of the radical state when this aromatic ring is oxidized by one electron to a phenoxyl radical.[114]

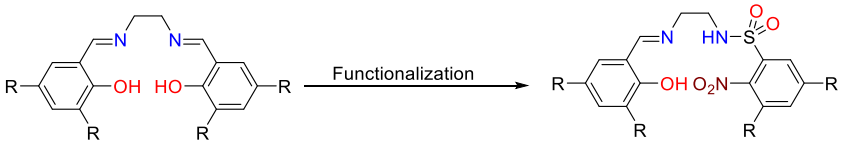

Scheme 2-1: Functionalization of classical salen-type ligand to obtain asymmetric salen-type ligand used in this work.

Past XoRG members had synthesized two different classes of nitro ligands viz: *t*Bu or unsubstituted aromatic derivatives with imine or amine sulfonamide functionalized backbones, giving rise to total of

four ligands (Scheme 2-2). From our previous report[115] on unsubstituted nitro ligands and their complexes, it was found that the pendant nitro group on the ligand remained uncoordinated to various metal centers (Fe(III), Co(II), Cu(II)) upon complexation, which does not give much information about its redox behavior. To have more insight into metal/functional group interaction and understanding redox versatility of nitrogen-containing moieties, the non-coordinating nitro group on the ligands is partially hydrogenated to provide the hydroxylamine analogues.

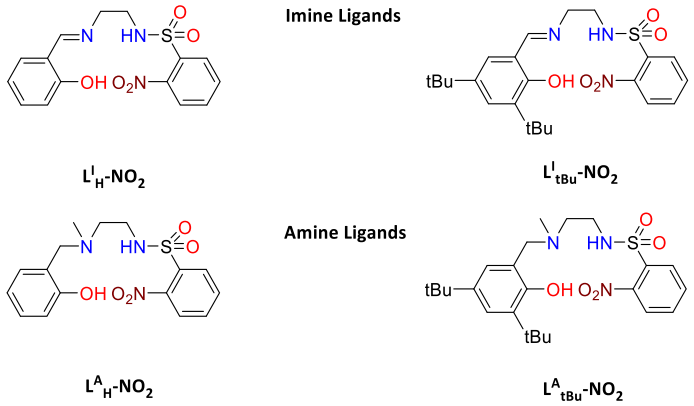

L^{I}_{H}-NO_2 L^{I}_{tBu}-NO_2 L^{A}_{H}-NO_2 L^{A}_{tBu}-NO_2

Scheme 2-2: Representative asymmetric imine and amine-based salen-type tridentate ligands employed in this research.

Our overall approach for this research project is summarize in Scheme 2-3. Although the synthesis of the nitro ligands was done by our previous research group members; Fei Chen, Maëlle Mosser and Nooshin Sheibany, I particularly focused on optimizing the hydrogenation conditions to get exclusively the NHOH function on the ligands. The partial hydrogenation can be done either catalytically or stoichiometrically. Reduction of imine-based ligands (L^{I}_{tBu}-NO_2 and L^{I}_{H}-NO_2) was carried out catalytically, under hydrogen pressure using Pd/C (10 wt.% Pd) catalyst poisoned by thioether to maximize the quantity of NHOH species and prevent its full reduction to NH_2, whereas the reduction of amine-based ligands (L^{A}_{tBu}-NO_2 and L^{A}_{H}-NO_2) was accomplished stoichiometrically *via* transfer hydrogenation employing a Zn/NH_4HCO_2 system.

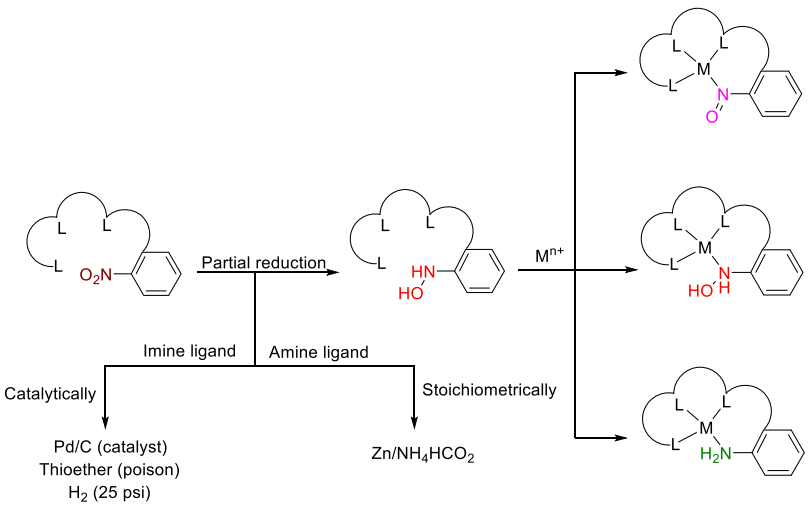

Scheme 2-3: Research approach: methods for partial reduction of nitro ligands and complexation.

2.2 Synthesis of Nitro Ligands

The synthesis of the L^{I}_{R}-NO_2 (R = H or *t*Bu) nitro ligands follows a two-step process.[115] In the first step, the mono-sulfonamide is formed *via* reaction of 2-nitrobenzenesulfonyl chloride with an excess ethylenediamine (en). After evaporation of the volatiles, including en, addition of concentrated hydrochloric acid allows to solubilize L^{I}_{R}-NO_2H^+ while the bis(sulfonamide) by-product is discarded as a precipitate. In the second step, the protonated L^{I}_{R}-NO_2H^+ is condensed with salicylaldehyde or 3,5-di-*tert*-butylsalicylaldehyde to get the L^{I}_{H}-NO_2 and L^{I}_{tBu}-NO_2 ligands in 65% and 81%, respectively (Scheme 2-4).

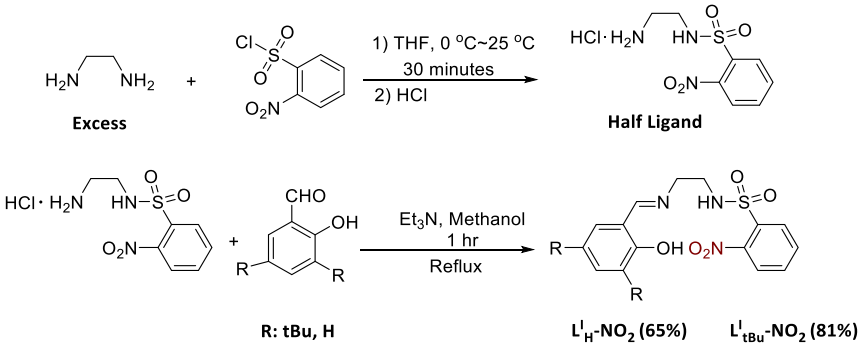

Scheme 2-4: Synthesis of L^{I}_{H}-NO_2 and L^{I}_{tBu}-NO_2 Ligands.

The other two ligands are prepared by reduction of the imine function in L^{I}_{H}-NO_2 and L^{I}_{tBu}-NO_2. L^{A}_{H}-NO_2 is synthesized *via* a one-step, one-pot reductive methylation of L^{I}_{H}-NO_2 in 70% yield (Scheme 2-5a). L^{A}_{tBu}-NO_2 is synthesized in two steps. The imine is first reduced with sodium cyanoborohydride

($NaBH_3CN$) to yield a secondary amine, which is then methylated by reductive amination of formaldehyde to yield L^A_{tBu}-NO_2 in 98% yield (Scheme 2-5b).

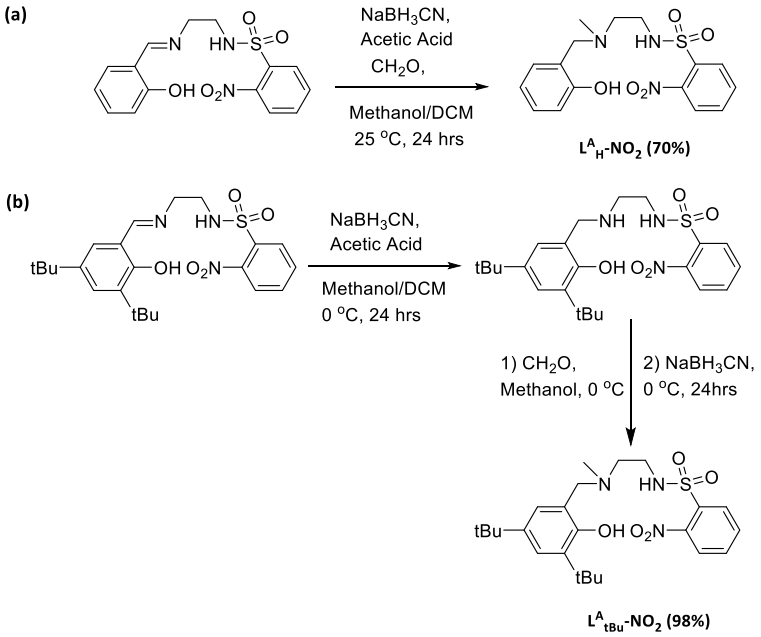

Scheme 2-5: Synthesis of (a) L^A_H-NO_2 and (b) L^A_{tBu}-NO_2.

2.3 Hydrogenation Optimization of Imine-Based Nitro Ligands

Partial hydrogenation of L^I_R-NO_2 was carried out catalytically in a Parr shaker pressure vessel under a 25 psi H_2 pressure using Pd/C (10 wt.% Pd) as catalyst. Due to presence of various reducible groups in the ligand, there is a possibility of mixture of products along with the target NHOH-containing ligand. The other products that can be formed are $H_2L^I_R$-NH_2, a fully reduced compound where both the nitro and the imine functions are reduced, L^I_R-NH_2, where the nitro is fully reduced but the imine is intact, along with some leftover starting material, L^I_R-NO_2 (Scheme 2-6). The separation of the reaction mixture is challenging due to the similar solubility of the products and the fact that they decompose on a chromatography column. Fortunately, the starting material, L^I_R-NO_2, can be easily removed by precipitation in diethyl ether if still present at the end of the reaction. The strategy is thus to operate at incomplete conversion, before any NHOH present is reduced to NH_2. To slow down the formation of the amine, L^I_R-NH_2, from the hydroxylamine intermediate, milder reduction conditions were found by deactivating the catalyst with a poison, diphenyl sulfide (Ph_2S)[116] and reducing the reaction time. The key in the optimization procedure was thus to maximize the amount of L^I_R-NHOH and minimize the amount of L^I_R-NH_2 or $H_2L^I_R$-NH_2 (if present) by careful monitoring by thin-layer chromatography (TLC).

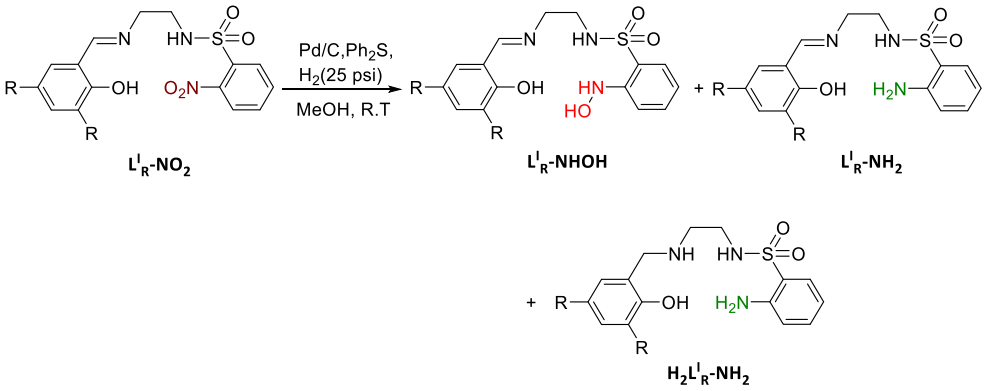

Scheme 2-6: Hydrogenated Products of Imine ligands.

Following the work of former XoRG member Fei Chen, I started to optimize the hydrogenation conditions starting with 2 mol% Pd/C catalyst per substrate, the amount of which remains same throughout different experimental conditions (Table 2-1). Without poison (additive), the ligand is fully reduced to $H_2L^I_R$-NH_2 (entry 1) in 5 h. Decreasing the reaction time while adding up the amount of additive increases the amount of formation of targeted hydroxylamine ligand, L^I_R-NHOH. The best results were obtained with 10 mol% of additive per Pd and for a reaction time of 50 min for H-substituted (entry 7), 1 h for *t*Bu-substituted ligand (entry 8), under 25 psi of hydrogen pressure.

The ratio of the compounds in the reaction mixtures are easily analyzed by ^{1}H-NMR by monitoring the characteristic signals for the CH_2CH_2 backbone for the nitro, hydroxylamine and amine species (in ppm): 3.54/3.73 (L^I_H-NO_2), 3.12/3.55 (L^I_H-NHOH), 3.27/3.58 (L^I_H-NH_2), and 3.53/3.73 (L^I_{tBu}-NO_2), 3.18/3.48 (L^I_{tBu}-NHOH), 3.26/3.59 (L^I_{tBu}-NH_2). This procedure afforded L^I_H-NHOH in 91% yield and 80% purity, the main contaminant being L^I_H-NH_2. The procedure was then adapted on L^I_{tBu}-NO_2 to afford 95% of L^I_{tBu}-NHOH in 84% purity.

Table 2-1: Hydrogenation Optimization[a] of Imine-based Ligands.

				% compounds[b]			
Entry	**R**	**Time (h)**	**Poison (%/Pd)**	**L^{I}_{R}-NO_2**	**L^{I}_{R}-NHOH**	**L^{I}_{R}-NH_2**	**$H_2L^{I}_{R}$-NH_2**
1	H	5	-	-	-	-	100
2	H	2	-	-	-	30	70
3	H	1	-	-	-	45	55
4	H	0.5	-	-	38	62	-
5	H	0.5	5	26	62	12	-
6	H	1	5	20	70	10	-
7	H	0.83	10	16	80	4	-
8	*t*Bu	1	10	13	84	3	-

[a] Pd/C (2 mol% Pd per substrate), Ph_2S (10 mol% per Pd), 25 psi H_2. MeOH, 25°C. [b] Quantities based on ^{1}H-NMR ratios.

2.4 Hydrogenation Optimization of Amine-Based Nitro Ligands

Because of the possible imine reduction with the above ligands, we designed more robust ligands having a tertiary amine linkage in the backbone. The reduction of amine-based ligands (L^{A}_{tBu}-NO_2 and L^{A}_{H}-NO_2) was accomplished *via* transfer hydrogenation employing a Zn/NH_4HCO_2 system. The general reduction procedure involves the addition of ammonium formate dissolved in methanol (1-3 mL) to a vigorously stirring solution of ligand in dichloromethane (2-4 mL). Zinc is then added in portions during reaction (0.5 equiv. zinc powder after every 15 min). After filtering out the reaction mixture, extraction, evaporation and drying, a yellow product was obtained, which was transferred to the glove box to prevent its decomposition. There could be possibility of formation of mixture containing L^{A}_{R}-NHOH and L^{A}_{R}-NH_2 along with some unreacted nitro ligand (Scheme 2-7).

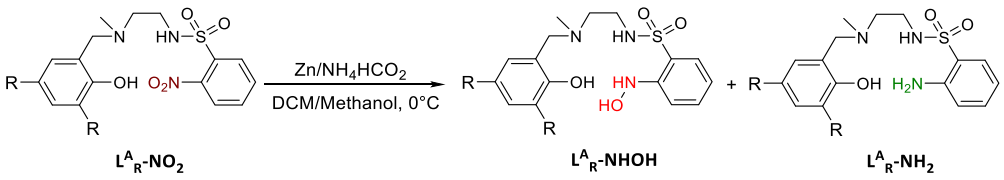

Scheme 2-7: Reduction of Amine Ligands.

The earlier attempts to optimize the hydrogenation conditions for amine-based ligands were made by a former XoRG member, Maëlle Mosser, and recently by Nooshin Sheibany. For L^{A}_{tBu}-NO_2, Mosser got a crude mixture containing 38% L^{A}_{tBu}-NHOH, 3% L^{A}_{tBu}-NH_2 and unconsumed starting material, L^{A}_{tBu}-NO_2 (59%) by employing 16 equiv. of NH_4Cl and 9 equiv. of activated zinc powder in DCM for 22 h at room

temperature, with respect to substrate. The zinc dust was activated by following a literature procedure.[117]

Although the optimization procedures for the hydrogenation of these ligands were previously developed by Nooshin Sheibany, I reoptimized the reduction conditions for better yield and maximum purity for the hydroxylamine ligand (Table 2-2). Starting with 1.6 equiv. of ammonium formate, an amount that remained constant throughout the set of reaction conditions, and 1.2 equiv. of zinc, we obtained L^{A}_{H}-NHOH (29%) in 30 minutes at room temperature with a small amount of fully reduced amine L^{A}_{H}-NH_2 (4%). The major portion in the mixture was left over starting material L^{A}_{H}-NO_2 (67%) (entry 1), which can be recycled. Increasing the reaction time to 1 h did not affect the relative yields of the products (entry 2). The main objective of optimizing the hydrogenation conditions is to procure maximum yield of hydroxylamine ligand, L^{A}_{R}-NHOH with highest purity by stopping the reaction after the complete consumption of starting material and before the formation of completely reduced amine ligand, L^{A}_{R}-NH_2. At first, to prevent over-reduction of hydroxylamine to amine, the reaction is performed at 0°C, which had the significant effect in the less production of amine derivative, L^{A}_{H}-NH_2. At the same time, the amount of zinc is increased to maximize the yield of hydroxylamine ligand. The progress of the reaction was monitored by TLC every 15 min, which clearly indicates the disappearance of nitro ligand at the best reduction conditions. Also, the amount of solvent is increased for more vigorous stirring and for better accumulation of zinc powder in the reaction mixture rather than sticking to the walls of the reaction pot. The best results were obtained by using 5 equiv. of zinc with a reaction time of 2.5 h. at 0°C for the reduction of L^{A}_{H}-NO_2 (entry 6). For the reduction of L^{A}_{tBu}-NO_2, 6 equiv. of zinc were used to afford the L^{A}_{H}-NHOH in 3.5 h (entry 8). This extra equivalent is used to compensate for the steric hinderance imparted by *tert*-butyl substituents. The ratio of the compounds in the mixtures was assessed by ^{1}H-NMR by analyzing the characteristic ethylene backbone signals which are at (in ppm): 2.67/3.28 (L^{A}_{H}-NO_2), 2.58/3.10 (L^{A}_{H}-NHOH), 2.73/3.06 (L^{A}_{H}-NH_2), and 2.66/3.27 (L^{A}_{tBu}-NO_2), 2.58/3.09 (L^{A}_{tBu}-NHOH), and 2.70/3.06 (L^{A}_{tBu}-NH_2). This procedure afforded L^{A}_{H}-NHOH in 85% yield and 98% purity and L^{A}_{tBu}-NHOH in 67% yield and 98% purity.

Table 2-2: Hydrogenation Optimization of Amine-based Ligands

							% compounds[a]		
Entry	**R**	**Time (h)**	**DCM (mL)**	**MeOH (mL)**	**NH_4HCO_2 (eq.)**	**Zn (eq.)**	**L^A_R-NO_2**	**L^A_R-NHOH**	**L^A_R-NH_2**
1[b]	H	0.5	2	1	1.6	1.2	67	29	4
2[b]	H	1	2	1	1.6	1.2	65	30	5
3	H	2	2	1	1.6	2	45	55	0
4	H	3	2	1	1.6	5	0	95	5
5	H	3	4	3	1.6	5	0	96	4
6	H	2.5	4	3	1.6	5	0	98	2
7	t-Bu	3.5	4	3	1.6	5	20	80	0
8	t-Bu	3.5	4	3	1.6	6	0	98	2

[a] Quantities based on ^{1}H-NMR ratios. [b] Reactions were carried out at room temperature.

2.5 Conclusion

In brief, to study the redox behavior of nitrogen-containing functional group near a metal center, salen-type ligands with a pendant nitro group were synthesized. Hydrogenation conditions were optimized to obtain the hydroxylamine function in the ligands with as much purity and yield as possible. For imine-based ligands (L^I_H-NO_2 and L^I_{tBu}-NO_2), the hydrogenation was carried out catalytically using Pd/C catalyst poisoned by diphenyl sulfide. The best hydrogenation conditions were achieved by using 2 mol% of catalyst w.r.t substrate and 10 mol% poison per Pd, under 25 psi hydrogen pressure, which afforded L^I_H-NHOH and L^I_{tBu}-NHOH ligands in 80% and 84% purity, respectively. On the other side, the partial reduction of the amine-based ligands (L^A_H-NO_2 and L^A_{tBu}-NO_2) was accomplished by using stoichiometric amount of zinc and ammonium formate *via* transfer hydrogenation. The optimized conditions afforded 98% pure L^A_R-NHOH (R= H, tBu) ligands in high yield up to 85%, using 5 equiv. of zinc (6 equiv. of zinc for L^A_{tBu}-NO_2) and 1.6 equiv. of ammonium formate at 0°C in DCM and methanol. The latter method proved to be more successful as it provides milder reaction conditions to get better yield and more pure hydroxylamine ligands.

Chapter 3: Synthesis of Transition Metal Complexes Supported by Hydroxylamine Containing Salen-Type Ligands

3.1 Previous Work on Complexes Derived from Nitro and Hydroxylamine Ligands

As reported by our past group member Fei Chen, the pendant nitro group remains uncoordinated upon complexation of ligand L^{I}_{H}-NO_2 with Fe(III), Co(II) and Cu(II) (Scheme 3-1).[115]

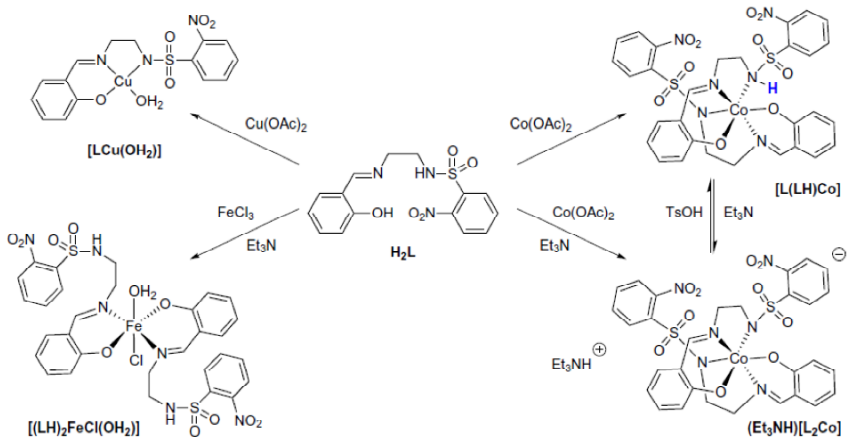

Scheme 3-1: Complexation of L^{I}_{H}-NO_2 with Fe(III), Co(II), Cu(II) having uncoordinated NO_2 group .[115]

Our former group member Maryam Habibian had previously studied the coordination behaviour of a NHOH-containing ligand, L_{py2}-NHOH, with a bis(2-picolyl)amine moiety in place of the salicylimine moiety in our L^{I}_{R}-NHOH ligands. She found that, upon reaction with Fe(II), the hydroxylamine function disproportionated to form nitroso (NO) and amine (NH_2) metal complexes, which were isolated and crystallographically characterized (Scheme 3-2).[118]

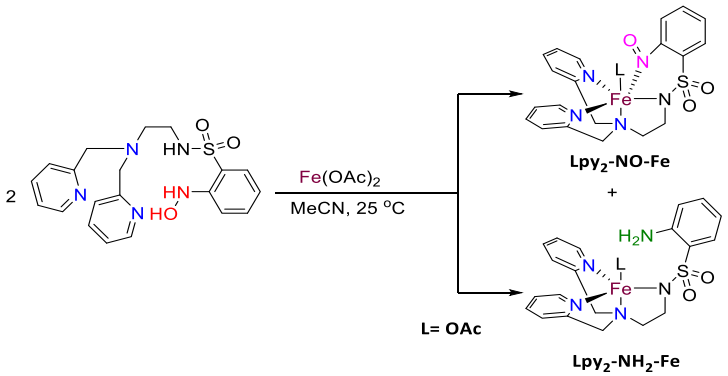

Scheme 3-2: Disproportionation of NHOH function upon complexation with Fe(II) to form nitroso (NO) and amine (NH_2) complexes.[118]

Using the same ligand, Nooshin Sheibany used copper salts and reported two different reaction outcomes (Scheme 3-3): (1) Upon reaction with Cu(I), the hydroxylamine function disproportionated to nitroso (formally) and amine species. (2) Upon reaction with Cu(II), however, the NHOH function only oxidized to the NO function, with negligible amounts of the NH_2 species.[119] X-ray studies of the (L_{py2}-NO)Cu complex were consistent with a copper in a +2 oxidation state and a NO function reduced by one electron to an aminoxyl anion (C–$NO^{\bullet-}$) based on the reduced N–O bond length compared with neutral nitroso moiety. This indicates that the reactive hydroxylamine function can show different reactivities depending on the metal ion it reacts with, as well as the coordination environment (reaction conditions, ligand scaffold and charge). It gives us an urge to study the redox behaviour of the NHOH moiety on the salen-type ligands when coordinating transition metal centers.

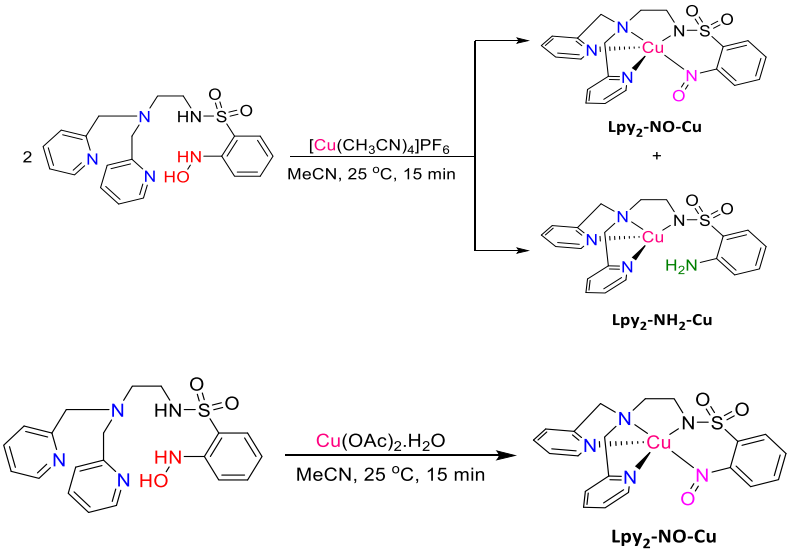

Scheme 3-3: Top: Direct oxidation of NHOH to NO upon complexation with Cu(II). Bottom: Disproportionation of NHOH function to form nitroso (NO) and amine (NH_2) complexes upon coordination with Cu(I).[119]

XoRG members Joseph Zsombor-Pindera, Farshid Effaty et al.[120] recently reported a novel copper(I)-arylhydroxylamine complex in which the weakly bounded hydroxylamine function is stabilized by intramolecular hydrogen bond between OH and Cl atom, as established by X-ray crystallography. Two-electron oxidation of this complex with diethyl azodicarboxylate (DEAD) affords a copper(II)-(arylnitrosyl radical) complex in which the arylnitroso is hemilabile (Scheme 3-4). To the best of our knowledge, this compound is the first reported, crystallographically characterized aromatic hydroxylamine complex of a transition metal.

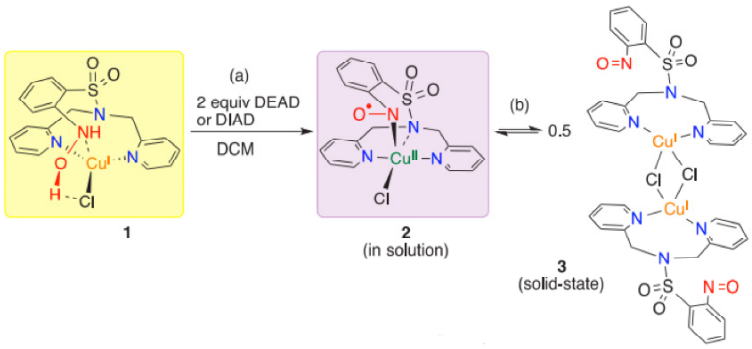

Scheme 3-4: Cu(I)-arylhydroxylamine complex and its oxidized products (adapted from reference 120).[120]

To have insight into possible behaviours of the NHOH function in the L^{I}_{R}-NHOH ligands, we decided to employ different divalent metal ions, *viz*.: copper(II), nickel(II) and zinc(II). In particular, Zn(II) is not redox-active and Its reactions will serve as a baseline to compare the other reactions to. The general procedure for complexation involves the dropwise addition of acetonitrile (ACN) solution of the hydroxylamine ligand onto a vigorously stirring ACN solution of metal acetate or nitrate salt (Scheme 3-5). The addition of 2 equivalents of base (acetate from the metal salt or added triethylamine) is required to deprotonate sulfonamide and phenolic protons. Following this procedure, we were able to isolate well-defined complexes from the dark, coloured solutions formed with the imine ligands (L^{I}_{H}-NHOH and L^{I}_{tBu}-NHOH), but not with the amine ligands (L^{A}_{H}-NHOH and L^{A}_{tBu}-NHOH). To our surprise, all the metal complexes we obtained bear an intact hydroxylamine function and no NHOH disproportionation was observed.

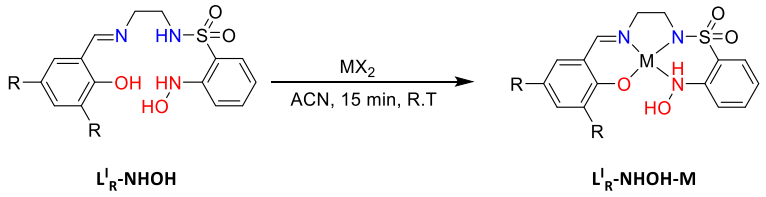

L^{I}_{R}-NHOH

L^{I}_{R}-NHOH-M

R= tBu, H; M= Cu(II), Ni(II), Zn(II); X= OAc^-, NO_3^-
2 eqvs. Et_3N in Zn(II) complexation

Scheme 3-5: General scheme for the complexation of Imine NHOH (L^{I}_{R}-NHOH) ligands with Cu(II), Ni(II) and Zn(II).

3.2 Complexation of L^{I}_{R}-NHOH Ligands with Cu(II)

Contrary to the disproportionation of NHOH function in PhNHOH by Cu(II), which had been reported in the literature,[84] Fei Chen had synthesized the Cu(II) complex with L^{I}_{tBu}-NHOH in which the hydroxylamine function remains intact upon coordination.[121] It was synthesized by reacting copper(II)

acetate [$Cu(OAc)_2.H_2O$] with L^{I}_{tBu}-NHOH solutions in ACN which afforded a purple precipitate. Crystals of the complex were grown by placing a small portion of Cu(II) acetate in a vial and then layering it with L^{I}_{tBu}-NHOH dissolved in acetonitrile inside an inert atmosphere of glovebox. Keeping the mixture in the –30°C freezer for 3 days afforded purple crystals suitable for X-ray diffraction analysis. The complex showed a well-defined 1:1 metal to ligand stoichiometry as determined by its solid-state structure (Figure 3-1). The copper center is in a square-pyramidal geometry where the equatorial positions are occupied by the phenolate, imine, sulfonamidate and the nitrogen of the hydroxylamine, and the apical position is occupied by the sulfonamide oxygen atom from a neighbour molecule. The +2 oxidation state of copper center is confirmed by the Cu–N bond lengths which are in the range of 1.923(2)-2.055(2) Å similar to those reported in similar type of compounds.[122] The $Cu–N3_{imine}$ bond (1.923(2) Å) is shorter than the $Cu–N2_{sulfonamide}$ bond (2.001(2) Å) as the electron density on the amide nitrogen is decreased due to electron withdrawing nature of $–SO_2R$ group. This indicates strong coordination of the imine nitrogen. Also, the retention of the NHOH group upon coordination is further supported by N–O bond length in the copper complex (1.428(3) Å), which is the typical value for single N–O bond.[123] Two absorption bands were observed in its UV-Vis spectrum at 510 nm (338 M^{-1} cm^{-1}) and 627 nm (150 M^{-1} cm^{-1}) (Figure 6-15). The unusual stability of arylhydroxylamine moiety is due to intramolecular hydrogen bond between the OH of NHOH and the O atom of phenolate. This hydrogen bonding is a characteristic property of all NHOH complexes synthesized in this work.

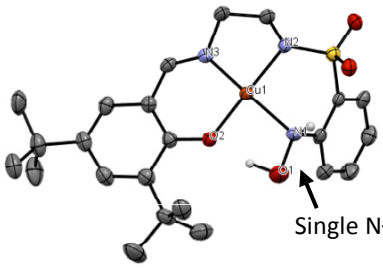

Figure 3-1: ORTEP representation of L^{I}_{tBu}-NHOH-Cu at 50% ellipsoid probability. Hydrogen atoms were omitted for clarity, except for NHOH ones. Selected bond lengths (Å) and angles (°): Cu1–N1, 2.055(2); Cu1–N2, 2.001(2); Cu1–N3, 1.923(2); Cu1–O2, 1.915(2); O1–N1, 1.428(3); O2–Cu1–N3, 93.28(9); N3–Cu1–N2, 84.27(10); O2–Cu1–N1, 87.95(9); N2–Cu1–N1, 92.85(9).

The L^{I}_{H}-NHOH-Cu complex was synthesized by the same procedure as for L^{I}_{tBu}-NHOH-Cu, which afforded green precipitates in 58% yield. Crystals suitable for X-ray measurements were obtained by subjecting a small portion of the complex dissolved in DCM to slow vapour diffusion of pentane at room

temperature. L^{I}_{H}-NHOH-Cu also crystallizes with Cu(II) adopting square-pyramidal geometry (Figure 3-2a). The NHOH function is intact with an N–O bond length of 1.423(3) Å, a typical value for single N–O bond.[123] The copper(II) center exhibits similar coordination features as in L^{I}_{tBu}-NHOH-Cu. The dihedral angles between the opposite planes N3–Cu1–O2 and N2–Cu1–N1 in L^{I}_{tBu}-NHOH-Cu and L^{I}_{H}-NHOH-Cu complexes are found to be 19° and 16.2°, which represents small tetrahedral distortions at the metal centers. Figure 3-2b represents the dimeric unit of the complex to show the coordination of O of SO_2 to metal center in a apical position of the geometry. From UV-Vis spectroscopy, it was observed that the complex exhibits a more intense band at 524 nm (231 M^{-1} cm^{-1}) and less intense band at 647 nm (104 M^{-1} cm^{-1}) compared with L^{I}_{tBu}-NHOH-Cu (Figure 6-15).

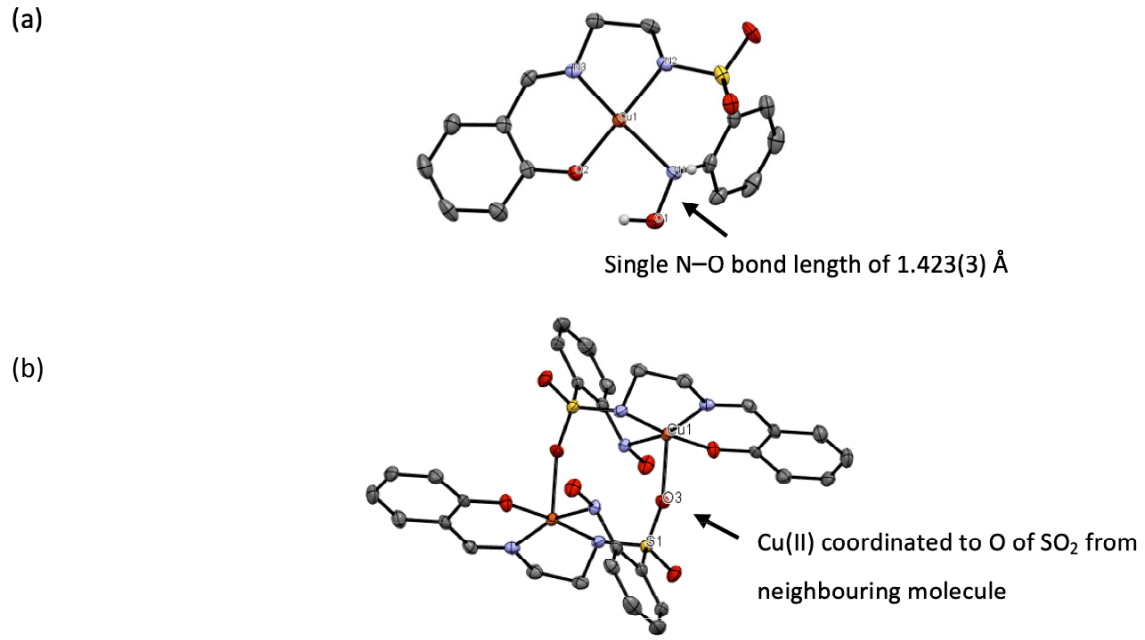

Figure 3-2: ORTEP representation of L^{I}_{H}-NHOH-Cu (a) at 50% ellipsoid probability. Hydrogen atoms, except those on the hydroxylamine, were omitted for clarity. Selected bond lengths (Å) and angles (°): Cu1–N1, 2.069(2); Cu1–N2, 1.987(2); Cu1–N3, 1.939(2); Cu1–O2, 1.914(2); O1–N1, 1.423(3); N3–Cu–N2, 84.44(9); O2–Cu–N1, 86.35(8); N2–Cu–N1, 94.67(9); O2–Cu1–N3, 92.89(9). (b) Coordination of Cu(II) with O of SO_2 of the neighbour complex.

3.3 Complexation of L^{I}_{R}-NHOH Ligands with Ni(II)

As Cu(II) complexes are paramagnetic, ^{1}H-NMR cannot be used to confirm the presence of the hydrogens on the hydroxylamine function. Therefore, we synthesized diamagnetic analogues with Ni(II) and Zn(II) metal centers. These complexes also show 1:1 metal-to-ligand stoichiometry in their solid-state structures. L^{I}_{tBu}-NHOH-Ni and L^{I}_{H}-NHOH-Ni complexes were synthesized by reacting nickel(II)

nitrate and L^{I}_{tBu}-NHOH and L^{I}_{H}-NHOH ligand solutions in acetonitrile in 72 and 74% yields, respectively. Crystallization by slow diffusion of pentane to the solution of complex in DCM at room temperature afforded green crystals suitable for X-ray diffraction analysis. In both the cases, the Ni(II) ion lies in a square-planar geometry with a ligand:metal ratio of 1:1 (Figure 3-3a, b). The dihedral angle between the two opposite N–Ni–O planes are 8.2° in L^{I}_{tBu}-NHOH-Ni and 4.4° in L^{I}_{H}-NHOH-Ni complexes, indicating small tetrahedral distortions consistent with reported values for similar nickel(II) complexes.[124,125] The crystal structure of these complexes showed an intact NHOH function with N–O bond lengths of 1.420(5) and 1.429(4) Å in L^{I}_{tBu}-NHOH-Ni and L^{I}_{H}-NHOH-Ni, respectively. These bond lengths are the typical values for single N–O bond.[123]

(a)

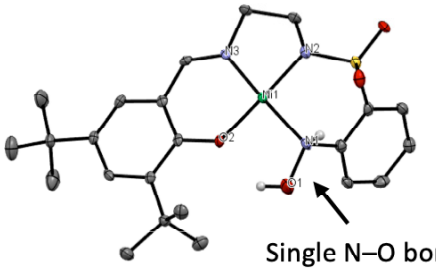

Single N–O bond length of 1.429(4) Å

(b)

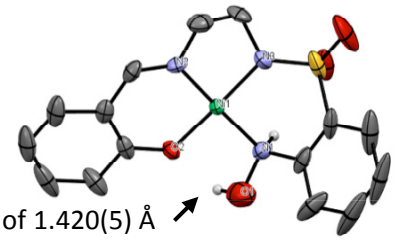

Single N–O bond length of 1.420(5) Å

Figure 3-3: ORTEP representations of (a) L^{I}_{tBu}-NHOH-Ni and (b) L^{I}_{H}-NHOH-Ni at 50% ellipsoid probability. Hydrogen atoms, except those on the hydroxylamine, were omitted for clarity. Selected bond lengths (Å) and angles (°) for (a): Ni1–N1, 1.974(4); Ni1–N2, 1.898(4); Ni1–N3, 1.839(3); Ni1–O2, 1.847(4); N1–O1, 1.420(5); O2–Ni–N3, 94.8(1); N3–Ni1–N2, 84.7(2); O2–Ni1–N1, 87.8(2); N2–Ni1–N1, 93.1(2); O2–Ni1–N2, 177.2(2); for (b) Ni1–N1, 1.958(3); Ni1–N2, 1.856(3); Ni1–N3, 1.881(3); Ni1–O2, 1.829(2); N1–O1, 1.429(4); O2–Ni1–N3, 177.8(1); N3–Ni1–N2, 84.4(1); O2–Ni1–N1, 86.9(1); N2–Ni1–N1, 175.6(1); O2–Ni1–N2, 95.2(1).

The presence of hydroxylamine hydrogen atoms in diamagnetic L^{I}_{tBu}-NHOH-Ni and L^{I}_{H}-NHOH-Ni complexes is supported by ^{1}H-NMR, which shows peaks at 8.66, 8.55 ppm and 8.89, 8.44 ppm for OH, NH protons in the respective complexes (Figure 3-4). The disappearance of protons of phenolic and sulfonamide groups in ^{1}H-NMR spectrum further supports that these groups are deprotonated and coordinated to the Ni(II) center.

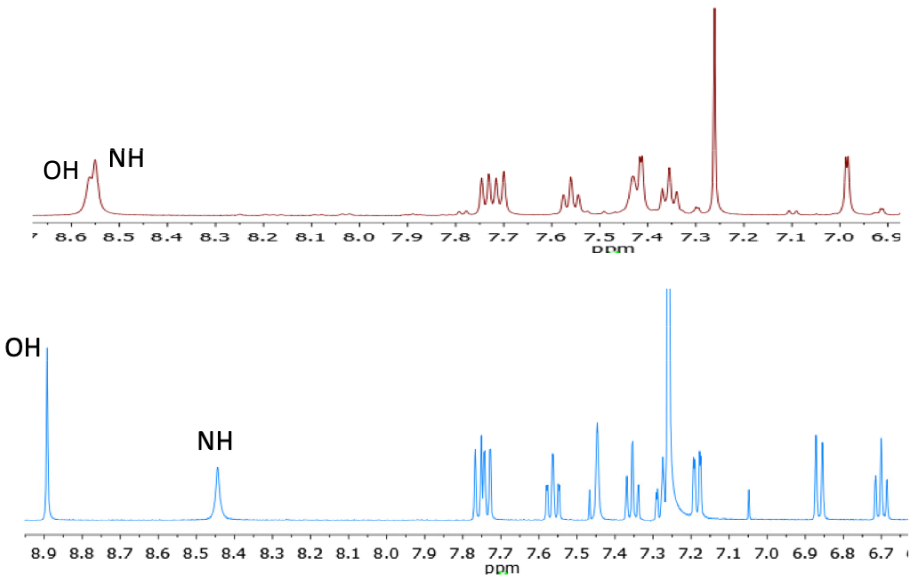

Figure 3-4: ^{1}H-NMR spectra of L^{I}_{tBu}-NHOH-Ni (top) and L^{I}_{H}-NHOH-Ni(II) (bottom) complexes in $CDCl_3$ at 25°C.

The diamagnetic low-spin configuration of Ni(II) in both complexes is also supported by the coordination bond lengths in L^{I}_{tBu}-NHOH-Ni: Ni1–$N3_{imine}$ (1.839(3) Å), Ni1–$O2_{phenolate}$ (1.847(4) Å), Ni1–$N2_{sulfonamide}$ (1.898(4) Å) and L^{I}_{H}-NHOH-Ni: Ni1–$N2_{imine}$ (1.856(3) Å), Ni1–$O2_{phenolate}$ (1.829(4) Å), Ni1–$N2_{sulfonamide}$ (1.881(4) Å), Ni1–$N1_{NHOH}$ (1.958(4) Å). These values are consistent with the values expected for similar type of Ni(II) square planar complexes.[125–127] However, the Ni–N_{NHOH} bond lengths, 1.974(4) Å (L^{I}_{tBu}-NHOH-Ni), 1.958(4) Å (L^{I}_{H}-NHOH-Ni), are longer than the other values. The UV-Vis spectra of the complexes show two absorption bands at 405 nm (2433 M^{-1} cm^{-1}) and 581 nm (186 M^{-1} cm^{-1}) for L^{I}_{H}-NHOH-Ni, and 409 nm (2079 M^{-1} cm^{-1}) and 591 nm (198 M^{-1} cm^{-1}) for L^{I}_{tBu}-NHOH-Ni (Figure 6-14).

3.4 Disproportionation of L^{I}_{R}-NHOH-Ni Complexes

Although the Ni(II) hydroxylamine complexes are stable at room temperature, refluxing in acetonitrile at 80°C for 1 h leads to disproportionation of NHOH to form NO and NH_2 moieties (Scheme 3-6).

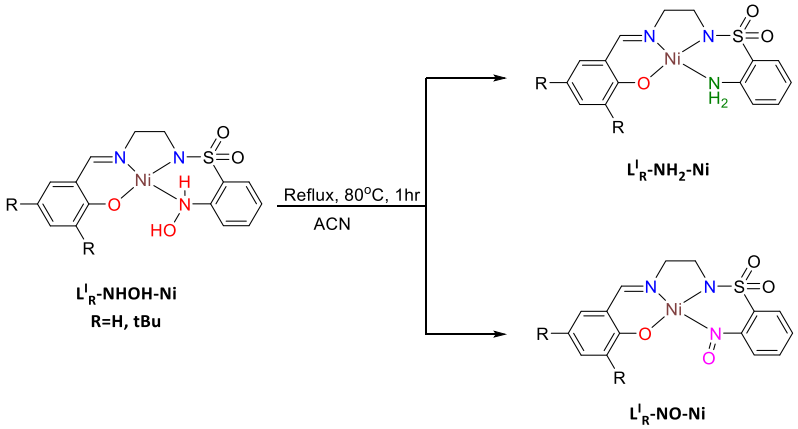

Scheme 3-6: Disproportionation of nickel(II) hydroxylamine complex to produce amine and nitroso derivatives.

When the acetonitrile solution of L^{I}_{tBu}-NHOH-Ni is refluxed, it resulted in colour change from green to dark purple after 1 h. (Figure 3-5a). The products were characterized by ESI-MS which showed peaks for m/z = 488.162, $[M+H]^+$ of L^{I}_{tBu}-NH_2-Ni and 502.151, $[M+H]^+$ of L^{I}_{tBu}-NO-Ni with expected isotopic pattern for $^{58/60}$Ni (Figure 3-5b). Unfortunately, we were unable to grow good quality crystals suitable for X-ray crystallography.

(a)

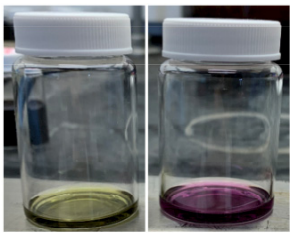

(b)

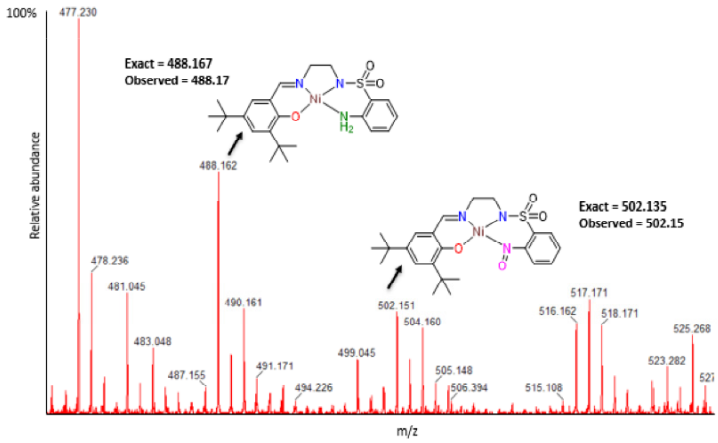

Figure 3-5: (a) Colour change observed after refluxing L^{I}_{tBu}-NHOH-Ni solution in acetonitrile; left (before reflux), right (after reflux), (b) Positive mode ESI-MS of [L^{I}_{tBu}-NHOH-Ni] after 1 h refluxing showing the disproportionated products.

For L^{I}_{H}-NHOH-Ni, the disproportionation was also observed with a change in colour from green to dark red after refluxing for 1 h. (Figure 3-6).

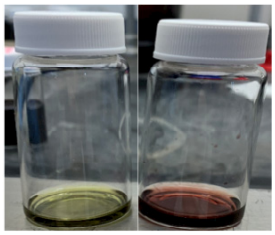

Figure 3-6: Colour change observed after refluxing L^{I}_{H}-NHOH-Ni solution in acetonitrile; left (before reflux), right (after reflux).

Crystals were grown by diffusing excess of pentane into the complex solution in dichloromethane at room temperature. Two types of crystals were obtained in a single vial based on their colours. The light orange crystals are of diamagnetic NH_2 complex (Figure 3-7). There were very small deep-red crystals, which we were expecting to be the nitroso species, but they did not diffract. The L^{I}_{H}-NH_2-Ni complex shows a Ni(II) center in a square-planar geometry. The dihedral angle between the two opposite N–Ni–O planes, 2.3°, indicates that Ni(II) ion sits within a near-perfect square-planar geometry. All the selected bond lengths shown in Figure 3-8 were in the same range as in L^{I}_{tBu}-NHOH-Ni and L^{I}_{H}-NHOH-Ni complexes.

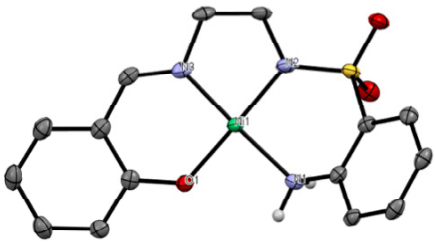

Figure 3-7: ORTEP representation of one independent molecule of L^{I}_{H}-NH_2-Ni at 50% ellipsoid probability. Hydrogen atoms, except those on the amine were omitted for clarity. Selected bond lengths (Å) and angles (°): Ni1–O1, 1.853(2); Ni1–N1, 1.964(3); Ni1–N2, 1.885(3); Ni1–N3; 1.847(3), N3–Ni1–N2, 84.5(1); O1–Ni1–N1, 87.5(1); N3–Ni1–O1, 94.6(1); N2–Ni1–N1, 93.5(1).

The presence of the amino group is further confirmed by ^{1}H-NMR, with the disappearance of the NH and OH protons of L^{I}_{H}-NHOH and formation of the NH_2 signal around 4.3 ppm in L^{I}_{H}-NH_2-Ni (Figure 3-8).

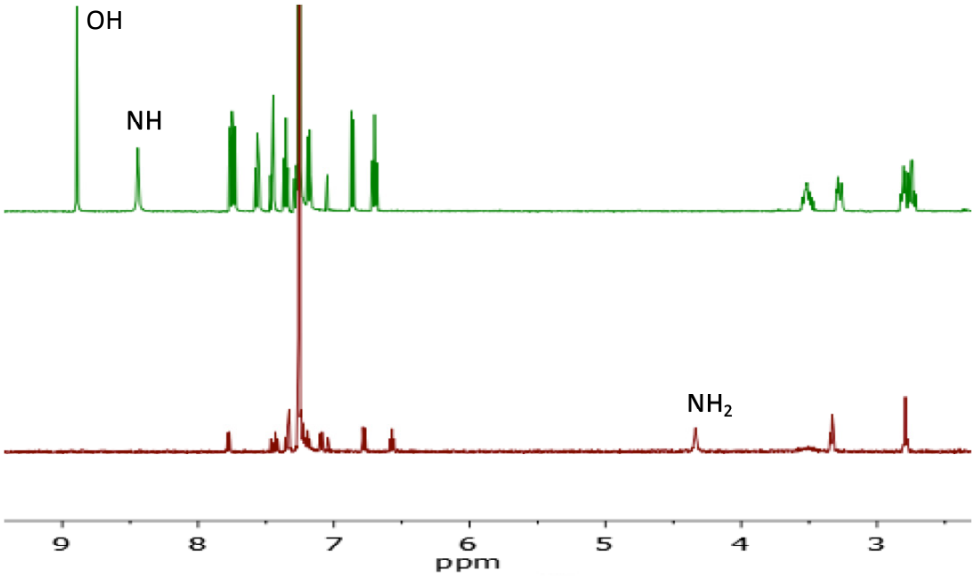

Figure 3-8: Comparison of the ^{1}H-NMR spectra of L^{I}_{H}-NHOH-Ni (top) and L^{I}_{H}-NH_2-Ni (bottom) in $CDCl_3$ at 25°C.

3.5 Zn(II) Complexes with L^{I}_{R}-NHOH Ligands

L^{I}_{tBu}-NHOH-Zn and L^{I}_{H}-NHOH-Zn complexes were synthesized by adding a Zn(II) nitrate solution in acetonitrile to a vigorously stirring corresponding ligands solutions in acetonitrile. To this mixture, two equiv. of triethylamine (Et_3N) were also added to deprotonate NH of sulfonamide and OH of phenolic groups. The reactions yield white solids in 61% and 55%, respectively. Colourless crystals were grown by slow layered diffusion of pentane into a dichloromethane solution of the complex at room temperature.

The L^{I}_{H}-NHOH-Zn complex is isostructural with L^{I}_{H}-NHOH-Ni (Figure 3-9a). The metal center adopts a square-planar geometry. The small 6° tetragonal distortion between the two opposite N–Zn–O planes shows that the Zn(II) ion fits well within the square-planar geometry. The N–O bond length of 1.42(1) Å is consistent with single N–O bond character in this intact NHOH group. The ^{1}H-NMR spectrum of the complex (Figure 3-9b) indicates the disappearance of phenolic and sulfonamide protons (at 8.22 ppm and 7.89 ppm in L^{I}_{H}-NHOH) and a shift in the imine proton from 8.41 ppm in ligand to 8.29 ppm in the complex, suggesting that the imine group binds to the metal center as well. Aromatic and methylene protons also show slight chemical shifts upon complexation. For example, the methylene protons, originally at 3.06 and 3.57 ppm in the ligand, are shifted to 2.77 and 3.46 ppm in the complex. Furthermore, NH and OH protons on hydroxylamine group in the complex resonate at 9.57 and 8.71 ppm in the complex, compared with 13.14 and 8.92 ppm in the ligand, respectively.

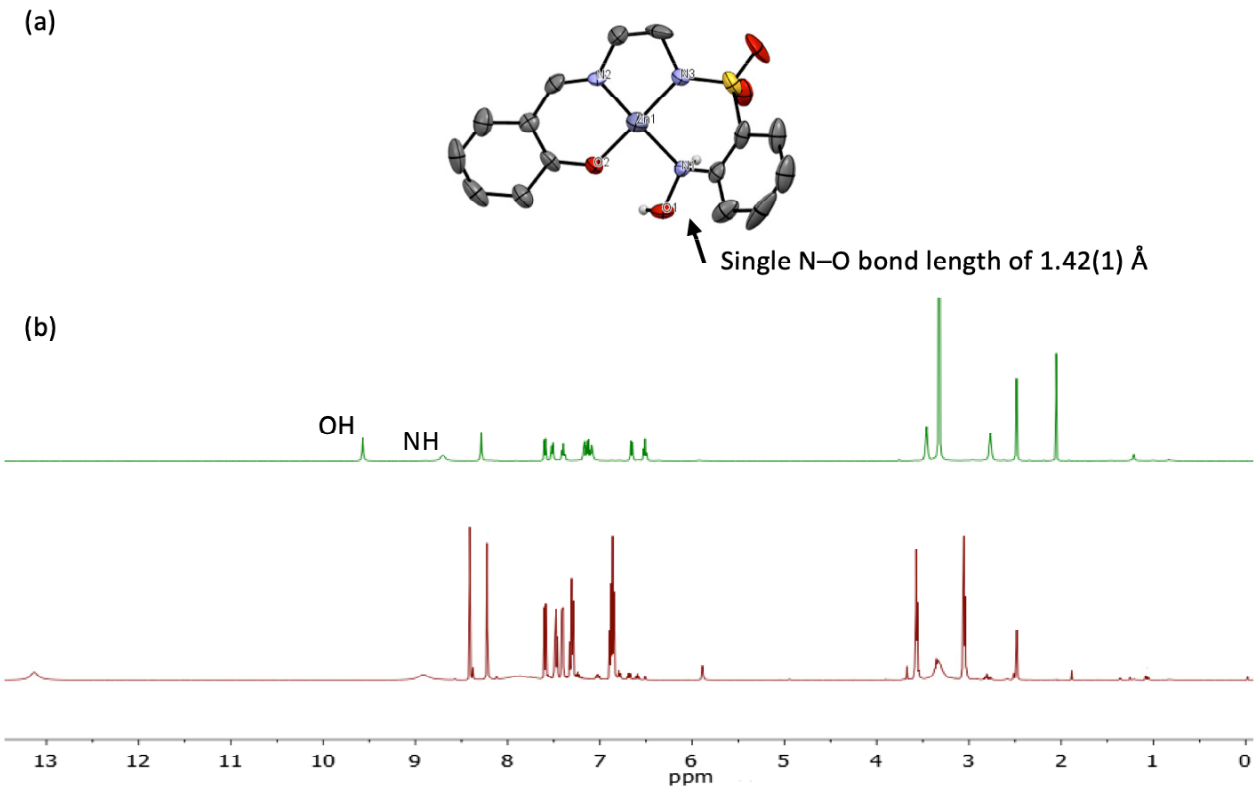

Figure 3-9: (a) ORTEP representation of L^{I}_{H}-NHOH-Zn at 50% ellipsoid probability. Hydrogen atoms were omitted for clarity, except for NHOH ones. Selected bond lengths (Å) and angles (°): Zn1–N1, 1.978(8); Zn1–N2, 1.865(9); Zn1–N3, 1.88(1); Zn1–O2, 1.840(8); N1–O1, 1.42(1); O2–Zn1–N3, 177.6(4); N3–Zn1–N2, 85.0(4); O2–Zn1–N1, 87.0(3); N2–Zn1–N1, 175.1(4); O2–Zn1–N2, 94.8(4).(b) Comparison of the ^{1}H-NMR spectra of ligand L^{I}_{H}-NHOH (bottom) and the L^{I}_{H}-NHOH-Zn complex (top) in DMSO-d_6 at 25°C.

The other Zn complex, L^{I}_{tBu}-NHOH-Zn, dimerizes in the solid state, with each Zn(II) in a trigonal-bipyramidal (TBP) environment (Figure 3-10). The distortion from the ideal geometries for the five coordinated complexes (square-pyramidal or trigonal-bipyramidal) can be estimated in terms of structural index parameter, called as geometric parameter (τ_5). [128] The value of τ_5 is zero for a perfectly square-pyramidal geometry whereas it is 1 for an ideal TBP geometry. In this dimer, the degrees of trigonality for Zn1 and Zn2 were found to be 0.841 and 0.805, respectively. These values indicate that both the metal centers are in a TBP geometry. The complex dimerizes through the coordination of N-atom of the sulfonamide group of each ligand to the Zn(II) center of the other unit. The dimer is based on two identical coordination bonds forming a Zn–N–Zn–N square. Therefore, the nitrogen of the sulfonamide group of each ligand forms a bridge between two Zn centers. Due to dimerization, significant changes in the Zn–$N_{sulfonamide}$ bond lengths can be observed within each monomer unit. For

instance, in zinc dimer, the Zn1–N4$_{sulfonamide}$ and Zn2–N6$_{sulfonamide}$ distances are 2.349(5) and 2.312(5) Å, respectively whereas in L^{I}_{H}-NHOH-Zn monomer, Zn1–N3$_{sulfonamide}$ is 1.88(1) Å. So, the Zn–N$_{sulfonamide}$ bond length increases upon coordination. The Zn1···Zn2 distance (3.082 Å) can be considered in the usual range reported in similar type of Zn(II) complexes.[129,130] The anti-parallel orientation of the two ligands minimizes the steric repulsion between the two *t*Bu groups of the individual units by forcing them to point away from each other in the adjacent molecules. Also, the coplanarity of the complex is not retained after the coordination, as can be clearly seen in Figure 3-6. There are multiple hydrogen bonds which can be seen between the OH of NHOH and O of the phenolate as well as the NH of NHOH and the O of SO_2. The N–O bond length in the related Ni(II) complex is found to be 1.420(5) Å whereas it is 1.421(6) and 1.425(7) Å in NHOH fragments of Zn dimer. These NO bond lengths confirm the presence of single N–O bonds.[123]

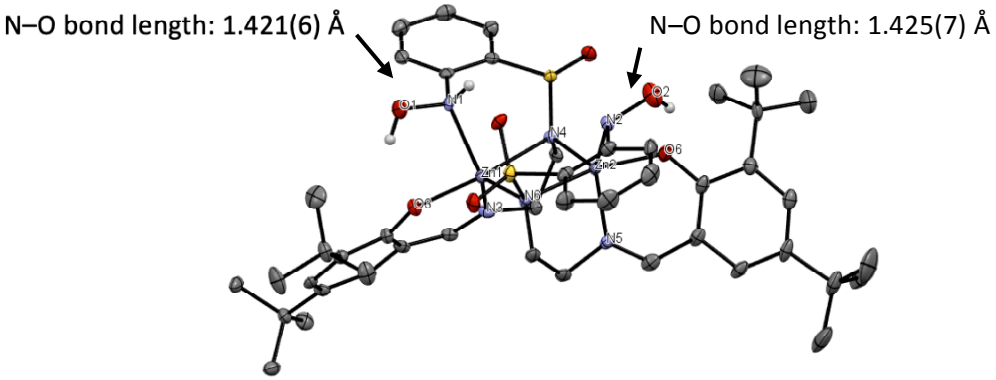

Figure 3-10: ORTEP representation of L^{I}_{tBu}-NHOH-Zn dimer. Thermal ellipsoids are drawn at 50% probability. Hydrogen atoms, except those on the hydroxylamine, were omitted for clarity. Selected bond lengths (Å) and angles (°): Zn1–O3, 1.993(4); Zn1–O1, 2.141(4); Zn1–N3, 1.989(4); Zn1–N4, 2.349(5); Zn1–N6, 2.045(3); Zn2–O6, 1.994(4); Zn2–N2, 2.144(4); Zn–N4, 2.041(3); Zn2–N5, 2.005(4); N1–O1, 1.421(6); N2–O2, 1.425(7); N4–Zn1–N1, 86.8(1); N6–Zn1–N3, 120.2(2); N3–Zn1–O3, 92.1(2); N5–Zn2–O6, 91.4(1); N5–Zn2–N6, 79.2(1); N4–Zn2–N6, 89.6(1).

3.6 Conclusion

In this project, we were successful at using imine ligands (L^{I}_{H}-NHOH and L^{I}_{tBu}-NHOH) to obtain well-defined complexes with different metal centers, whereas the amine ligands (L^{A}_{H}-NHOH and L^{A}_{tBu}-NHOH) led to darkly coloured solutions from which we were unable to isolate pure metal complexes. The obtained complexes were well characterized by single crystal X-ray diffraction analysis, ^{1}H-NMR and mass spectrometry. The Cu(II) and Ni(II) adopt square-pyramidal and square-planar geometry, respectively. On the other side, Zn(II) exhibits square-planar geometry in L^{I}_{H}-NHOH-Zn and TBP geometry

(TBP) in zinc(II) dimer L^{I}_{tBu}-NHOH-Zn. All these novel salen-type metal complexes with Cu(II), Ni(II) and Zn(II) are bearing an intact hydroxylamine group. Hence, contrary to our original assumption, the hydroxylamine group present in the ligands do not disproportionate upon coordination. We hypothesize that the presence of and intramolecular hydrogen bond at the distal OH position stabilizes the NHOH function. These examples are among the first crystallographically characterized aromatic hydroxylamine complex of a transition metal.

Chapter 4: Catalysis: An Aerobic Oxidation of Alcohols to Aldehydes

The oxidation of alcohols is an important organic transformation that is traditionally carried out by various stoichiometric oxidants such as hypochlorite,[131] high-valent Mn[132] and Cr species,[133,134] hypervalent iodine,[135] and oxalyl chloride/DMSO[136], which are not ideal because they produce high amount of hazardous and toxic wastes or undesirable by-products. Herein, we report a novel earth-abundant copper(II) catalysts based on Schiff base ligand systems which can selectively oxidize alcohols to aldehydes under mild conditions. The reactions use oxygen as the terminal oxidant, which generates water as by-product and therefore constitutes "greener" conditions. We tested the catalytic performance of the series of Cu(II), Ni(II) and Zn(II) complexes with L^{I}_{tBu}-NHOH and L^{I}_{H}-NHOH ligands for the selective oxidation of alcohols to aldehydes. Of all complexes reported in this thesis, only the Cu(II) complexes (L^{I}_{tBu}-NHOH-Cu and L^{I}_{H}-NHOH-Cu) show catalytic activity for this organic transformation. Although they show promising results for benzylic alcohols oxidation, they are ineffective towards the oxidation of primary aliphatic alcohols.

The hydroxylamine function (NHOH) present in our complexes is redox noninnocent and can be interconverted to two-electrons oxidized nitroso group (NO) and/or two-electrons reduced amine moiety (NH_2) *via* disproportionation or oxidation/reduction processes. This two-electron shuttle can be used to mediate two-electron oxidation process such as oxidation of alcohols to aldehydes. The two-electron transfer series for nitrogen functional moieties is shown in Scheme 4-1.

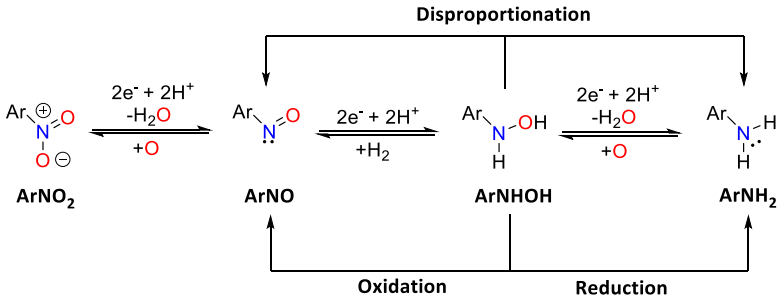

Scheme 4-1: Redox versatility of nitrogen-containing functional groups.

4.1 Oxidation of Primary Aliphatic Alcohols

We tested our catalytic system for the oxidation of various primary aliphatic alcohols, *viz.*: propanol, hexanol and octanol under the conditions including the complex (5 mol% catalyst loading), 4 Å molecular sieves (MS 4 Å), 4-*N,N*-dimethylaminopyridine (DMAP, 20 mol% w.r.t substrate) as an additive, in DCM for 3h at room temperature under O_2 pressure ($P(O_2)$ = 2 atm, i.e. 1 atm above room

atmosphere). The general scheme is shown in Scheme 4-2 and the results are collected in Table 4-1. Under these conditions, there is almost 0% conversion. In order to facilitate this transformation for good results, several additives were tested. Changing the additives from DMAP to potassium *tert*-butoxide (*t*BuOK), K_2CO_3, Et_3N, *N*-methylimidazole (NMI), and increasing the reaction time from 3 h to 24 h has negligible effect on this transformation (entries 1-3). Also, the use of hydrogen peroxide as an oxidant did not facilitate the oxidation process. However, using THF as a solvent under same set of conditions listed earlier with elevated temperature (50°C) afforded 14% conversion (based on GC) of octanol to octanal in 20 h (entry 4), which we have still to confirm for reproducibility.

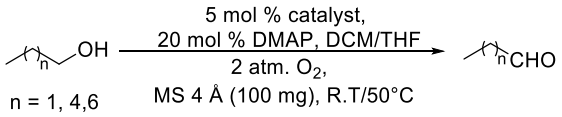

Scheme 4-2: Copper(II)-catalyzed aerobic oxidation of primary aliphatic alcohols.

Table 4-1: Aerobic Oxidation of Primary Aliphatic Alcohols[a]

Entry	Substrate	Catalyst	Additive	Solvent	T (°C)	Time (h)	Yield [b] (%)
1	Propanol	L^{I}_{tBu}-NHOH-Cu	DMAP/*t*BuOK/ Et_3N/NMI/ K_2CO_3	DCM	25	24	0
2	Hexanol	L^{I}_{tBu}-NHOH-Cu	DMAP/*t*BuOK/ Et_3N/ NMI/K_2CO_3	DCM	25	24	0
3	Octanol	L^{I}_{tBu}-NHOH-Cu	DMAP/*t*BuOK/ Et_3N/ NMI/K_2CO_3	DCM	25	24	0
4	Octanol	L^{I}_{tBu}-NHOH-Cu	DMAP	THF	50	20	14

[a]Alcohol (0.5 mmol), catalyst (0.025 mmol, 5 mol%), DMAP (0.1 mmol, 20mol%), O_2 (2 atm), 4 Å molecular sieves (MS) (100 mg), Solvent (4 mL). [b] GC yield using hexamethylbenzene as an internal standard.

4.2 Oxidation of Benzyl Alcohols and their Substituted Derivatives

These conditions were next applied to benzyl alcohol and its various substituted derivatives (Scheme 4-2). Some selected results are shown in the Table 4-2. Using DCM as a solvent and DMAP (20 mol% w.r.t substrate) as an additive, there is 44% conversion (entry 1) of benzyl alcohol to benzaldehyde in 24 h, which gets increased to 89% in 48 h at room temperature (entry 2). Elevating the temperature to 50 °C in THF using DMAP as an additive did not improve the rate and conversion significantly (entries 3 and 4), thus we continued with the room-temperature conditions in DCM. The reaction is as efficient with a 3-nitro or 3-methoxy substituent on the substrate (entries 5-8). 3-methoxybenzyl alcohol shows the highest conversion among these substrates at the 24 h mark. The least sterically encumbered

complex, L^{I}_{H}-NHOH-Cu, is surprisingly not as effective as L^{I}_{tBu}-NHOH-Cu, with quite low conversions. For benzylic alcohols, there is maximum of 18% conversion in 48 h (entry 10). Whereas 3-nitro and 3-methoxy substituted benzyl alcohols show 52% and 64% conversions in 48 h, respectively (entries 11-14). The addition of other additives like *t*BuOK and Et_3N leads to 0% conversion (entries 17, 18). It underscores the important role of DMAP in the catalytic cycle. We also conducted some control experiments to determine the actual role of catalyst and the additive. These experiments showed 0% conversion in the absence of DMAP and using Cu(II) acetate instead of L^{I}_{tBu}-NHOH-Cu as a catalyst (entries 15, 16). Interestingly, the nitro-containing L^{I}_{tBu}-NO_2-Cu and L^{I}_{H}-NO_2-Cu(OH_2) complexes (entries 19 and 20) were not conducive for catalysis, thereby demonstrating the crucial role of the NHOH function. Similarly, Cu is essential to the reaction, as neither L^{I}_{tBu}-NHOH-Ni, L^{I}_{tBu}-NHOH-Zn, L^{I}_{H}-NHOH-Ni or L^{I}_{H}-NHOH-Zn led to no significant conversion (entries 21-24).

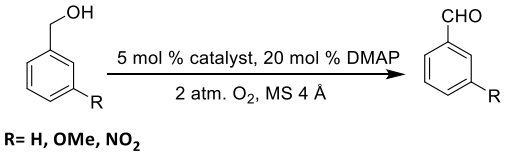

Scheme 4-3: Oxidation conditions for primary benzylic alcohols and their *meta*-substituted derivatives.

Table 4-2: Oxygen-mediated Oxidation of Benzyl Alcohols and its Substituted Derivatives[a]

Entry	R	Catalyst	Solvent	T (°C)	Time (h)	Yield [b] (%)
1	H	L^{I}_{tBu}-NHOH-Cu	DCM	25	24	44
2	H	L^{I}_{tBu}-NHOH-Cu	DCM	25	48	89
3	H	L^{I}_{tBu}-NHOH-Cu	THF	50	24	75
4	H	L^{I}_{tBu}-NHOH-Cu	THF	50	30	80
5	NO_2	L^{I}_{tBu}-NHOH-Cu	DCM	25	24	76
6	NO_2	L^{I}_{tBu}-NHOH-Cu	DCM	25	48	95
7	MeO	L^{I}_{tBu}-NHOH-Cu	DCM	25	24	93
8	MeO	L^{I}_{tBu}-NHOH-Cu	DCM	25	48	97
9	H	L^{I}_{H}-NHOH-Cu	DCM	25	24	13
10	H	L^{I}_{H}-NHOH-Cu	DCM	25	48	18
11	NO_2	L^{I}_{H}-NHOH-Cu	DCM	25	24	40
12	NO_2	L^{I}_{H}-NHOH-Cu	DCM	25	48	52
13	OMe	L^{I}_{H}-NHOH-Cu	DCM	25	24	60
14	OMe	L^{I}_{H}-NHOH-Cu	DCM	25	48	64
15[c]	H	L^{I}_{tBu}-NHOH-Cu	DCM	25	48	0
16	H	$Cu(OAc)_2 \cdot H_2O$	DCM	25	48	0
17[d]	H	L^{I}_{tBu}-NHOH-Cu	DCM	25	48	0
18[e]	H	L^{I}_{tBu}-NHOH-Cu	DCM	25	48	0
19	H	L^{I}_{tBu}-NO_2-Cu	DCM	25	24	0
20	H	L^{I}_{H}-NO_2-Cu(OH_2)	DCM	25	24	0
21	H	L^{I}_{tBu}-NHOH-Ni	DCM	25	24	0
22	H	L^{I}_{tBu}-NHOH-Zn	DCM	25	24	0
23	H	L^{I}_{H}-NHOH-Ni	DCM	25	24	0
24	H	L^{I}_{H}-NHOH-Zn	DCM	25	24	0

[a]Alcohol (0.5 mmol), Catalyst (0.025 mmol, 5mol%), DMAP (0.1 mmol, 20mol%), O_2 (2 atm), 4Å molecular sieves (MS) (100 mg), Solvent (4 mL). [b] GC yield using hexamethylbenzene as an internal standard. [c] Control experiment without DMAP. [d] Et3N, [e] tBuOK are used as an additives.

This research work was inspired by previous, related chemistry of transition metal complexes which catalyze oxygen-mediated oxidation of alcohols to give carbonyl compounds as reported in the literature.[5,55,56] These complexes in presence of simple and inexpensive additives (bases) exhibit ligand participatory catalytic cycle. For example, the catalytic system consisting of Cu^{I}(phenanthroline) and diethyl azodicarboxylate (DEAD) reported by Markó et al. in 1996[55] involved a simple ligand-participatory catalytic cycle, which was further improved to become a highly efficient protocol for this organic transformation.[56] As discussed earlier in the introduction,[57] the mechanistic reinvestigation of

this system further suggested a new catalytic bicycle which involves two pathways: (i) a fast Cu(II)/DBAD pathway involving DBAD as an oxidant, and (ii) a slow Cu(II)-only pathway in which Cu(II) acts as an oxidant.

Based on this observation in which metal center incorporated with redox noninnocent ligand system catalyzes the oxidation process, we choose to work with our complexes to screen their reactivity towards aerobic alcohol oxidation. Also, the speculated ArNO species (Scheme 4-4b) produced from ArNHOH present in our system can be depicted as the monosubstituted electronic mimics of azo functionality (–N=N–) (Scheme 4-4a) encountered in six-membered transition state of Markó's catalytic system as proposed by Stahl.[57] A general demonstration of the speculative mechanism for aerobic alcohol oxidation by our system is shown in Scheme 4-4c.

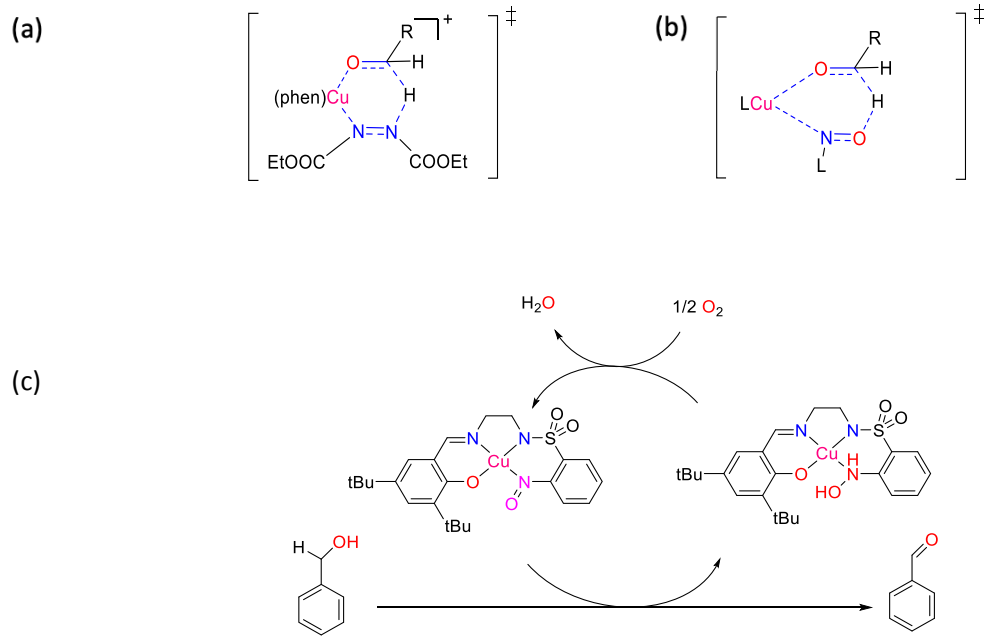

Scheme 4-4: Structural similarity of the (a) Transition state proposed by Stahl, (b) speculated species in our systems, and (c) a plausible mechanism for the oxidation of benzyl alcohol by L^{I}_{tBu}-NHOH-Cu.

4.3 Conclusion

Preliminary results obtained from these experiments are very interesting, especially the requirement of the NO bond for turnover. The catalytic system we developed is somewhat inactive for aliphatic alcohols, but works well (up to 97%) for benzyl alcohols to form benzaldehydes with no trace of overoxidized carboxylic acids. This catalytic system under these novel conditions is a good example of ligand-participatory catalytic cycle since the hydroxylamine is crucial for turnover. We hypothesize that

the NHOH/NO conversion is part of the catalytic cycle based on the similarity to Markó's conditions. Mechanistic studies still need to be performed for further modifications in the catalytic system to improve the conversion and rate.

Chapter 5: Conclusion

In summary, we studied the redox behavior of nitrogen-containing functional group near a metal center, by designing and preparing salen-type ligands with a pendant nitrogen-containing group and partial hydrogenation of this group to the redox-noninnocent hydroxylamine function. Two different approaches were used for partial reduction. For imine-based ligands (L^{I}_{tBu}-NO_2 and L^{I}_{H}-NO_2), the hydrogenation was carried out catalytically using Pd/C catalyst poisoned by diphenyl sulfide under H_2 pressure. The use of a poison is to slow down the hydrogenation and enable to stop the reaction at the hydroxylamine point before further reduction to amine. The best hydrogenation conditions were achieved by using 2 mol% of catalyst w.r.t substrate and 10 mol% poison per Pd, under 25 psi hydrogen pressure which afforded up to maximum of 84% purity of L^{I}_{R}-NHOH (R = H, tBu) ligands. For the amine-based ligands (L^{A}_{tBu}-NO_2 and L^{A}_{H}-NO_2), the partial reduction was accomplished using zinc dust and ammonium formate (stoichiometric reducing agent) *via* transfer hydrogenation. For amine-based ligands, the optimized conditions afforded 98% pure L^{A}_{R}-NHOH (R= H, tBu) ligands in high yield up to 85 %, using 5 equiv. of zinc (6 equiv. of zinc for L^{A}_{tBu}-NO_2) and 1.6 equiv. of ammonium formate at 0°C in DCM and methanol. The extra one equivalent of Zn in case of *t*Bu-substituted ligand is used to compensate the steric hinderance.

Imine-based hydroxylamine ligands were successfully used for complexation with Cu(II), Ni(II) and Zn(II), leading to novel complexes bearing an intact hydroxylamine function, confirmed by crystallography and, whenever possible, ^{1}H-NMR spectroscopy. The normally reactive NHOH function in these complexes is stabilized by intramolecular hydrogen bonding with the phenolate of the salicylimine moiety. This unusual stability goes against the belief that NHOH disproportionates upon interaction with transition metal centers to form amine and nitroso derivatives. Complexes L^{I}_{tBu}-NHOH-Ni and L^{I}_{H}-NHOH-Ni disproportionate upon refluxing to form dark coloured solutions containing disproportionated products (NO and NH_2 derivatives), characterized by mass spectrometry. For L^{I}_{H}-NHOH-Ni, we were also able to obtain the crystal structure for one of its disproportionated products (L^{I}_{H}-NH_2)-Ni.

The hydroxylamine-containing complexes were screened for the catalytic conversion of alcohols to aldehydes using a green terminal oxidant, dioxygen. They selectively oxidize alcohols to aldehydes with no traces of overoxidized carboxylic acids found. Of all these complexes, only copper based complexes (L^{I}_{tBu}-NHOH-Cu and L^{I}_{H}-NHOH-Cu) show promising results under milder reaction conditions. The reaction can also be carried out at 50°C in THF instead of DCM. Several control experiments were carried out to determine the significance of additive and catalyst. It was found that there is 0% conversion when the

additive (DMAP) or copper catalysts are removed. Although, primary alcohols almost show 0% conversion (except octanol, 14%), but we observe up to 97% conversion for benzyl alcohol and its *meta*-substituted derivatives in two days.

For future work, we aim to test these complexes for catalyzing other reactions. For example, two-electron oxidized derivative of copper(I) complex bearing NHOH can generate radical/anionic species (Scheme 5-1a).[120] We may explore its reactivity to catalyze a very famous reaction Chan-Evans-Lam coupling (CEL)[137–139] as the presence of nucleophilic site can foster coordination to boronic acid. For example, a sulfonate group incorporated into the ligand allows coordination to boron and helps in transmetalation (Scheme 5-1b) .[140]

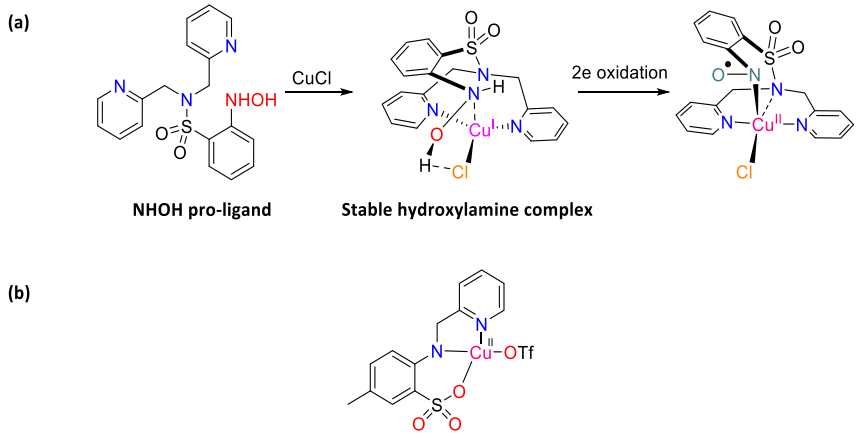

Scheme 5-1: Two-electron oxidation to form radical/anionic species in NHOH bearing complex.[120] (b) Copper(II) pyridyliminoarylsulfonate complex incorporated with nucleophilic sulfonate group for catalyzing CEL.

Furthermore, the catalytic conversion of alcohols to aldehydes can be improved and expanded. We will thus explore other oxidants or reoptimized reaction conditions to get better yields in shorter reaction time.

Chapter 6: Experimental Section

6.1 Materials and Instrumentation

Organic reagents, solvents and metal salts for synthesis were commercially available reagent grade and used as received. All non-protic solvents used were dried on an MBraun solvent purification system and stored over activated 4 Å molecular sieves inside an inert-atmosphere (N_2) glovebox filled with a dry nitrogen atmosphere (O_2 < 0.1 ppm; H_2O < 0.1 ppm). Air-sensitive samples were also stored in the glovebox. Oxidation experiments were carried out in Radleys® carrousel reaction station attached to a compressed O_2 tank.

All the prepared ligands and complexes were characterized by ^{1}H-NMR spectra recorded in $CDCl_3$, DMSO-d_6 or acetone-d_6 at 25°C on a Varian Innova 500 MHz or Bruker Fourier 300 MHz instrument and referenced to an internal standard, TMS (tetramethylsilane). Chemical shifts for ^{1}H-NMR spectra are recorded in parts per million from TMS. Electrospray ionization mass-spectrometry (ESI-MS) measurements were performed *via* direct injection on a Micromass Quattro LC at Concordia's Centre for Biological Applications of Mass Spectrometry. UV-Visible spectra were recorded on a B&W Tek iTrometer equipped with quartz cell of 1.00 cm pathlength. GC measurements were performed on an Agilent 6850 GC system equipped with an HP-5 capillary column (5%-Phenyl)-methylpolysiloxane stationary phase. Hexamethylbenzene (HMB) was used as an internal standard. Calibration curves were generated for the products to determine yields.

Crystallographic analysis was performed on a Bruker APEX-DUO diffractometer at the Cu-Kα or Mo-Kα source. The frames were integrated with the Bruker SAINT software package using a narrow-frame algorithm. Data were corrected for absorption effects using the multiscan method (SADABS or TWINABS). The structures were solved by direct methods and refined using the APEX3 software package. All non-H atoms were refined with anisotropic thermal parameters. H atoms were generated in idealized positions, riding on the carrier atoms with isotropic thermal parameters.

6.2 Synthesis of Nitro Ligands

L^{I}_{H}-NO_2

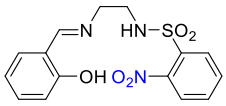

In a 250 mL round-bottom flask readied with a magnetic stir bar, ethylenediamine (10 mL, 8.94 g, 148.75 mmol) was dissolved in anhydrous THF (25 mL) at 0°C followed by the dropwise addition of 2-

nitrobenzenesulfonyl chloride (10.98 g , 49.54 mmol) in anhydrous THF (50 mL). After the entire addition, the solution was warmed to room temperature, stirred for further 30 min, then evaporated to dryness to give the oily residue, which was partitioned between DCM (50 mL) and water (50 mL). The aqueous layer was further extracted with 3 × 50 mL of dichloromethane. The organics were combined, dried over Na_2SO_4, filtered, and the solvent was removed on a rotary evaporator to give a brown oil. Concentrated HCl (50 mL, 12 M) was added to the oil, thereupon the bis(sulfonamide) by-product precipitated as a white solid. The solid was filtered off and the filtrate was concentrated in a 250 mL round-bottom flask to give a brown oil of the mono-substituted ethylenediammonium salt, which was used directly for the next step. Methanol (50 mL) was added to this oil, followed by salicylaldehyde (6.40 mL, 7.26 g, 59.45 mmol) and triethylamine (6.91 mL, 5.01 g, 49.54 mmol). The solution was refluxed under stirring for 30 min, then cooled to 25 °C and then to 0 °C. The yellow microcrystalline solid was filtered off and washed with cold methanol (50 mL). Yield: 11 g, 65% based on 2-nitrobenzenesulfonyl chloride. ^{1}H-NMR (500 MHz, $CDCl_3$, δ/ppm): 12.59 (s, 1H), 8.24 (s, 1H), 8.10 (dd, *J* = 7.8, 1.4 Hz, 1H), 7.71-7.67 (m, 1H), 7.65 (dd, *J* = 7.7, 1.4 Hz, 1H), 7.58 (td, *J* = 7.7, 1.4 Hz, 1H), 7.29 (ddd, *J* = 8.4, 7.3, 1.7 Hz, 1H), 7.14 (dd, *J* = 7.6, 1.7 Hz, 1H), 6.87 (dd, *J* = 9.5, 0.9 Hz, 1H), 6.84 (dd, *J* = 7.5, 1.0 Hz, 1H), 5.51 (s, 1H), 3.73 (td, *J* = 5.7, 1.0 Hz, 2H), 3.54 (s, 2H).

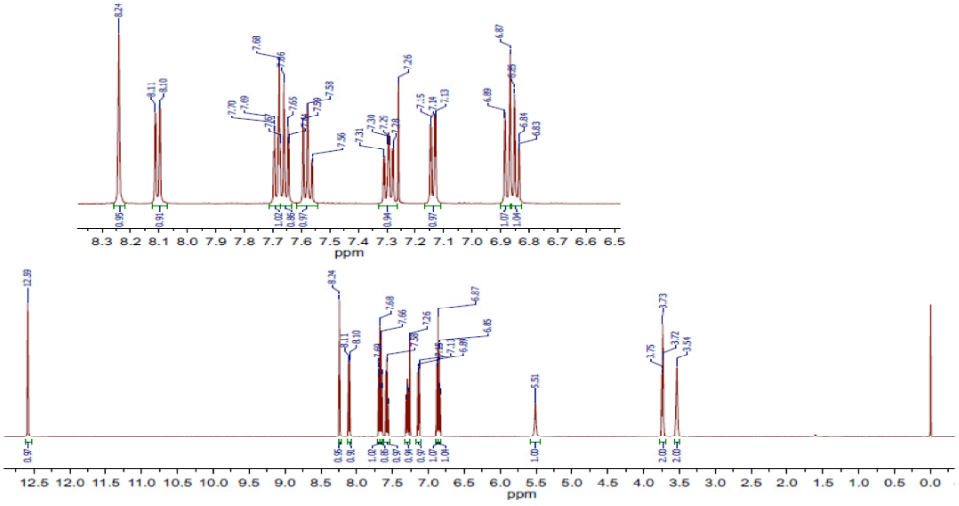

Figure 6-1: ^{1}H-NMR (500 MHz) spectra of L^{I}_{H}-NO_2 in $CDCl_3$ at 25 °C with inset showing zoom in of aromatic region.

L^{I}_{tBu}-NO_2

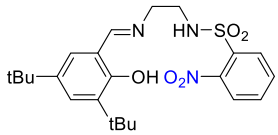

The half ligand (mono-substituted ethylenediammonium salt) was synthesized as *per* the above procedure for L^{I}_{H}-NO_2. It was then dissolved in a methanol (50 mL) in a 250 mL round-bottom flask equipped with a stir bar. To this solution, triethylamine (6.91 mL, 5.01 g, 49.54 mmol) and 3,5-di-*tert*-butylsalicyaldehyde (13. 930 g, 56.45 mmol) were added. After been reflux under stirring for 1 h, the reaction mixture was cooled down to room temperature and then to 0 °C. The yellow microcrystalline solid was filtered off and further washed with 50 mL of cold methanol. Yield: 18.56 g, 81% based on 2-nitrobenzenesulfonyl chloride. ^{1}H-NMR (500 MHz, $CDCl_3$, δ/ppm): 13.01 (s, 1H), 8.24 (s, 1H), 8.13 (dd, *J* = 7.8, 1.2 Hz, 1H), 7.75 (dd, *J* = 7.9, 1.1 Hz, 1H), 7.67 (td, *J* = 7.7, 1.2 Hz, 1H), 7.60 (td, *J* = 7.8, 1.3 Hz, 1H), 7.38 (d, *J* = 2.4 Hz, 1H), 6.96 (d, *J* = 2.4 Hz, 1H), 5.54 (s, 1H), 3.73 (t, *J* = 5.7 Hz, 2H), 3.52 (dd, *J* = 11.6, 5.9 Hz, 2H), 1.42 (s, 9H), 1.30 (s, 9H).

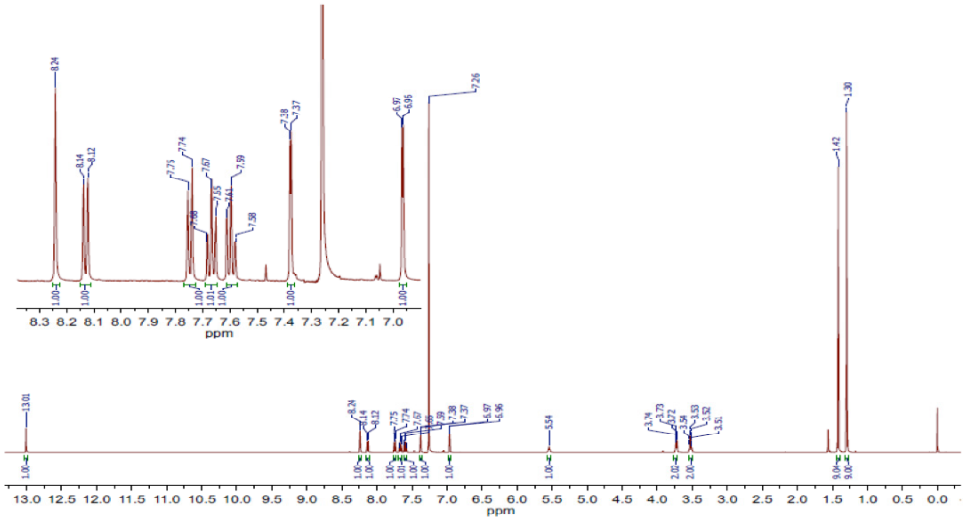

Figure 6-2: ^{1}H-NMR (500 MHz) spectra of L^{I}_{tBu}-NO_2 in $CDCl_3$ at 25 °C with inset showing zoom in of aromatic region.

L^{A}_{H}-NO_2

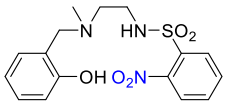

L^{I}_{H}-NO_2 (1 g, 2.86 mmol) was dissolved in a minimum quantity of methanol (ca. 2 mL). To this solution, acetic acid (0.163 mL, 171.1 mg, 2.86 mmol), formaldehyde (37%) (0.157 mL, 171.1 mg, 5.72 mmol) and sodium cyanoborohydride (449 mg, 7.15 mmol) were added sequentially. In a few minutes to an hour, a pinkish-grey precipitated formed. The reaction mixture was stirred for 24 h. The precipitate was then

filtered off, washed with portions of cold methanol and diethyl ether, and dried *in vacuo*. Yield: 776 mg, 74%. ^{1}H-NMR (500 MHz, $CDCl_3$) δ 10.21 (s, 1H), 8.13-8.04 (m, 1H), 7.90-7.83 (m, 1H), 7.74-7.72 (m, 1H), 7.71 (dd, *J* = 6.5, 4.6 Hz, 1H), 7.16 (td, *J* = 8.0, 1.7 Hz, 1H), 6.97-6.90 (m, 1H), 6.82-6.79 (m, 1H), 6.77 (dd, *J* = 7.4, 1.1 Hz, 1H), 5.48 (s, 1H), 3.69 (s, 2H), 3.28 (t, *J* = 6.7 Hz, 2H), 2.67 (t, *J* = 6.7 Hz, 2H), 2.33 (s, 3H).

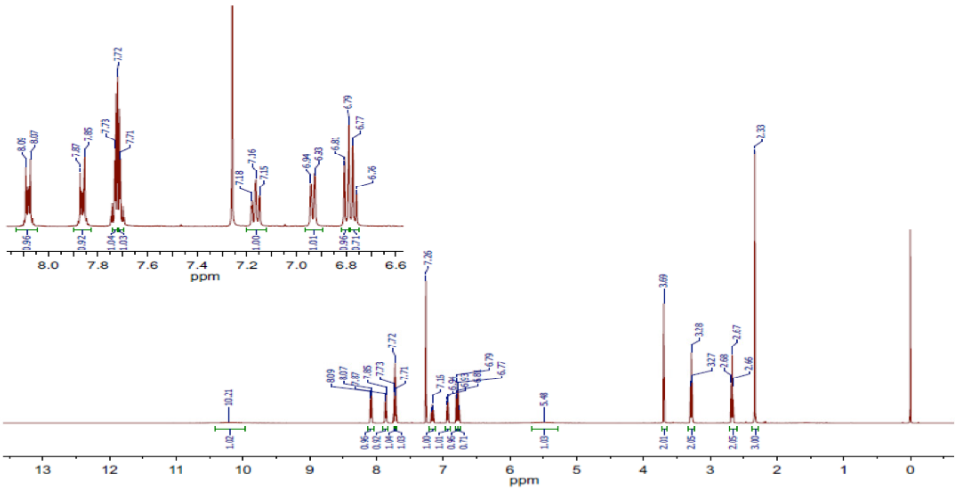

Figure 6-3: ^{1}H-NMR (500 MHz) spectra of L^{A}_{H}-NO_2 in $CDCl_3$ at 25 °C with inset showing zoom in of aromatic region.

L^{A}_{tBu}-NO_2

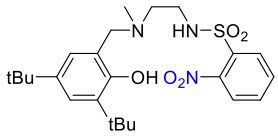

In a 250 mL round bottom flask in an ice bath, L^{I}_{tBu}-NO_2 (5 g, 10.83 mmol) was dissolved in DCM (40 mL). To this solution, $NaBH_3CN$ (748.8 mg, 11.91 mmol, 1.1 eq.) was added slowly and portion-wise while stirring. After 30 min, methanol (40 mL) was added and the mixture was further stirred for 30 min. Acetic acid (0.681 mL, 715 mg, 11.91 mmol) was then added to the reaction mixture and further stirred for 3 h in the ice bath. The mixture was left stirring overnight while it warmed up to room temperature. If TLC monitoring on alumina (100% DCM) shows incomplete conversion, another 0.5 equiv. of $NaBH_3CN$ was added while the mixture was stirring at 0°C. After completion of the reaction, formaldehyde (37%) (0.531 mL, 487.9 mg, 16.2 mmol) and $NaBH_3CN$ (1.02 mg, 16.2 mmol, 1.5 eq.) were added and the mixture stirred. As TLC monitoring (alumina, 100% DCM) after 1 h revealed incomplete conversion, another 0.5 equiv. of formaldehyde was added to the mixture and the reaction stirred for another 1 h and monitored by TLC (alumina, 100% DCM). Solvents were evaporated and the viscous residue was dissolved in DCM. While cooling and stirring on the ice bath, an aqueous solution of Na_2CO_3 (10 g Na_2CO_3 in 100 mL water) was added slowly with frequent testing for pH of the reaction until indication

of a neutral solution. The mixture was stirred for 15 min and then kept undisturbed for two minutes to form two distinct layers with the product in the DCM phase. The organic layer was collected, and the aqueous layer was extracted thrice with DCM (3x100 mL). The combined organic fractions were dried over sodium sulfate, filtered, evaporated and dried under vacuum for 48 h to yield the product as a off-white solid. Yield: 5.175 g, 98%. ^{1}H-NMR (500 MHz, $CDCl_3$) δ 10.38-10.04 (s, 1H), 8.12-8.08 (m, 1H), 7.87 (ddd, *J* = 8.5, 5.0, 2.5 Hz, 1H), 7.76-7.70 (m, 2H), 7.23 (t, *J* = 3.6 Hz, 1H), 6.81 (d, *J* = 2.4 Hz, 1H), 5.49 (s, 1H), 3.67 (d, *J* = 6.2 Hz, 2H), 3.30-3.26 (m, 2H), 2.67 (t, *J* = 6.7 Hz, 2H), 2.33 (s, 3H), 1.39 (s, 9H), 1.28 (s, 9H).

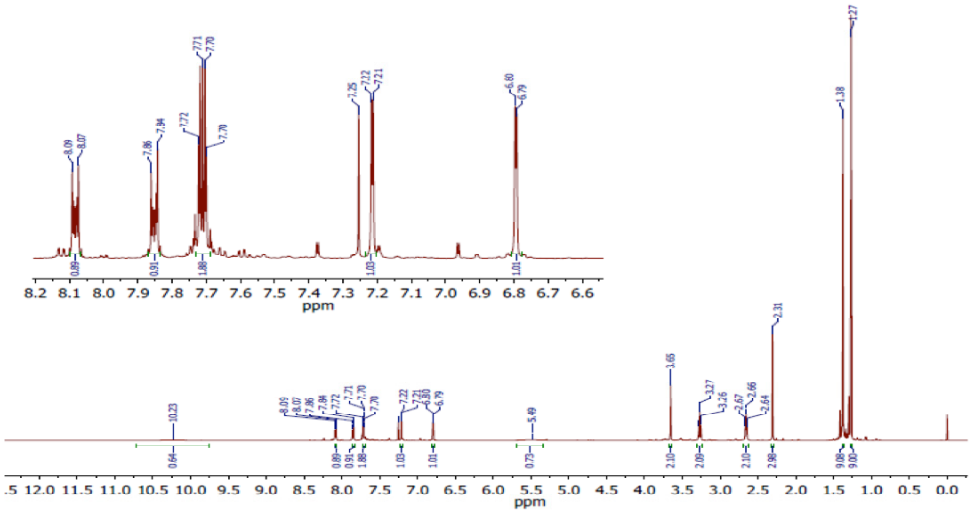

Figure 6-4: ^{1}H-NMR (500 MHz) spectra of L^{A}_{tBu}-NO_2 in $CDCl_3$ at 25 °C with inset showing zoom in of aromatic region.

6.3 Synthesis of Hydroxylamine Ligands

L^{I}_{H}-NHOH

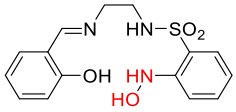

To a medium-pressure hydrogenation flask configured in a Parr shaker was added Pd/C (10 wt.% Pd) (0.0286 mmol, 30.4 mg) followed by slow addition of methanol (30 mL). Then, 100 µL of a 0.0286 M diphenyl sulfide (0.00286 mmol, 0.533 mg) solution in methanol (5 mL) was added, followed by another 20 mL of methanol and L^{I}_{H}-NO_2 (1.43 mmol, 500 mg) dissolved in DCM (25 mL). The hydrogenation was carried out at 25 psi of H_2 at 25 °C for 50 min. The catalyst was then filtered off over a pad of Celite, which was well rinsed with methanol (ca. 100 mL). After evaporating the filtrate to dryness, a minimum quantity of diethyl ether (ca. 9 mL) was added to the residue. The solid, which is the starting material, was filtered off and the filtrate was evaporated to dryness to give L^{I}_{H}-NHOH as a yellow powder. Yield:

434 mg, 91%. ^{1}H-NMR (500 MHz, $CDCl_3$, δ/ppm): 13.21 (s, 1H), 8.26 (s, 1H), 7.81 (dd, *J* = 7.7, 1.3 Hz, 1H), 7.55 (dd, *J* = 8.2, 1.3 Hz, 1H), 7.54-7.49 (m, 1H), 7.40-7.35 (m, 1H), 7.24 (dd, *J* = 7.6, 1.7 Hz, 1H), 7.07-7.03 (m, 1H), 7.01-6.97 (m, 1H), 6.95 (td, *J* = 7.5, 1.1 Hz, 1H), 6.48 (s, 1H), 5.66 (s, 1H), 3.57-3.53 (m, 1H), 3.12 (s, 1H).

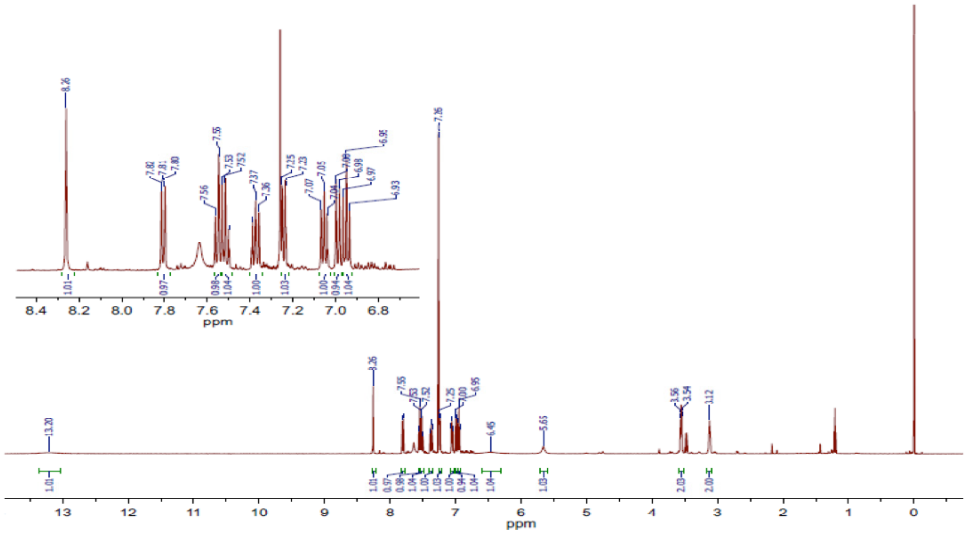

Figure 6-5: ^{1}H-NMR (500 MHz) spectra of L^{I}_{H}-NHOH in $CDCl_3$ at 25 °C with inset showing zoom in of aromatic region.

L^{I}_{tBu}-NHOH

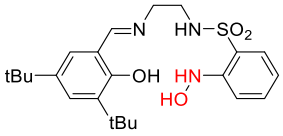

In a medium-pressure hydrogenation flask mounted on a Parr shaker, Pd/C (10 wt.% Pd) (0.0216 mmol, 22.98 mg) was placed with slow addition of methanol (30 mL). To this mixture, 100 µL of a 0.0216 M diphenyl sulfide (0.00216 mmol, 0.402 mg) solution in methanol (5 mL) was added, followed by another 20 mL of methanol and L^{I}_{tBu}-NO_2 (1.08 mmol, 500 mg) dissolved in DCM (25 mL). The hydrogenation was carried out at 25 psi of H_2 pressure at 25 °C for 1 h. The work-up was the same as for L^{I}_{H}-NHOH to yield L^{I}_{tBu}-NHOH as a yellow powder. Yield: 459 mg, 95%. ^{1}H-NMR (500 MHz, $CDCl_3$, δ/ppm): 13.49 (s, 1H), 8.19 (s, 1H), 7.81 (d, *J* = 7.4 Hz, 1H), 7.69 (s, 1H), 7.53 (d, *J* = 3.0 Hz, 1H), 7.52 (d, *J* = 1.2 Hz, 1H), 7.44 (d, *J* = 2.4 Hz, 1H), 7.05 (d, *J* = 2.4 Hz, 1H), 6.10 (s, 1H), 5.71 (s, 1H), 3.47 (t, *J* = 10.5 Hz, 2H), 3.17 (dd, *J* = 11.0, 5.8 Hz, 1H), 1.55 (s, 9H), 1.45 (s, 9H).

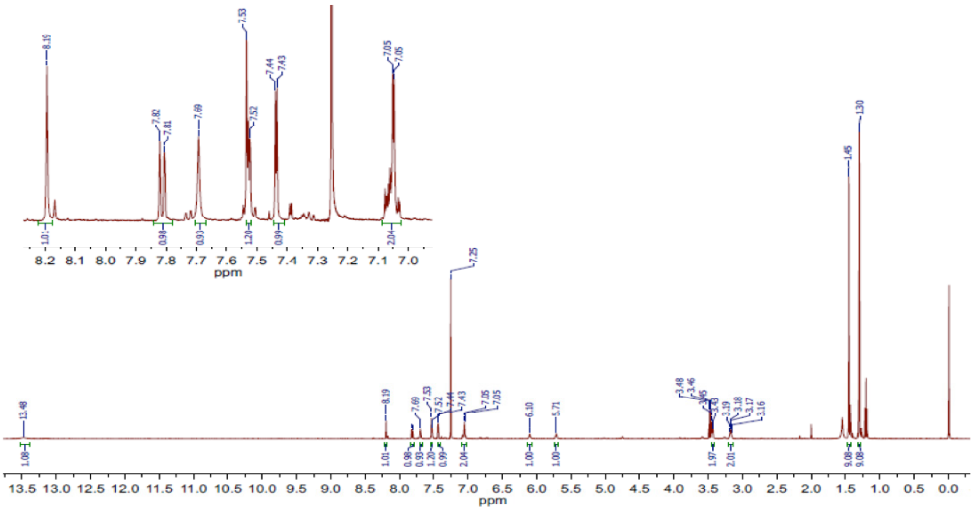

Figure 6-6: ^{1}H-NMR (500 MHz) spectra of L^{I}_{tBu}-NHOH in $CDCl_3$ at 25 °C with inset showing zoom in of aromatic region.

L^{A}_{H}-NHOH

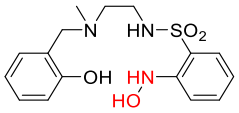

To a vigorously stirring solution of L^{A}_{H}-NO_2 (100 mg, 0.273 mmol) in DCM (4 mL) was added ammonium formate (20.6 mg, 0.437 mmol, 1.6 eq.) dissolved in methanol (3 mL). The reaction mixture was placed and kept on an ice bath during the reaction. Initially, activated zinc powder (35.89 mg, 0.547 mmol, 2 eq.) was added to the solution followed by its addition in portions (0.5 eq, 8.94 mg) every 15 min up to the total amount of 5 equiv. The reaction was monitored by TLC (alumina, 100% DCM) and around 2.5 h, no sign of starting material (L^{A}_{H}-NO_2) remained. The reaction mixture was immediately filtered over celite to prevent further reduction. Aqueous tetrasodium ethylenediaminetetraacetate (0.1 M, 10 mL) was added to the filtrate, followed by three extractions in DCM (3x10 mL). The combined organic phase was dried over sodium sulfate and the solvent was evaporated *in vacuo*. A yellow solid was recovered. It was dried under vacuum and was stored in a glovebox to avoid deterioration. Yield: 81 mg, 85%. ^{1}H-NMR (500 MHz, acetone) δ 8.28 (s, 1H), 8.00 (s, 1H), 7.70 (dd, *J* = 7.9, 1.4 Hz, 1H), 7.53 (ddd, *J* = 8.6, 7.2, 1.5 Hz, 1H), 7.49-7.45 (m, 1H), 7.16-7.09 (m, 1H), 7.00-6.94 (m, 2H), 6.75-6.71 (m, 2H), 3.65 (s, 2H), 3.10 (t, *J* = 6.6 Hz, 2H), 2.61-2.56 (m, 2H), 2.18 (d, *J* = 7.9 Hz, 3H).

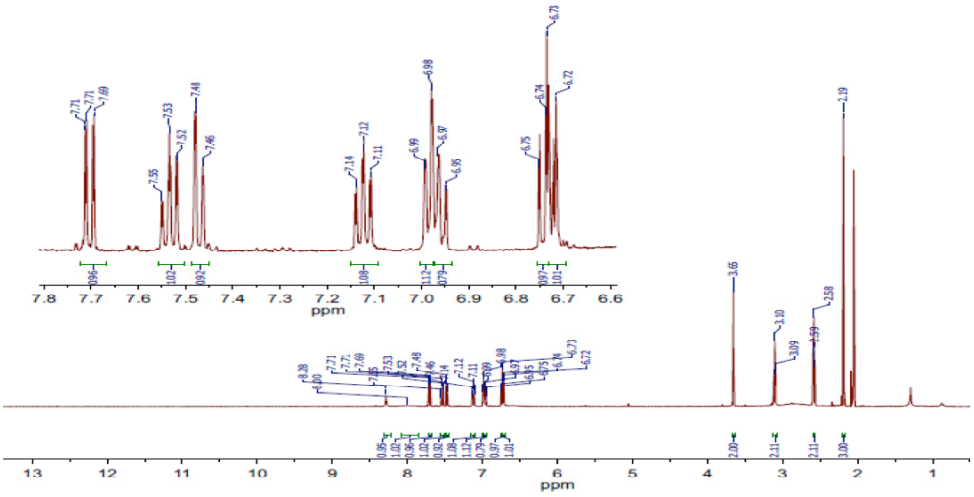

Figure 6-7: ^{1}H-NMR (500 MHz) spectra of L^{A}_{H}-NHOH in $CDCl_3$ at 25 °C with inset showing zoom in of aromatic region.

L^{A}_{tBu}-NHOH

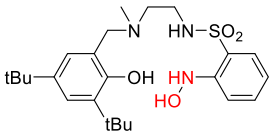

Ammonium formate (1.6 eq.) dissolved in methanol (3 mL) was added to a vigorously stirring solution of L^{A}_{tBu}-NO_2 (50 mg, 0.105 mmol) in DCM (4 mL), the solution was placed and kept on an ice bath during the course of the reaction. Initially, activated zinc powder (2 eq.) was added to the solution followed by its addition in portions (0.5 eq., 8.94 mg) every 15 min up to the total amount of 6 equiv. The reaction was monitored by TLC (alumina, 100% DCM) and around 3 h, there are still sign of starting material (L^{A}_{tBu}-NO_2) remained on the plate. Thus, 0.5 equivalents of zinc along with 0.5 equivalent of ammonium formate was added. The reaction was monitored by TLC (alumina, 100% DCM) and around 3.5 h, no sign of starting material (L^{A}_{tBu}-NO_2) remained. The reaction mixture was immediately filtered over celite to prevent further reduction. Aqueous tetrasodium ethylenediaminetetraacetate (0.1 M, 10 mL) was added to the filtrate, followed by three extractions in DCM (3x10 mL). The combined organic phase was dried over sodium sulfate and the solvent was evaporated *in vacuo*. A foamy yellow product was recovered. It was dried under vacuum and stored in a glove box to avoid deterioration. Yield: 31 mg, 67%.^{1}H-NMR (500 MHz, acetone) δ 8.31 (s, *J* = 11.0 Hz, 1H), 8.04 (s, 1H), 7.69 (dd, *J* = 7.9, 1.5 Hz, 1H), 7.56-7.51 (m, 1H), 7.49-7.44 (m, 1H), 7.21 (t, *J* = 3.3 Hz, 1H), 6.98-6.91 (m, 1H), 6.88 (d, *J* = 2.4 Hz, 1H), 6.55 (s, 1H), 3.67 (s, *J* = 9.7 Hz, 2H), 3.09 (t, *J* = 6.8 Hz, 2H), 2.58 (t, *J* = 6.9 Hz, 2H), 2.25 (d, *J* = 6.6 Hz, 3H), 1.39 (s, 10H), 1.26 (s, 9H).

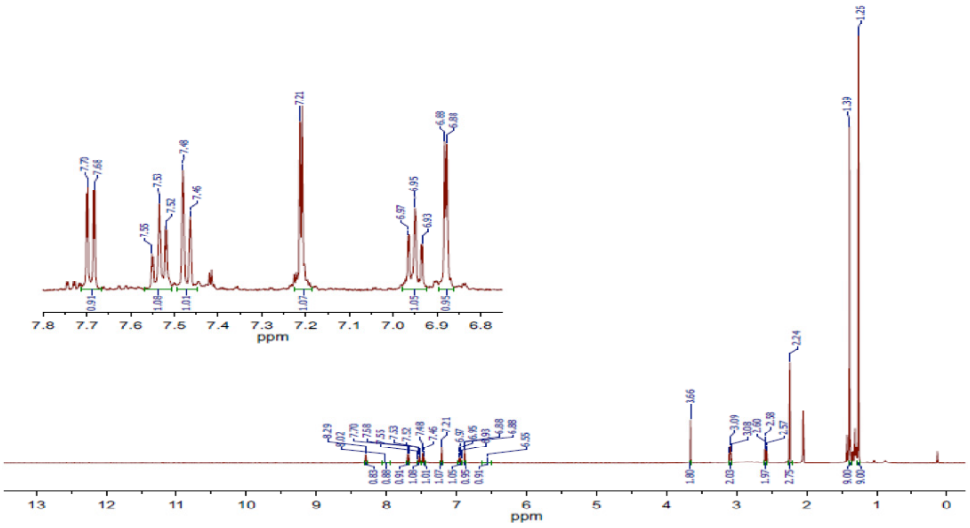

Figure 6-8: ^{1}H-NMR (500 MHz) spectra of L^{A}_{tBu}-NHOH in $CDCl_3$ at 25 °C with inset showing zoom in of aromatic region.

6.4 Synthesis of Hydroxylamine Metal Complexes

L^{I}_{H}-NHOH-Ni

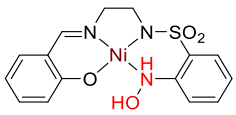

To a stirring solution of $Ni(NO_3)_2{\cdot}6H_2O$ (216.6 mg, 0.75 mmol) in ACN (5 mL), a solution of L^{I}_{H}-NHOH (250 mg, 0.7454 mmol) in ACN (5 mL) was added dropwise. The mixture was stirred vigorously for 15 min, during which a green solid precipitated out. The solid was collected by filtration, washed with diethyl ether (20 mL) and then dried under vacuum to give a muddy-green powder. Yield: 215 mg, 74%. Crystals suitable for X-ray diffraction analysis were obtained by subjecting a small portion of the complex dissolved in DCM to vapour-diffusion of pentane at room temperature. ^{1}H-NMR (500 MHz, $CDCl_3$, δ/ppm): 8.89 (s, 1H), 8.44 (s, 1H), 7.76 (d, *J* = 8.0 Hz, 1H), 7.74 (dd, *J* = 7.5, 1.2 Hz, 1H), 7.56 (td, *J* = 7.9, 1.4 Hz, 1H), 7.46 (d, *J* = 10.0 Hz, 1H), 7.35 (t, *J* = 7.6 Hz, 1H), 7.29-7.27 (m, 1H), 7.18 (dd, *J* = 7.9, 1.6 Hz, 1H), 6.86 (d, *J* = 8.5 Hz, 1H), 6.70 (d, *J* = 14.9 Hz, 1H), 3.51 (ddd, *J* = 22.5, 11.2, 6.3 Hz, 1H), 3.31-3.25 (m, 1H), 2.81 (ddd, *J* = 9.1, 5.8, 3.2 Hz, 1H), 2.74 (td, *J* = 10.2, 5.2 Hz, 1H).

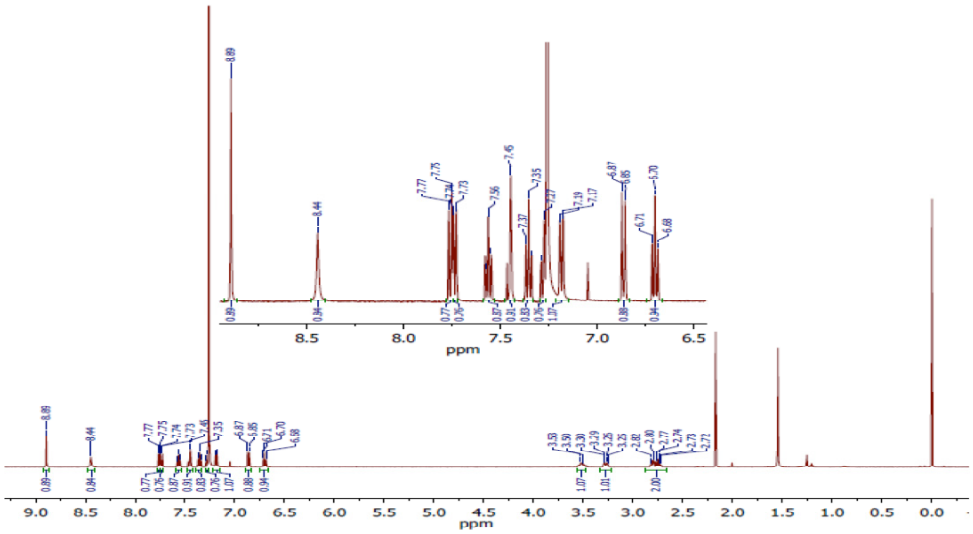

Figure 6-9: ^{1}H-NMR (500 MHz) spectra of L^{I}_{H}-NHOH-Ni in $CDCl_3$ at 25 °C with inset showing zoom in of aromatic region.

L^{I}_{tBu}-NHOH-Ni

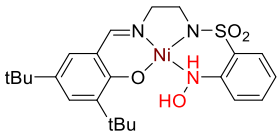

To a stirring solution of $Ni(NO_3)_2{\cdot}6H_2O$ (33.73 mg, 0.116 mmol) in ACN (5 mL), a solution of L^{I}_{tBu}-NHOH (52 mg, 0.116 mmol) in ACN (5 mL) was added dropwise. The mixture was stirred vigorously in air for 15 min, during which a green solid precipitated out. The solid was collected by filtration, washed with diethyl ether (20 mL) and then dried under vacuum to give a light-green powder. Yield: 42 mg, 72%. Crystals suitable for X-ray diffraction analysis were obtained by subjecting a small portion of the complex dissolved in DCM to vapour-diffusion of pentane at room temperature. ^{1}HNMR (300 MHz, $CDCl_3$, δ/ppm): 8.56 (s, 1H), 8.55 (s, 1H), 7.71 (d, *J* = 8.1 Hz, 1H), 7.56 (td, *J* = 7.9, 1.3 Hz, 1H), 7.43 (s, 1H), 7.41 (d, *J* = 2.6 Hz, 1H), 7.35 (d, *J* = 15.1 Hz, 1H), 6.99 (d, *J* = 2.5 Hz, 1H), 3.49 (t, *J* = 13.8 Hz, 1H), 3.24 (dd, *J* = 22.2, 10.0 Hz, 1H), 2.79 (d, *J* = 3.8 Hz, 1H), 2.77 (d, *J* = 5.9 Hz, 1H), 1.34 (s, 9H), 1.25 (s, 9H).

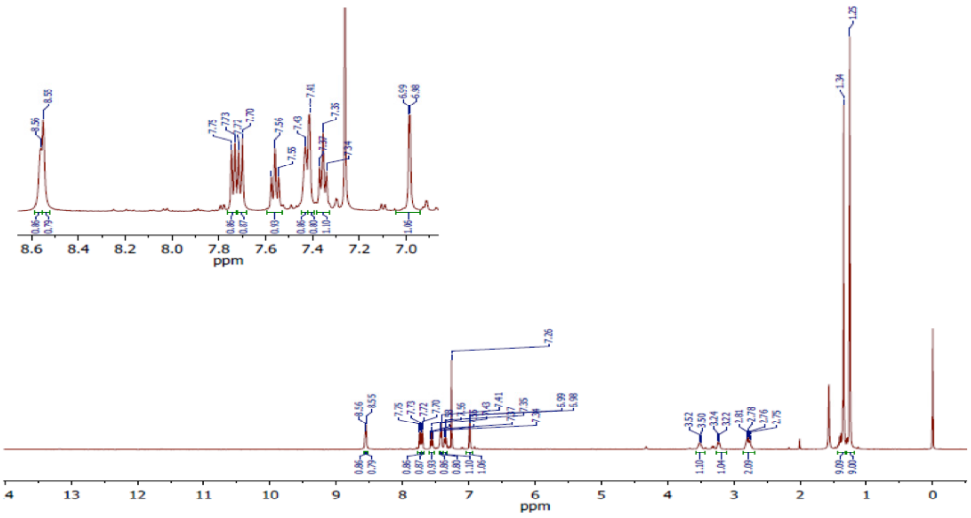

Figure 6-10: ^{1}H-NMR (500 MHz) spectra of L^{I}_{tBu}-NHOH-Ni in $CDCl_3$ at 25 °C with inset showing zoom in of aromatic region.

L^{I}_{H}-NHOH-Cu

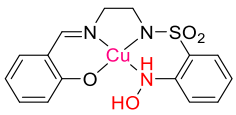

To a stirring solution of L^{I}_{H}-NHOH (110 mg, 0.327 mmol) in ACN (5 mL), a solution of $Cu(OAc)_2 \cdot H_2O$ (65.4 mg, 0.327 mmol) in ACN (5 mL), was added dropwise. The mixture was stirred vigorously for 15 min, during which a green solid precipitated out. The solid was collected by filtration, washed with diethyl ether (20 mL) and dried under vacuum to give a dark green powder. Yield: 75 mg, 58 %. Crystals suitable for X-ray diffraction analysis were obtained by subjecting a small portion of the complex dissolved in DCM to vapour-diffusion of pentane at room temperature.

L^{I}_{tBu}-NHOH-Cu

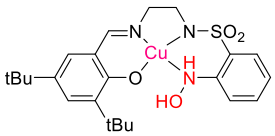

To a stirring solution of $Cu(OAc)_2.H_2O$ (127.9 mg, 0.641 mmol) in ACN (5 mL), a solution of L^{I}_{tBu}-NHOH (287 mg, 0.641 mmol) in ACN (5 mL) was added dropwise. The mixture was stirred vigorously for 15 minutes, during which a purple solid precipitated out. The solid was collected by filtration, washed with diethyl ether (20 mL) and dried under vacuum to give a purple powder. Crystals suitable for X-ray diffraction analysis were obtained by placing a small portion of copper(II) acetate dihydrate (0.0447 mmol, 13 mg) in a vial and then layering it with L^{I}_{tBu}-NHOH (0.0447 mmol, 30 mg) dissolved in 5 mL ACN

inside an inert atmosphere of glovebox. The mixture was left standing in the –30°C freezer for 3 days to yield purple crystals. Yield: 217 mg, 67%.

L^{I}_{H}-NHOH-Zn

To a stirring solution of $Zn(NO_3)_2{\cdot}6H_2O$ (150.8 mg, 0.507 mmol) in ACN (5 mL), a solution of L^{I}_{H}-NHOH (170 mg, 0.507 mmol) and triethylamine (140 µL, 102.6 mg, 1.013 mmol) in ACN (5 mL) was added dropwise. The mixture was stirred vigorously in air for 30 min, during which a white solid precipitated out. The solid was collected by filtration, washed with acetonitrile (10 mL) following by diethyl ether (20 mL) and then dried under vacuum to give a white powder. Yield: 112 mg, 55%. Crystals suitable for X-ray diffraction were grown by slow layered diffusion of pentane into a DCM solution of the complex at –20 °C. ^{1}H-NMR (500 MHz, DMSO) δ 9.57 (s, 1H), 8.70 (s, 1H), 8.29 (s, 1H), 7.60 (d, *J* = 7.5 Hz, 1H), 7.52 (d, *J* = 7.9 Hz, 1H), 7.40 (t, *J* = 7.5 Hz, 1H), 7.17 (t, *J* = 7.0 Hz, 1H), 7.16 – 7.11 (m, 1H), 7.09 (t, *J* = 7.4 Hz, 1H), 6.66 (d, *J* = 8.3 Hz, 1H), 6.51 (t, *J* = 7.3 Hz, 1H), 3.46 (t, *J* = 5.3 Hz, 2H), 2.77 (t, 2H).

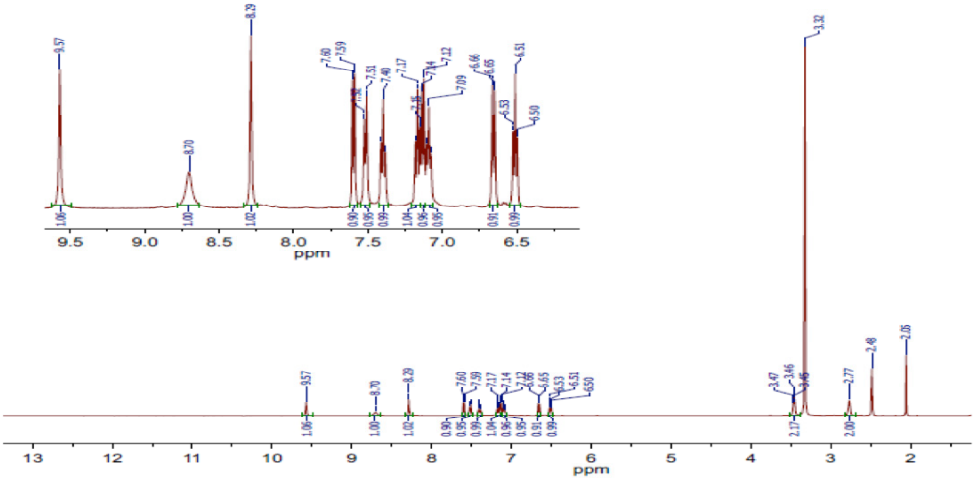

Figure 6-11: ^{1}H-NMR (500 MHz) spectra of L^{I}_{H}-NHOH-Zn in DMSO at 25 °C, inset representing zoom of aromatic region and NHOH proton peaks.

L^{I}_{tBu}-NHOH-Zn

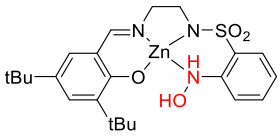

To a stirring solution of $Zn(NO_3)_2{\cdot}6H_2O$ (66.3 mg, 0.223 mmol) in ACN (5 mL), a solution of L^{I}_{tBu}-NHOH (100 mg, 0.223 mmol) and triethylamine (62 µL, 45.1 mg, 0.446 mmol) in ACN (5 mL) was added

dropwise. The mixture was stirred vigorously in air for 30 min, during which a white solid precipitated out. The solid was collected by filtration, washed with acetonitrile (10 mL) following by diethyl ether (20 mL) and dried under vacuum to give a white powder. Yield: 69 mg, 61 %. Crystals suitable for X-ray diffraction were grown by slow layered diffusion of pentane into dichloromethane solution of the complex at room temperature. ^{1}H-NMR (500 MHz, $CDCl_3$, δ/ppm) δ 9.30 (s, 2H), 8.07 (s, 1H), 8.01 (d, *J* = 8.8 Hz, 1H), 7.76 (d, *J* = 8.1 Hz, 1H), 7.54 (s, 1H), 7.51 (s, 1H), 7.24 (d, *J* = 7.5 Hz, 1H), 6.79 (d, *J* = 2.5 Hz, 1H), 3.19 (d, *J* = 45.1 Hz, 1H), 3.00 (d, *J* = 42.7 Hz, 1H), 1.59 (s, 9H), 1.27 (s, 9H).

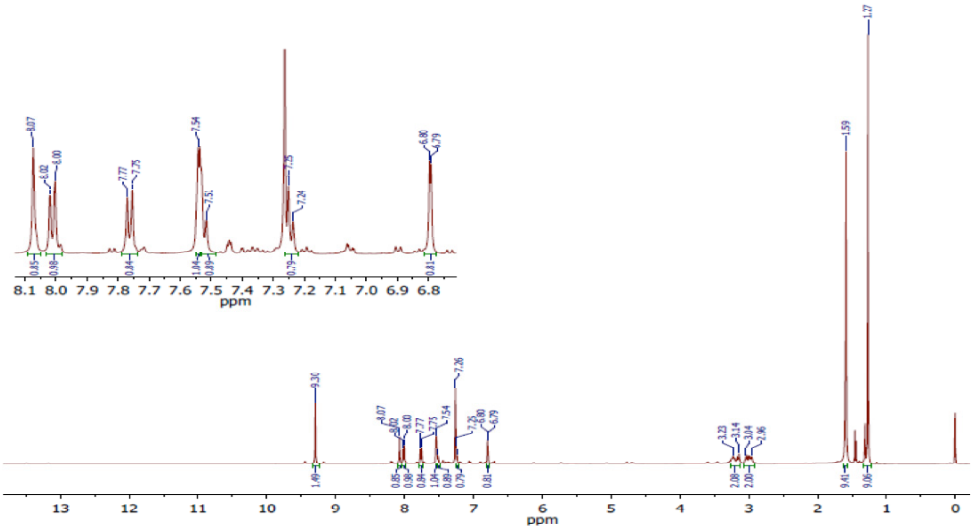

Figure 6-12: ^{1}H-NMR (500 MHz) spectra of L^{I}_{tBu}-NHOH-Zn in $CDCl_3$ at 25 °C, inset representing zoom of aromatic region and NHOH proton peaks.

6.5 Synthesis of Nitro Metal Complex

L^{I}_{tBu}-NO_2-Cu

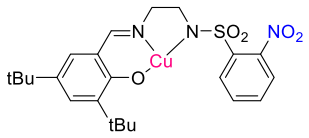

To a stirring methanol (5 mL) solution of $Cu(OAc)_2.H_2O$ (43.1 mg, 0.216 mmol), a solution of L^{I}_{tBu}-NO_2 (100 mg, 0.216 mmol) in DCM (5 mL) was added dropwise. The colour changed immediately to deep green. The solution was stirred for 15 min and then diethyl ether (10 mL) was added. The precipitated green solid was filtered off, washed with diethyl ether, and dried under vacuum. Yield: 82 mg, 70%. MS (ESI, CH_3CN): 523.116 $[M\text{-}L]H^{+}$.

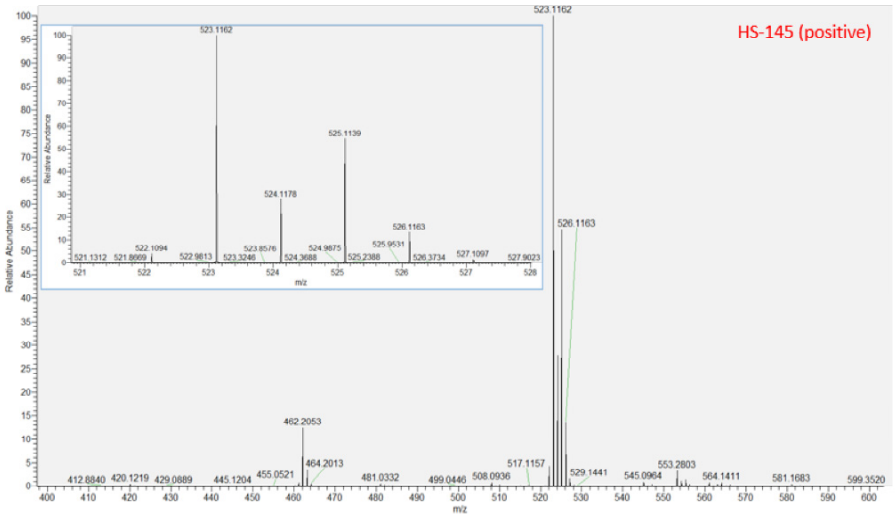

Figure 6-13: Positive mode ESI-MS of [L^{I}_{tBu}-NO_2-Cu] complex in HPLC-grade ACN. The peak at 523.116 corresponds to [M-L]H^+.

6.6 UV-Vis of L^{I}_{R}-NHOH-Ni and L^{I}_{R}-NHOH-Cu Complexes

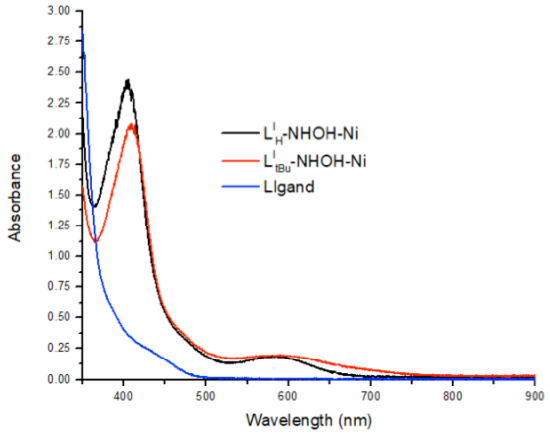

Figure 6-14: UV-Vis spectra of 1 mM L^{I}_{H}-NHOH-Ni (black) and L^{I}_{tBu}-NHOH-Ni (red) complexes solutions in DCM at room temperature with ligand overlay (blue). Pathlength of quartz cell used is 1.00 cm.

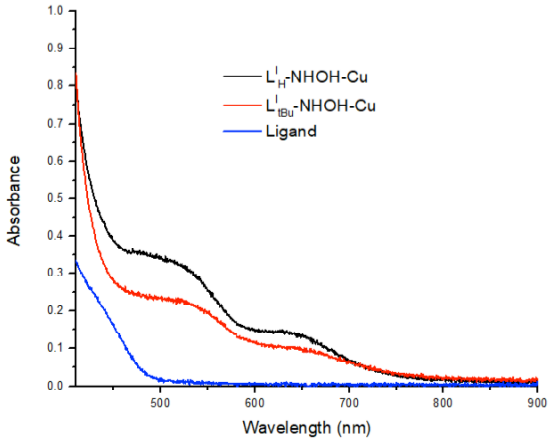

Figure 6-15: UV-Vis spectra of 1mM L^{I}_{H}-NHOH-Cu (black) and L^{I}_{tBu}-NHOH-Cu (red) complexes solutions in DCM at room temperature with ligand overlay (blue). Pathlength of quartz cell used is 1.00 cm.

6.7 General Procedure for the Oxidation of Alcohols to Aldehydes

In the glovebox, a Radleys® glass reaction tube was charged with 0.5 mmol of alcohol in 4 mL of solvent (DCM or THF). To this solution, L^{I}_{tBu}-NHOH-Cu (0.25 mmol, 5 mol%), 4-(*N,N*-dimethylamino)pyridine (DMAP, 0.1 mmol, 20 mol%) and 100 mg 4 Å MS were added sequentially. After the addition, a cross-shaped stirring bar was added, and the tube was sealed with the Radleys® perfluoroalkoxyalkane cap. The tube was then transferred to Radleys® carrousel (heated to 50 °C when the solvent is THF) and purged with oxygen (+1 atm vs. ambient atmosphere, *i.e.* 2 atm total), and kept under O_2 pressure throughout the course of reaction, with stirring. The reaction was monitored by taking small aliquots using a long-needled syringe. Each aliquot sample was passed over a small Celite-filled Pasteur pipette to remove metal, followed by the addition of known amount of hexamethylbenzene (HMB) as an internal standard (IS) in 1 mL HPLC grade MeOH in a GC vial. The resulting diluted solution was then injected into the GC-FID.

6.8 GC Chromatogram of Oxidation Catalysis Experiments

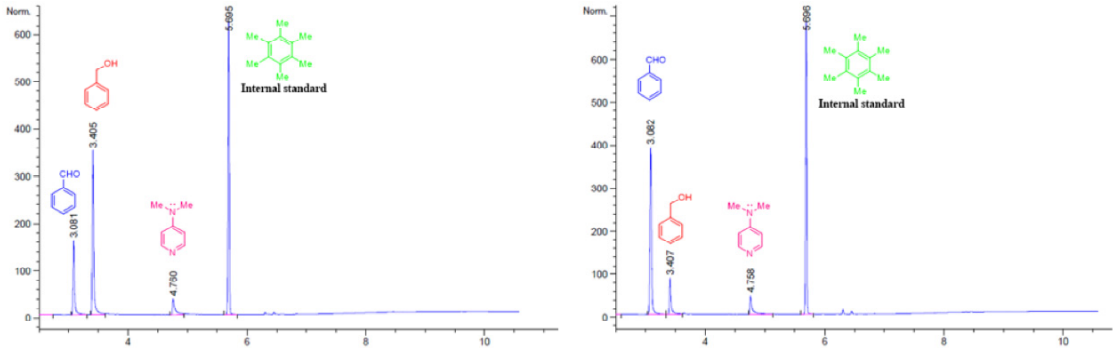

Figure 6-16: GC chromatogram showing the conversion of benzyl alcohol to benzaldehyde after 24 h(left) and 48 h (right) in DCM using L^{I}_{tBu}-NHOH-Cu as catalyst, DMAP as an additive and HMB as an internal standard.

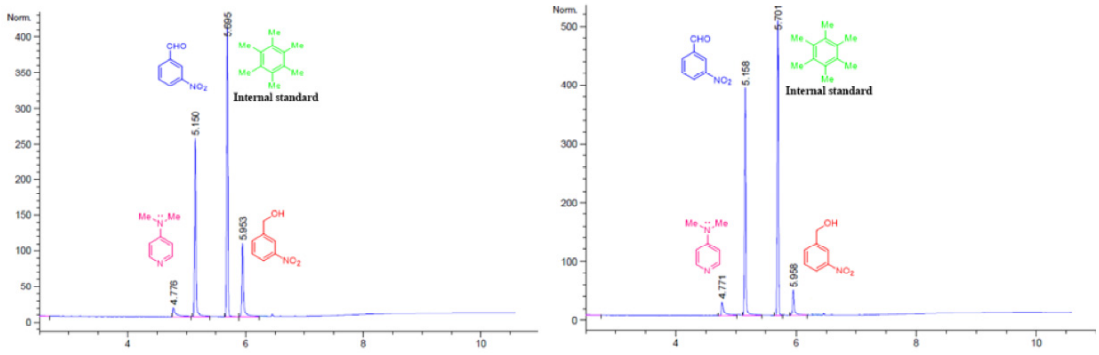

Figure 6-17: GC chromatogram showing the conversion of 3-nitro benzyl alcohol to 3-nitro benzaldehyde after 24 h (left) and 48 h (right) in DCM using L^{I}_{tBu}-NHOH-Cu as catalyst, DMAP as an additive and HMB as an internal standard.

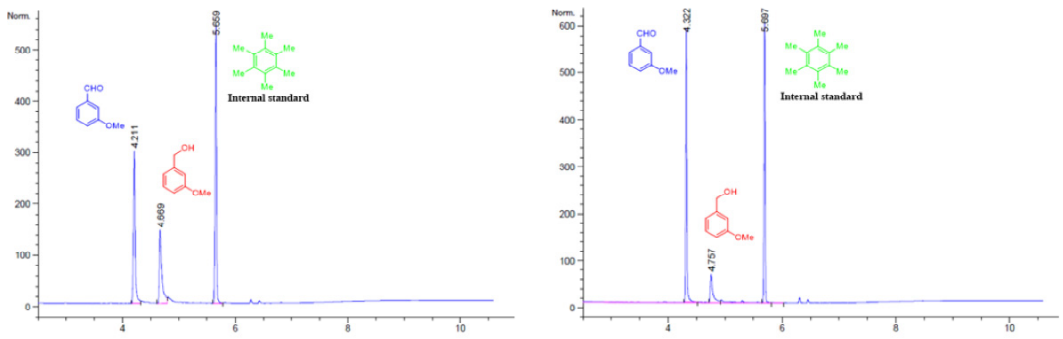

Figure 6-18: GC chromatogram showing the conversion of 3-methoxy benzyl alcohol to 3-methoxy benzaldehyde after 24 h (left) and 48 h (right) in DCM using L^{I}_{tBu}-NHOH-Cu as catalyst, DMAP as an additive and HMB as an internal standard.

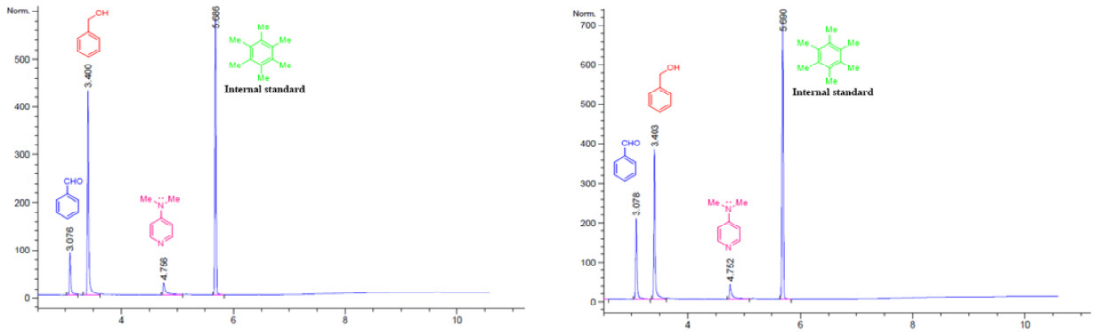

Figure 6-19: GC chromatogram showing the conversion of benzyl alcohol to benzaldehyde after 24 h (left) and 48 h (right) in DCM using L^{I}_{H}-NHOH-Cu as catalyst, DMAP as an additive and HMB as an internal standard.

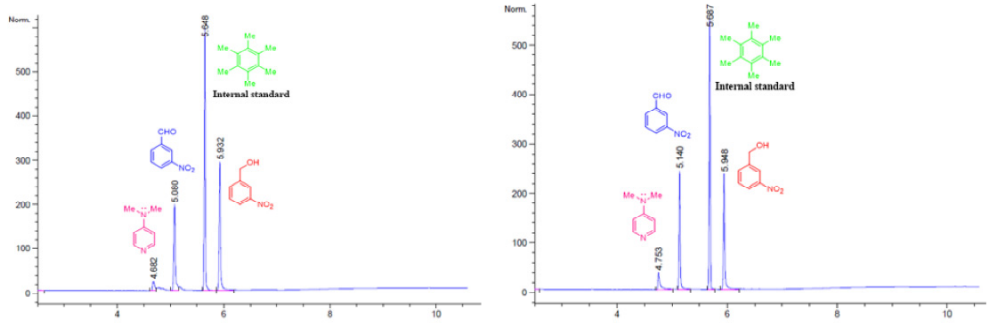

Figure 6-20: GC chromatogram showing the conversion of 3-nitro benzyl alcohol to 3-nitro benzaldehyde after 24 h (left) and 48 h (right) in DCM using L^{I}_{H}-NHOH-Cu as catalyst, DMAP as an additive and HMB as an internal standard.

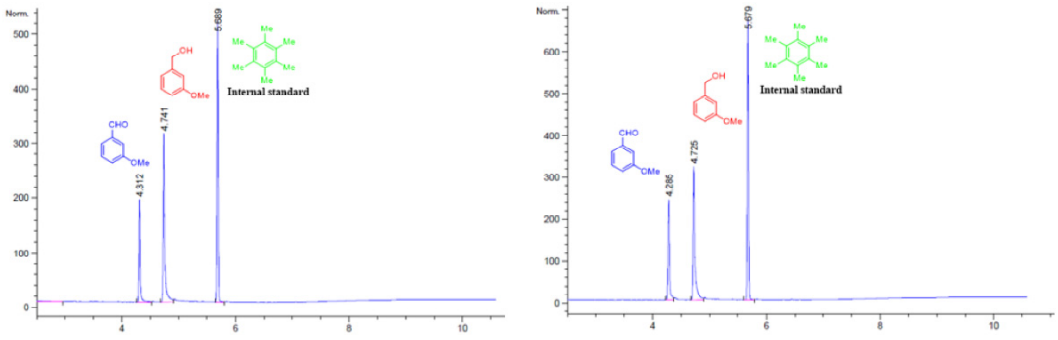

Figure 6-21: GC chromatogram showing the conversion of 3-methoxy benzyl alcohol to 3- benzaldehyde after 24 h (left) and 48 h (right) in DCM using L^{I}_{H}-NHOH-Cu as catalyst, DMAP as an additive and HMB as an internal standard.

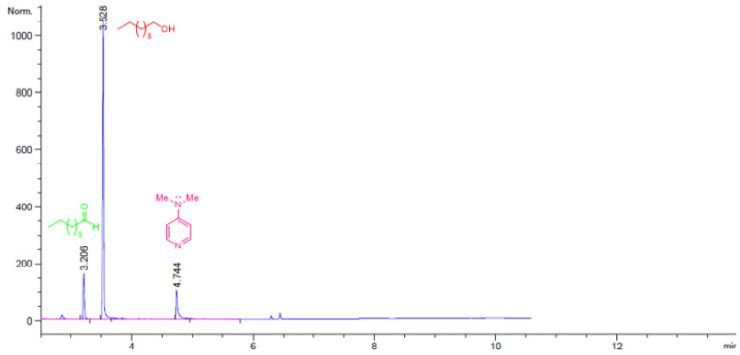

Figure 6-22: GC chromatogram showing the conversion of 1-octanol to octanal after 20 h in DCM using L^{I}_{tBu}-NHOH-Cu as catalyst and DMAP as an additive.

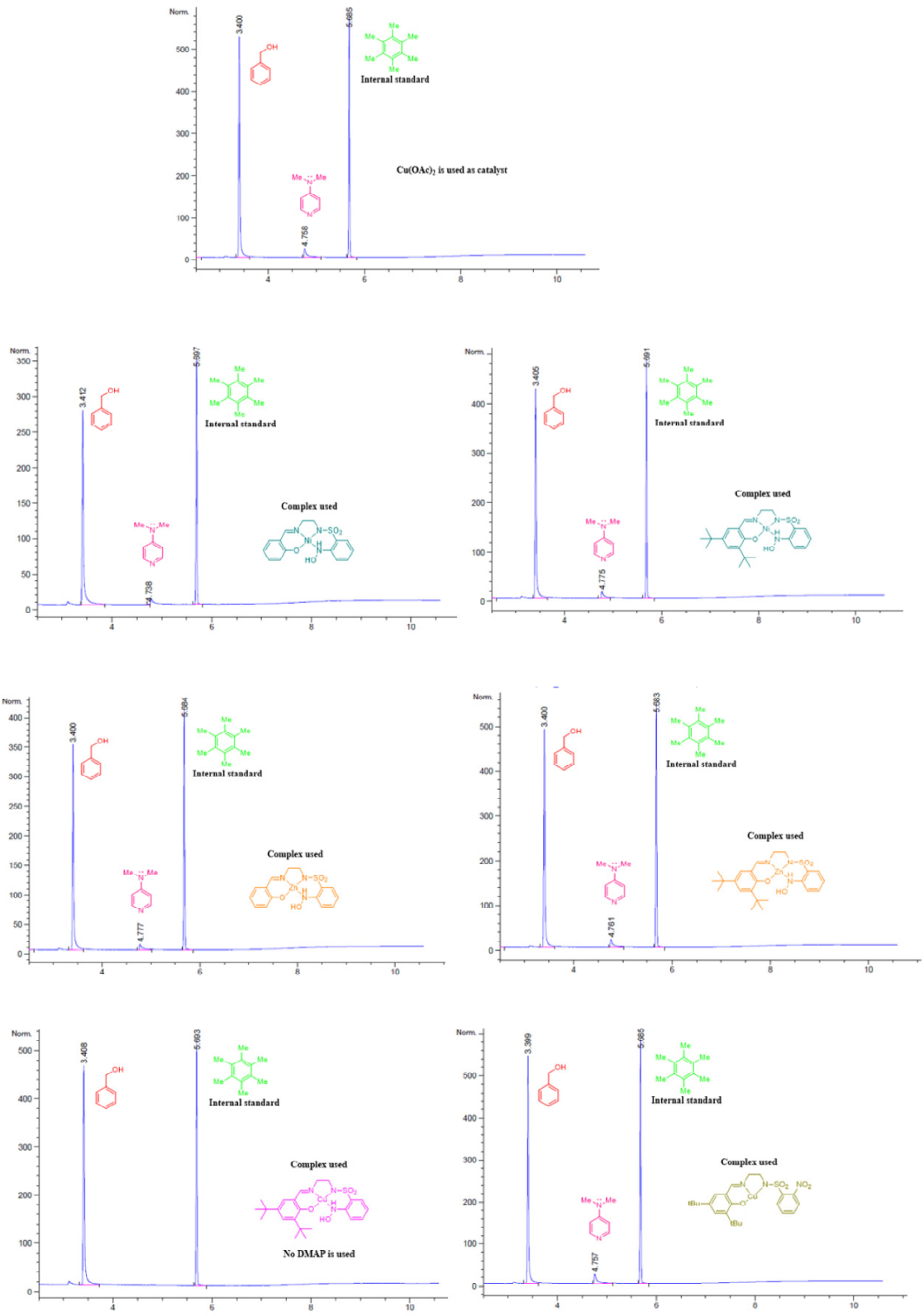

Figure 6-23: GC chromatogram for control experiments for the oxidation of benzyl alcohol.

6.9 X-ray crystallography

Table 6-1: Crystallography data for L^{I}_{H}-NHOH-M (M = Ni, Cu, Zn) and L^{I}_{H}-NH_2-Ni

	L^{I}_{H}-NHOH-Ni	L^{I}_{H}-NHOH-Cu	L^{I}_{H}-NHOH-Zn	L^{I}_{H}-NH_2-Ni
Sample code	Hardeep1	Hardeep5	Hardeep3	Hardeep4
Formula	$C_{15}H_{15}N_3NiO_4S$	$C_{30}H_{30}Cu_2N_6O_8S_2$	$C_{15}H_{15}N_3O_4SZn$	$C_{15}H_{15}N_3NiO_3S$, 0.5(H_2O)
Formula Weight (g mol^{-1})	392.07	793.80	398.73	385.08
T/K	300(2)	150(2)	300(2)	110(2)
Wavelength/Å	0.71073	0.71073	1.54178	1.54178
Size/mm^3	0.43×0.12×0.11	0.17×0.15×0.09	0.3×0.1×0.1	0.19×0.11×0.04
Crystal System	Orthorhombic	Monoclinic	Orthorhombic	Triclinic
Space Group	*Pbcn*	$P2_1/c$	*Pbcn*	*P-1*
a/Å	14.964(2)	11.2868(12)	15.0116(7)	11.9552(9)
b/Å	14.964(2)	9.6560(10)	15.0137(9)	12.1760(9)
c/Å	13.6852(19)	14.3063(15)	13.9214(8)	12.7970(9)
α/°	90	90	90	98.838(4)
β/°	90	94.4720(10)	90	112.789(4)
γ/°	90	90	90	108.273(4)
V/$Å^3$	3064.8(7)	1554.4(3)	3137.6(3)	1548.2(2)
Z	8	2	8	4
$D_{calc.}$/ g cm^{-3}	1.699	1.696	1.688	1.652
μ/mm^{-1}	1.429	1.565	3.660	3.274
θ_{min}/°	1.361	1.810	2.943	3.947
θ_{max}/°	27.463	25.341	54.049	68.802
Measured Reflections	22491	15265	35142	20646
Independent reflections	3630	2830	1863	5327
Reflexions with I > 2σ(I)	3248	2329	1610	4556
R_{int}	0.0498	0.0565	0.1057	0.0554
Parameters	229	218	229	432
Restraints	0	0	0	0
Largest Peak	0.512	0.373	0.397	0.353
Deepest Hole	-0.523	-0.364	-0.672	-0.425
Goodness of fit	1.047	1.051	1.202	1.097
wR_2 (all data)	0.1016	0.0787	0.1549	0.0953
wR_2	0.0972	0.0736	0.1498	0.0914
R_1 (all data)	0.0427	0.0451	0.0912	0.0461
R_1	0.0365	0.0328	0.0770	0.0375

Table 6-2: Crystallography data for L^{I}_{tBu}-NHOH-M (M = Ni, Cu, Zn)

	L^{I}_{tBu}-NHOH-Ni	L^{I}_{tBu}-NHOH-Cu	L^{I}_{tBu}-NHOH-Zn
Sample code	Hardeep2b	Fei18	Hardeep6
Formula	$C_{23}H_{31}N_3NiO_4S$	$C_{23}H_{31}CuN_3O_4S$	$C_{46}H_{62}N_6O_8S_2Zn_2$, 0.75($C_4O$), 0.25($CCl_2$)
Formula Weight (g mol^{-1})	504.28	509.11	1090.62
T/K	296(2)	110(2)	110(2)
Wavelength/Å	0.71073	1.54178	0.71073
Size/mm^3	0.27×0.20×0.05	0.19×0.15×0.10	0.28×0.10×0.07
Crystal System	Monoclinic	Monoclinic	Triclinic
Space Group	$P2_1/c$	$P2_1/c$	*P-1*
a/Å	16.4967(19)	18.1906(3)	12.0902(17)
b/Å	12.7673(15)	12.7306(2)	14.849(2)
c/Å	11.5945(14)	10.9264(2)	16.669(2)
α/°	90	90	111.874(2)
β/°	107.073(2)	100.5390(10)	106.757(2)
γ/°	90	90	94.825(2)
V/Å^3	2334.4(5)	2487.62(7)	2596.8(6)
Z	4	4	2
$D_{calc.}$/ g cm^{-3}	1.435	1.359	1.395
μ/mm^{-1}	0.955	2.293	1.088
θ_{min}/°	1.291	2.471	1.403
θ_{max}/°	25.379	68.494	27.475
Measured Reflections	-	22219	-
Independent reflections	7103	4524	11667
Reflexions with I > 2σ(I)	5748	3562	7302
R_{int}	0.0819	0.0492	0.1056
Parameters	296	293	658
Restraints	0	0	0
Largest Peak	1.121	0.712	0.907
Deepest Hole	-0.675	-0.838	-0.648
Goodness of fit	1.019	1.103	1.027
wR_2 (all data)	0.1654	0.1342	0.1697
wR_2	0.1540	0.1197	0.1509
R_1 (all data)	0.0795	0.0636	0.1231
R_1	0.0627	0.0435	0.0695

References

(1) Jørgensen, C. K. Differences between the Four Halide Ligands, and Discussion Remarks on Trigonal-Bipyramidal Complexes, on Oxidation States, and on Diagonal Elements of One-Electron Energy. *Coord. Chem. Rev.* **1966**, *1*, 164–178.

(2) Blanchard, S.; Derat, E.; Desage-El Murr, M.; Fensterbank, L.; Malacria, M.; Mouriès-Mansuy, V. Non-Innocent Ligands: New Opportunities in Iron Catalysis. *Eur. J. Inorg. Chem*. **2012**, *3*, 376–389.

(3) Tezgerevska, T.; Alley, K. G.; Boskovic, C. Valence Tautomerism in Metal Complexes: Stimulated and Reversible Intramolecular Electron Transfer between Metal Centers and Organic Ligands. *Coord. Chem. Rev.* **2014**, *268*, 23–40.

(4) Römelt, C.; Weyhermüller, T.; Wieghardt, K. Structural Characteristics of Redox-Active Pyridine-1,6-Diimine Complexes: Electronic Structures and Ligand Oxidation Levels. *Coord. Chem. Rev.* **2019**, *380*, 287–317.

(5) Sinha, S.; Das, S.; Sikari, R.; Parua, S.; Brandaõ, P.; Demeshko, S.; Meyer, F.; Paul, N. D. Redox Noninnocent Azo-Aromatic Pincers and Their Iron Complexes. Isolation, Characterization, and Catalytic Alcohol Oxidation. *Inorg. Chem.* **2017**, *56*, 14084–14100.

(6) Kaim, W.; Schwederski, B. Non-Innocent Ligands in Bioinorganic Chemistry-An Overview. *Coord. Chem. Rev.* **2010**, *254*, 1580–1588.

(7) Que, L.; Tolman, W. B. Biologically Inspired Oxidation Catalysis. *Nature* **2008**, *455*, 333–340.

(8) Lyaskovskyy, V.; De Bruin, B. Redox Non-Innocent Ligands: Versatile New Tools to Control Catalytic Reactions. *ACS Catal*. **2012**, *2*, 270–279.

(9) Sherbow, T. J.; Fettinger, J. C.; Berben, L. A. Control of Ligand PKa Values Tunes the Electrocatalytic Dihydrogen Evolution Mechanism in a Redox-Active Aluminum(III) Complex. *Inorg. Chem.* **2017**, *56*, 8651–8660.

(10) Dub, P. A.; Gordon, J. C. Metal-Ligand Bifunctional Catalysis: The “Accepted” Mechanism, the Issue of Concertedness, and the Function of the Ligand in Catalytic Cycles Involving Hydrogen Atoms. *ACS Catal.* **2017**, *7*, 6635–6655.

(11) Kaim, W. The Shrinking World of Innocent Ligands: Conventionaland Non-Conventional Redox-Active Ligands. *Eur. J. Inorg. Chem*. **2012**, *2012*, 343–348.

(12) de Bruin, B.; Gualco, P.; Paul, N. D. Redox Non-Innocent Ligands. In *Ligand Design in Metal Chemistry*; John Wiley & Sons, Ltd, **2016**; pp 176–204.

(13) Broere, D. L. J.; Plessius, R.; Van Der Vlugt, J. I. New Avenues for Ligand-Mediated Processes-Expanding Metal Reactivity by the Use of Redox-Active Catechol, o-Aminophenol and o-Phenylenediamine Ligands. *Chem. Soc. Rev.* **2015**, *44*, 6886–6915.

(14) Day, P. Christian Klixbull Jørgensen (1931-2001): Inorganic Spectroscopist Extraordinaire. *Coord. Chem. Rev*. **2003**, *238*, 3–8.

(15) Szilagyi, R. K.; Lim, B. S.; Glaser, T.; Holm, R. H.; Hedman, B.; Hodgson, K. O.; Solomon, E. I. Description of the Ground State Wave Functions of Ni Dithiolenes Using Sulfur K-Edge x-Ray Absorption Spectroscopy. *J. Am. Chem. Soc.* **2003**, *125*, 9158–9169.

(16) Samanta, S.; Ghosh, P.; Goswami, S. Recent Advances on the Chemistry of Transition Metal Complexes of 2-(Arylazo)Pyridines and Its Arylamino Derivatives. *Dalton Trans*. **2012**, *41*, 2213–2226.

(17) Chirik, P. J.; Wieghardt, K. Radical Ligands Confer Nobility on Base-Metal Catalysts. *Science* **2010**, *327*, 794–795.

(18) Ward, M. D.; McCleverty, J. A. Non-Innocent Behaviour in Mononuclear and Polynuclear Complexes: Consequences for Redox and Electronic Spectroscopic Properties. *J. Chem. Soc., Dalton Trans*. **2002**, *3*, 275–288.
(19) Eikey, R. A.; Abu-Omar, M. M. Nitrido and Imido Transition Metal Complexes of Groups 6-8. *Coord. Chem. Rev*. **2003**, *243*, 83–124.
(20) Ray, K.; Begum, A.; Weyhermüller, T.; Piligkos, S.; Van Slageren, J.; Neese, F.; Wieghardt, K. The Electronic Structure of the Isoelectronic, Square-Planar Complexes $[Fe^{II}(L)_2]^{2-}$ and $[Co^{III}(L^{Bu})_2]^{-}$ (L^{2-} and $(L^{Bu})^{2-}$ = Benzene-1,2-Dithiolates): An Experimental and Density Functional Theoretical Study. *J. Am. Chem. Soc.* **2005**, *127*, 4403–4415.
(21) Kaim, W. The Transition Metal Coordination Chemistry of Anion Radicals. *Coord. Chem. Rev.* **1987**, *76*, 187–235.
(22) Stubbe, J. A.; Van Der Donk, W. A. Protein Radicals in Enzyme Catalysis. *Chem. Rev.* **1998**, *98*, 705–762.
(23) Chaudhuri, P.; Wieghardt, K. Phenoxyl Radical Complexes. In *Prog. Inorg. Chem.* **2001**, Vol. *50*, pp 151–216.
(24) Schaefer, W. P. The Structure of Decaammine-μ-Peroxo-Dicobalt Disulfate Tetrahydrate. *Inorg. Chem.* **1968**, *7*, 725–731.
(25) Perutz, M. F.; Fermi, G.; Luisi, B.; Shaanan, B.; Liddington, R. C. Stereochemistry of Cooperative Mechanisms in Hemoglobin. *Acc. Chem. Res.* **1987**, *20*, 309–321.
(26) Pauling, L. Nature of the Iron-Oxygen Bond in Oxyhemoglobin. *Nature*. **1964**, *203*, 182–183.
(27) Weiss, J. J. Nature of the Iron-Oxygen Bond in Oxyhemoglobin. *Nature*. **1964**, *202*, 83–84.
(28) Kaim, W.; Schwederski, B. Non-Innocent Ligands in Bioinorganic Chemistry-An Overview. *Coord. Chem. Rev.* **2010**, *254*, 1580–1588.
(29) Pierpont, C. G. Studies on Charge Distribution and Valence Tautomerism in Transition Metal Complexes of Catecholate and Semiquinonate Ligands. *Coord. Chem. Rev*. **2001**, *216*, 99–125.
(30) Pierpont, C. G.; Lange, C. W. The Chemistry of Transition Metal Complexes Containing Catechol and Semiquinone Ligands. In *Prog. Inorg. Chem.* **2007**, *41*, 331–442.
(31) Balch, A. L. Oxidation of O-Quinone Adducts of Transition Metal Complexes. *J. Am. Chem. Soc.* **1973**, *95*, 2723–2724.
(32) Ketterer, N. A.; Fan, H.; Blackmore, K. J.; Yang, X.; Ziller, J. W.; Baik, M. H.; Heyduk, A. F. $\Pi^{\bullet-}\Pi^{\bullet}$ Bonding Interactions Generated by Halogen Oxidation of Zirconium(IV) Redox-Active Ligand Complexes. *J. Am. Chem. Soc.* **2008**, *130*, 4364–4374.
(33) Ringenberg, M. R.; Nilges, M. J.; Rauchfuss, T. B.; Wilson, S. R. Oxidation of Dihydrogen by Iridium Complexes of Redox-Active Ligands. *Organometallics* **2010**, *29*, 1956–1965.
(34) Murad, F. Discovery of Some of the Biological Effects of Nitric Oxide and Its Role in Cell Signaling (Nobel Lecture). *Angew. Chem. Int. Ed*. **1999**, *38*, 1856–1868.
(35) Wang, P. G.; Cai, T. B.; Taniguchi, N. Nitric Oxide Donors: For Pharmaceutical and Biological Applications. Wiley-VCH: Weinheim, **2005**.
(36) Feelish, M.; Stamler, J. S. Methods in Nitric Oxide Research. J. Wiley: Chichester, UK, **1996**.
(37) Culotta, E.; Koshland, D. E. NO News Is Good News. *Science* **1992**, *258*, 1862–1865.
(38) Ivanović-Burmazović, I.; Van Eldik, R. Metal Complex-Assisted Activation of Small Molecules. from NO to Superoxide and Peroxides. *Dalton Trans.* **2008**, *39*, 5259–5275.
(39) McCleverty, J. A. Chemistry of Nitric Oxide Relevant to Biology. *Chem. Rev*. **2004**, *104*, 403–418.
(40) Teillet-Billy, D.; Fiquet-Fayard, F. The NO-3Σ- and 1Δ Resonances: Theoretical Analysis of Electron Scattering Data. *J. Phys. B: Atom. Molec. Phys.* **1977**, *10*, L111-L117.
(41) Krüger, H. J. What Can We Learn from Nature about the Reactivity of Coordinated Phenoxyl Radicals? - A Bioinorganic Success Story. *Angew. Chem. Int. Ed*. **1999**, *38*, 627–631.

(42) Nobles, M. K.; Madhosingh, C. Dactylium Dendroides (Bull.) Fr. Misnamed as Polyporus Circinatus Fr. *Biochem. Biophys. Res. Commun.* **1963**, *12*, 146–147.
(43) Whittaker, J. W. Free Radical Catalysis by Galactose Oxidase. *Chem. Rev.* **2003**, *103*, 2347–2363.
(44) Whittaker, M. M.; Whittaker, J. W. A tyrosine-derived free radical in apogalactose oxidase. *J. Biol. Chem.* **1990**, *265*, 9610–9613.
(45) Das, A.; Ren, Y.; Hessin, C.; Desage-El Murr, M. Copper Catalysis with Redox-Active Ligands. *Beilstein J. Org. Chem.* **2020**, *16*, 858–870.
(46) Gamez, P.; Koval, I. A.; Reedijk, J. Bio-Mimicking Galactose Oxidase and Hemocyanin, Two Dioxygen-Processing Copper Proteins. *Dalton Trans*. **2004**, 4079–4088.
(47) Rittle, J.; Green, M. T. Cytochrome P450 Compound I: Capture, Characterization, and C-H Bond Activation Kinetics. *Science* **2010**, *330*, 933–937.
(48) Ortiz De Montellano, P. R. Hydrocarbon Hydroxylation by Cytochrome P450 Enzymes. *Chem. Rev.* **2010**, *110*, 932–948.
(49) Meunier, B.; de Visser, S. P.; Shaik, S. Mechanism of Oxidation Reactions Catalyzed by Cytochrome P450 Enzymes. *Chem. Rev.* **2004**, *104*, 3947–3980.
(50) Groves, J. T. Enzymatic C-H Bond Activation: Using Push to Get Pull. *Nat. Chem*. **2014**, *6*, 89–91.
(51) Grützmacher, H. Cooperating Ligands in Catalysis. *Angew. Chem. Int. Ed*. **2008**, 47, 1814–1818.
(52) Van Der Vlugt, J. I.; Reek, J. N. H. Neutral Tridentate PNP Ligands and Their Hybrid Analogues: Versatile Non-Innocent Scaffolds for Homogeneous Catalysis. *Angew. Chem. Int. Ed.* **2009**, *48*, 8832–8846.
(53) Luca, O. R.; Crabtree, R. H. Redox-Active Ligands in Catalysis. *Chem. Soc. Rev.* **2013**, *42*, 1440–1459.
(54) Zhang, G.; Wu, J.; Zheng, S.; Neary, M. C.; Mao, J.; Flores, M.; Trovitch, R. J.; Dub, P. A. Redox-Noninnocent Ligand-Supported Vanadium Catalysts for the Chemoselective Reduction of Ca=X (X = O, N) Functionalities. *J. Am. Chem. Soc.* **2019**, *141*, 15230–15239.
(55) Markó, I. E.; Tsukazaki, M.; Giles, P. R.; Brown, S. M.; Urch, C. J. Anaerobic Copper-Catalyzed Oxidation of Alcohols to Aldehydes and Ketones. *Angew. Chem. Int. Ed.* **1997**, *36*, 2208–2210.
(56) Markó, I. E.; Gautier, A.; Dumeunier, R.; Doda, K.; Philippart, F.; Brown, S. M.; Urch, C. J. Efficient, Copper-Catalyzed, Aerobic Oxidation of Primary Alcohols. *Angew. Chem. Int. Ed.* **2004**, *43*, 1588–1591.
(57) McCann, S. D.; Stahl, S. S. Mechanism of Copper/Azodicarboxylate-Catalyzed Aerobic Alcohol Oxidation: Evidence for Uncooperative Catalysis. *J. Am. Chem. Soc.* **2016**, *138*, 199–206.
(58) Blaser, H. U. A Golden Boost to an Old Reaction. *Science*. **2006**, *313*, 312–313.
(59) Corma, A.; Concepción, P.; Serna, P. A Different Reaction Pathway for the Reduction of Aromatic Nitro Compounds on Gold Catalysts. *Angew. Chem. Int. Ed.* **2007**, *46*, 7266–7269.
(60) Beaudoin, D.; Wuest, J. D. Dimerization of Aromatic C-Nitroso Compounds. *Chem. Rev*. **2016**, *116*, 258–286.
(61) Lee, J.; Chen, L.; West, A. H.; Richter-Addo, G. B. Interactions of Organic Nitroso Compounds with Metals. *Chem. Rev.* **2002**, *102*, 1019–1065.
(62) Zuman, P.; Shah, B. Addition, Reduction, and Oxidation Reactions of Nitrosobenzene. *Chem. Rev.* **1994**, *94*, 1621–1641.
(63) Adam, W.; Krebs, O. The Nitroso Ene Reaction: A Regioselective and Stereoselective Allylic Nitrogen Functionalization of Mechanistic Delight and Synthetic Potential. *Chem. Rev*. **2003**, *103*, 4131–4146.
(64) Druelinger, M. L.; Shelton, R. W.; Lammert, S. R. Photochemistry of Methylenenitrones and Related Compounds. A Study of Oxaziridine and Nitrene Formation. *J. Heterocycl. Chem.* **1976**, *13*, 1001–1007.

(65) Oppolzer, W.; Tamura, O. Asymmetric Synthesis of α-Amino Acids and α-N-Hydroxyamino Acids via Electrophilic Amination of Bornanesultam-Derived Enolates with 1-Chloro-1-Nitrosocyclohexane. *Tetrahedron Lett.* **1990**, *31*, 991–994.
(66) Oppolzer, W.; Tamura, O.; Sundarababu, G.; Signer, M. Asymmetric α-Amination of Ketone Enolates by Chiral α-Chloro-α-Nitroso Reagents: A New Approach to Optically Pure Erythro-β-Amino Alcohols. *J. Am. Chem. Soc.* **1992**, *114*, 5900–5902.
(67) Momiyama, N.; Yamamoto, H. Simple Synthesis of α-Hydroxyamino Carbonyl Compounds: New Scope of the Nitroso Aldol Reaction. *Org. Lett.* **2002**, *4*, 3579–3582.

(68) Adam, W.; Bottle, S. E.; Peters, K. Cycloaddition of Nitrosobenzene to a Trimethylenemethane Diradical: The First Case of Isoxazoline Formation from in Situ Generated Nitroxides through Spin Trapping. *Tetrahedron Lett.* **1991**, *32*, 4283–4286.
(69) Torssell, K. Investigation of Radical Intermediates in Organic Reactions by Use of Nitroso Compounds as Scavengers the Nitroxide Method. *Tetrahedron* **1970**, *26*, 2759–2773.
(70) Forrester, A. R.; Henderson, J.; Reid, K. Nitrosocarbonylbenzene as a Spin Trap. *Tetrahedron Lett.* **1983**, *24*, 5547–5550.
(71) Gowenlock, B. G.; Richter-Addo, G. B. Preparations of C-Nitroso Compounds. *Chem. Rev.* **2004**, *104*, 3315–3340.
(72) Gowenlock, B. G.; Richter-Addo, G. B. Dinitroso and Polynitroso Compounds. *Chem. Soc. Rev.* **2005**, *34*, 797–809.
(73) Xu, N.; Richter-Addo, G. B. Interactions of Nitrosoalkanes/Arenes, Nitrosamines, Nitrosothiols, and Alkyl Nitrites with Metals. In *Progress in Inorganic Chemistry*; Wiley Blackwell, 2014; Vol. 59, pp 381–446. https://doi.org/10.1002/9781118869994.ch06.
(74) Askari, M. S.; Effaty, F.; Gennarini, F.; Orio, M.; Le Poul, N.; Ottenwaelder, X. Tuning Inner-Sphere Electron Transfer in a Series of Copper/Nitrosoarene Adducts. *Inorg. Chem.* **2020**, *59*, 8678–8689.
(75) Di Girolamo, F.; Campanella, L.; Samperi, R.; Bachi, A. Mass Spectrometric Identification of Hemoglobin Modifications Induced by Nitrosobenzene. *Ecotoxicol. Environ. Saf.* **2009**, *72*, 1601–1608.
(76) Vyas, P. M.; Roychowdhury, S.; Woster, P. M.; Svensson, C. K. Reactive Oxygen Species Generation and Its Role in the Differential Cytotoxicity of the Arylhydroxylamine Metabolites of Sulfamethoxazole and Dapsone in Normal Human Epidermal Keratinocytes. *Biochem. Pharmacol.* **2005**, *70*, 275–286.
(77) Irvine, J. C.; Ritchie, R. H.; Favaloro, J. L.; Andrews, K. L.; Widdop, R. E.; Kemp-Harper, B. K. Nitroxyl (HNO): The Cinderella of the Nitric Oxide Story. *Trends in Pharm. Sci.* **2008**, *29*, 601–608.
(78) Spooren, A. A. M. G.; Evelo, C. T. A. Hydroxylamine Treatment Increases Glutathione-Protein and Protein- Protein Binding in Human Erythrocytes. *Blood Cells Mol. Dis.* **1997**, *23*, 323–336.
(79) Srivastava, R. S.; Nicholas, K. M. Mechanistic Aspects of Molybdenum-Promoted Allylic Amination. *J. Org. Chem.* **1994**, *59*, 5365–5371.
(80) Srivastava, R. S.; Nicholas, K. M. On the Mechanism of Allylic Amination Catalyzed by Iron Salts. *J. Am. Chem. Soc.* **1997**, *119*, 3302–3310.
(81) Ho, C. M.; Lau, T. C. Copper-Catalyzed Amination of Alkenes and Ketones by Phenylhydroxylamine. *New J. Chem.* **2000**, *24*, 859–863.
(82) Hogan, G. A.; Gallo, A. A.; Nicholas, K. M.; Srivastava, R. S. Cu(I)-Catalyzed Allylic Amination of Olefins. *Tetrahedron Lett.* **2002**, *43*, 9505–9508..
(83) Srivastava, R. S.; Khan, M. A.; Nicholas, K. M. Nitrosoarene-Cu(I) Complexes Are Intermediates in Copper-Catalyzed Allylic Amination. *J. Am. Chem. Soc.* **2005**, *127*, 7278–7279.

(84) Srivastava, R. S.; Tarver, N. R.; Nicholas, K. M. Mechanistic Studies of Copper(I)-Catalyzed Allylic Amination. *J. Am. Chem. Soc.* **2007**, *129* , 15250–15258.
(85) G. Booth. *Ullmann's Encyclopedia of Industrial Chemistry*; Wiley-VCH Verlag, Weinheim, **2000**.
(86) Travis, A. S. Manufacture and Uses of the Anilines: A Vast Array of Processes and Products. In *PATAI'S Chemistry of Functional Groups*; John Wiley & Sons, Ltd, **2009**, 764.
(87) Li, Z.; Xu, M.; Xing, S.; Ho, W. T.; Ishii, T.; Li, Q.; Fu, X.; Zhao, Z. J. Erlotinib Effectively Inhibits JAK2V617F Activity and Polycythemia Vera Cell Growth. *J. Biol. Chem.* **2007**, *282*, 3428–3432.
(88) Smith G. V.; Nothesiz, F. *Heterogeneous Catalysis in Organic Chemistry*; Academic Press: New York, 1**999**, pp 71-79.
(89) Larock, R. C. *Comprehensive Organic Transformations: A Guide to Functional Group Preparations*, 2nd ed.; Wiley-VCH: New York, **1999**, pp 821-828.
(90) Makaryan, J. A.; Savchenko, V. I. N-Arylhydroxylamines Transformation in the Presense of Heterogeneous Catalysts. *Stud. Surf. Sci. Catal.* **1993**, *75*, 2439–2442.
(91) Axet, M. R.; Conejero, S.; Gerber, I. C. Ligand Effects on the Selective Hydrogenation of Nitrobenzene to Cyclohexylamine Using Ruthenium Nanoparticles as Catalysts. *ACS Appl. Nano Mater.* **2018**, *1*, 5885–5894.
(92) Merlic, C. A.; Motamed, S.; Quinn, B. Structure Determination and Synthesis of Fluoro Nissl Green: An RNA-Binding Fluorochrome. *J. Org. Chem.* **1995**, *60*, 3365–3369.
(93) Burawoy, A.; Critchley, J. P. Electronic Spectra of Organic Molecules and Their Interpretation-V. Effect of Terminal Groups Containing Multiple Bonds on the K-Bands of Conjugated Systems. *Tetrahedron* **1959**, *5*, 340–351.
(94) Kock, E. Entstehung Halogensubstituirter Amidoverbindungen Bei Der Reduction von Nitrokohlenwasserstoffen. *Berichte der deutschen chemischen Gesellschaft* **1887**, *20*, 1567–1569.
(95) Doxsee, K. M.; Feigel, M.; Stewart, K. D.; Canary, J. W.; Knobler, C. B.; Cram, D. J. Host—Guest Complexation. 42. Preorganization Strongly Enhances The Tendency of Hemispherands To Form Hemispheraplexes. *J. Am. Chem. Soc.* **1987**, *109*, 3098–3107.
(96) Tsukinoki, T.; Tsuzuki, H. Organic Reaction in Water. Part 5. Novel Synthesis of Anilines by Zinc Metal-Mediated Chemoselective Reduction of Nitroarenes. *Green Chem.* **2001**, *3*, 37–38.
(97) Favre, T. L. F.; Seijsener, P. J.; Kooyman, P. J.; Maltha, A.; Zuur, A. P.; Ponec, V. Selective Reduction of Nitrobenzene to Nitrosobenzene on Oxidic Catalysts. *Catal. Let.* **1988**, *1*, 457–460.
(98) Entwistle, I. D.; Gilkerson, T.; Johnstone, R. A. W.; Telford, R. P. Rapid Catalytic Transfer Reduction of Aromatic Nitro Compounds to Hydroxylamines. *Tetrahedron* **1978**, *34*, 213–215.
(99) Marvel, C. S.; Kamm, O. Organic Chemical Reagents.3 III. β-Phenylhydroxylamine and Cupferron. *J. Am. Chem. Soc.* **1919**, *41*, 276–282.
(100) Kamm, O. B-PHENYLHYDROXYLAMINE. *Org. Synth.* **1925**, *4*, 57.
(101) Liu, S.; Wang, Y.; Jiang, J.; Jin, Z. The Selective Reduction of Nitroarenes to N-Arylhydroxylamines Using Zn in a CO_2/H_2O System. *Green Chem.* **2009**, *11*, 1397–1400.
(102) Liu, S.; Wang, Y.; Yang, X.; Jiang, J. Selective Reduction of Nitroarenes to N-Arylhydroxylamines by Use of Zn in a CO2-H2O System, Promoted by Ultrasound. *Research on Chemical Intermediates* **2012**, *38* (9), 2471–2478. https://doi.org/10.1007/s11164-012-0562-5.
(103) Effaty, F.; Zsombor-Pindera, J.; Kazakova, A.; Girard, B.; Askari, M. S.; Ottenwaelder, X. Ligand and Electronic Effects on Copper-Arylnitroso Self-Assembly. *New J. Chem.* **2018**, *42*, 7758–7764.
(104) Baleizão, C.; Garcia, H. Chiral Salen Complexes: An Overview to Recoverable and Reusable Homogeneous and Heterogenous Catalysts. *Chem. Rev.* **2006**, *106*, 3987–4043.
(105) Cozzi, P. G. Metal-Salen Schiff Base Complexes in Catalysis: Practical Aspects. *Chem. Soc. Rev.* **2004**, *33*, 410–421.

(106) Jacobsen, E. N.; Zhang, W.; Güler, M. L. Electronic Tuning of Asymmetric Catalysts. *J. Am. Chem. Soc.* **1991**, *113*, 6703–6704.
(107) Crane, A. K.; MacLachlan, M. J. Portraits of Porosity: Porous Structures Based on Metal Salen Complexes. *Eur. J. Inorg. Chem.* **2012**, *2012*, 17–30.
(108) Gupta, K. C.; Sutar, A. K. Catalytic Activities of Schiff Base Transition Metal Complexes. *Coord. Chem. Rev*. **2008**, *252*, 1420–1450.
(109) McGarrigle, E. M.; Gilheany, D. G. Chromium-and Manganese-Salen Promoted Epoxidation of Alkenes. *Chem. Rev.* **2005**, *105*, 1563–1602.
(110) Katsuki, T. Catalytic Asymmetric Oxidations Using Optically Active (Salen)Manganese(III) Complexes as Catalysts. *Coord. Chem. Rev*. **1995**, *140*, 189–214.
(111) Mukherjee, C.; Weyhermüller, T.; Bothe, E.; Chaudhuri, P. Targeted Oxidase Reactivity with a New Redox-Active Ligand Incorporating N_2O_2 Donor Atoms. Complexes of Cu(II), Ni(II), Pd(II), Fe(III), and V(V). *Inorg. Chem.* **2008**, *47*, 11620–11632.
(112) Min, K. S.; Weyhermüller, T.; Bothe, E.; Wieghardt, K. Tetradentate Bis(o-Iminobenzosemiquinonate(1-)) π Radical Ligands and Their o-Aminophenolate(1-) Derivatives in Complexes of Nickel(II), Palladium(II), and Copper(II). *Inorg. Chem.* **2004**, *43*, 2922–2931.
(113) Pfeiffer, P.; Breith, E.; Lübbe, E.; Tsumaki, T. Tricyclische Orthokondensierte Nebenvalenzringe. *Justus Liebigs Ann. Chem.* **1933**, *503*, 84–130.
(114) K. Asatkar, A.; Tripathi, M.; Asatkar, D. Salen and Related Ligands. In *Stability of Coordination Compounds*. *IntechOpen*, 2020.
(115) Chen, F.; Askari, M. S.; Ottenwaelder, X. Synthesis of a Sulfonamide-Schiff Base Ligand and Its Cu(II), Fe(III) and Co(III) Complexes. *Inorg. Chim. Acta* **2013**, *407*, 25–30.
(116) Mori, A.; Miyakawa, Y.; Ohashi, E.; Haga, T.; Maegawa, T.; Sajiki, H. Pd/C-Catalyzed Chemoselective Hydrogenation in the Presence of Diphenylsulfide. *Org. Lett.* **2006**, *8*, 3279–3281.
(117) Yamamura, S.; Toda, M.; Hirata, Y. MODIFIED CLEMMENSEN REDUCTION: CHOLESTANE. *Org. Synth.* **1973**, *53*, 86.
(118) Habibian, M. Oxygen- and Nitrogen-Group Transfers in Aryl-Nitroso Iron Complexes. **2011**.
(119) Sheibany, N. Hydroxylamine-Containing Ligands:Synthesis and Reactions with Copper Ions. **2017**.
(120) Zsombor-Pindera, J.; Effaty, F.; Escomel, L.; Patrick, B.; Kennepohl, P.; Ottenwaelder, X. Five Nitrogen Oxidation States from Nitro to Amine: Stabilization and Reactivity of a Metastable Arylhydroxylamine Complex. *J. Am. Chem. Soc.* **2020**. https://doi.org/10.1021/jacs.0c09300.
(121) Chen, F. CHEM 450. **2012**.
(122) Li, S. N.; Zhai, Q. G.; Hu, M. C.; Jiang, Y. C. Synthesis, Crystal Structures and Characterization of Two Cu(II) Complexes with Asymmetric Sulfonamide Schiff-Base Ligands. *J. Coord. Chem.* **2009**, *62*, 2709–2718.
(123) Cameron, M.; Gowenlock, B. G.; Vasapollo, G. Coordination Chemistry of C-Nitroso-Compounds. *Chem. Soc. Rev*. **1990**, *19*, 355–379.
(124) Kochem, A.; Gellon, G.; Leconte, N.; Baptiste, B.; Philouze, C.; Jarjayes, O.; Orio, M.; Thomas, F. Stable Anilinyl Radicals Coordinated to Nickel: X-Ray Crystal Structure and Characterization. *Chem. Eur. J.* **2013**, *19*, 16707–16721.
(125) Li, J.; Song, H.; Cui, C.; Cheng, J. P. Synthesis and Characterization of Linear and Square-Planar Nickel Complexes with Primary Amido Ligands. *Inorg. Chem.* **2008**, *47*, 3468–3470.
(126) Li, J.; Tian, D.; Song, H.; Wang, C.; Zhu, X.; Cui, C.; Cheng, J. P. Synthesis, Structures, and Reactivity of Nickel Complexes Incorporating Sulfonamido-Imine Ligands. *Organometallics* **2008**, *27*, 1605–1611.

(127) Taylor, M. K.; Reglinski, J.; Wallace, D. Coordination Geometry of Tetradentate Schiff's Base Nickel Complexes: The Effects of Donors, Backbone Length and Hydrogenation. *Polyhedron* **2004**, *23*, 3201–3209.
(128) Addison, A. W.; Rao, T. N.; Reedijk, J.; Van Rijn, J.; Verschoor, G. C. Synthesis, Structure, and Spectroscopic Properties of Copper(II) Compounds Containing Nitrogen-Sulphur Donor Ligands; the Crystal and Molecular Structure of Aqua[1,7-Bis(N-Methylbenzimidazol-2';-Yl)-2,6-Dithiaheptane]Copper(II) Perchlorate. *J. Chem. Soc., Dalton Trans.* **1984**, *7*, 1349–1356.
(129) Reglinski, J.; Morris, S.; Stevenson, D. E. Supporting Conformational Change at Metal Centres. Part 2: Four and Five Coordinate Geometry. *Polyhedron* **2002**, *21*, 2175–2182.
(130) Singer, A. L.; Atwood, D. A. Five-Coordinate Salen(TBu) Complexes of Zinc. *Inorg. Chim. Acta* **1998**, *277*, 157–162.
(131) Stevens, R. V.; Chapman, K. T.; Weller, H. N. Convenient and Inexpensive Procedure for Oxidation of Secondary Alcohols to Ketones. *J. Org. Chem.* **1980**, *45*, 2030–2032.
(132) Highet, R. J.; Wildman, W. C. Solid Manganese Dioxide as an Oxidizing Agent. *J. Am. Chem. Soc.* **1955**, *77*, 4399–4401.
(133) Lee, D. G.; Spitzer, U. A. The Aqueous Dichromate Oxidation of Primary Alcohols. *J. Org. Chem.* **1970**, *35*, 3589–3590.
(134) Holum, J. R. Study of the Chromium(VI) Oxide—Pyridine Complex. *J. Org. Chem.* **1961**, *26*, 4814–4816.
(135) Dess, D. B.; Martin, J. C. Readily Accessible 12-I-51 Oxidant for the Conversion of Primary and Secondary Alcohols to Aldehydes and Ketones. *J. Org. Chem.* **1983**, *48*, 4155–4156.
(136) Omura, K.; Swern, D. Oxidation of Alcohols by "Activated" Dimethyl Sulfoxide. a Preparative, Steric and Mechanistic Study. *Tetrahedron* **1978**, *34*, 1651–1660.
(137) Chan, D. M. T.; Monaco, K. L.; Wang, R. P.; Winters, M. P. New N- and O-Arylations with Phenylboronic Acids and Cupric Acetate. *Tetrahedron Lett.* **1998**, *39*, 2933–2936.
(138) Evans, D. A.; Katz, J. L.; West, T. R. Synthesis of Diaryl Ethers through the Copper-Promoted Arylation of Phenols with Arylboronic Acids. An Expedient Synthesis of Thyroxine. *Tetrahedron Lett.* **1998**, *39*, 2937–2940.
(139) Lam, P. Y. S.; Clark, C. G.; Saubern, S.; Adams, J.; Winters, M. P.; Chan, D. M. T.; Combs, A. New Aryl/Heteroaryl C-N Bond Cross-Coupling Reactions via Arylboronic Acid/Cupric Acetate Arylation. *Tetrahedron Lett.* **1998**, *39*, 2941–2944.
(140) Hardouin Duparc, V.; Bano, G. L.; Schaper, F. Chan-Evans-Lam Couplings with Copper Iminoarylsulfonate Complexes: Scope and Mechanism. *ACS Catal.* **2018**, *8*, 7308–7325.